
Doctoral Dissertations


Student Theses and Dissertations

Fall 2020

Investigation of urea decomposition and deposit formation in diesel exhaust after-treatment system

Anand Alembath

Follow this and additional works at: https://scholarsmine.mst.edu/doctoral_dissertations

 Part of the [Automotive Engineering Commons](#), [Chemical Engineering Commons](#), and the [Environmental Engineering Commons](#)

Department: Chemical and Biochemical Engineering

Recommended Citation

Alembath, Anand, "Investigation of urea decomposition and deposit formation in diesel exhaust after-treatment system" (2020). *Doctoral Dissertations*. 3085.
https://scholarsmine.mst.edu/doctoral_dissertations/3085

This thesis is brought to you by Scholars' Mine, a service of the Missouri S&T Library and Learning Resources. This work is protected by U. S. Copyright Law. Unauthorized use including reproduction for redistribution requires the permission of the copyright holder. For more information, please contact scholarsmine@mst.edu.

INVESTIGATION OF UREA DECOMPOSITION AND DEPOSIT FORMATION IN
DIESEL EXHAUST AFTER-TREATMENT SYSTEM

by

ANAND ALEMBATH

A DISSERTATION

Presented to the Graduate Faculty of the
MISSOURI UNIVERSITY OF SCIENCE AND TECHNOLOGY

In Partial Fulfillment of the Requirements for the Degree
DOCTOR OF PHILOSOPHY IN CHEMICAL ENGINEERING

2020

Approved by:

Joseph D Smith, Advisor
Ali Rownaghi
Brian Mooney
Douglas Ludlow
Fatih Dogan

© 2020

Anand Alembath

All Rights Reserved

ABSTRACT

Urea-selective catalytic reduction (SCR) system has proved to be an effective solution to reduce NO_x emissions in commercial vehicle (CV) diesel engines. A significant challenge in urea injection is to comprehend its decomposition chemistry that leads to formation of undesired deposits in the exhaust system unit. Due to complex interaction of multi-phase fluid flow and transport processes, significant uncertainty is associated with the identification of interacting factors that control the deposit initiation and its growth. To meet the future ultra-low NO_x emissions and to deliver ammonia without deposit formation, there is an imminent need to develop the urea-SCR technology.

The overall objective is to guide new product development and design a better exhaust mixer that would minimize deposits.

A systematic investigation into the mechanism of deposit formation was conducted through numerous experiments and deposits were characterized to measure their chemical composition. Effect of pressure on urea deposits was investigated for the first time by heating aqueous urea solution in a closed system maintained between 30-200psia. The deposit forming temperatures and phase change compositions were identified in both open and closed system. Based on this understanding, deposit test was conducted on a hot gas test setup with a typical after-treatment system layout. Deposit initiating temperatures were identified, and the effect of gas flow rate was studied. The chemical characterization procedure was carried out using different analytical techniques such as thermogravimetric analysis (TGA), electrospray ionization (ESI) and liquid chromatography (LC).

ACKNOWLEDGMENTS

I would first like to thank my advisor Dr. Joseph Smith. He has always believed in me and has provided the support that I have needed. Under his guidance, I have learned to be an independent researcher. I am grateful to Faurecia Clean Mobility for funding my research. My heartfelt thanks to all the collaborators at Faurecia: Atul Shinde, R. Shashidhara and Robin Willats. It was great to have an opportunity to spend a part of my research at Faurecia's R&D facility.

I would like to thank all the professors on my PhD committee who have each provided helpful feedback. I would like to acknowledge the contribution of Dr. Brian Mooney and for piquing my interest in mass spectroscopy. Sincere thanks to Dr. Al-Dahhan, Dr. Forciniti and their graduate students Dr. Humayun and Dr. Paul for sharing their lab facility. Special thanks to Dr. Ownby who flew me on his plane to Columbus, IN during my first visit to Faurecia.

My research would have been impossible without the aid and support of undergraduate students: Maria, Jonathan, Olivia and Austin. I am indebted to many friends in my research group: Dr. Aso, Dr. Al-Rubaye, Hassan Alabedi, Shyam, Hayder, Dr. Yu, Dr. Nagapurkar and Dr. Rao. I want to express my gratitude to the chemical engineering department staff- Michael, Dean, Marlene and Chandra. I would like to acknowledge the valuable help of Eileen for structuring my manuscripts.

My deepest appreciation belongs to my parents, my brother and my in-laws who have backed me and helped me realize my dreams. Finally, I want to thank my wife Parvathy for her unconditional love and support throughout my entire academic journey.

TABLE OF CONTENTS

| | Page |
|---|------|
| ABSTRACT..... | iii |
| ACKNOWLEDGMENTS | iv |
| LIST OF ILLUSTRATIONS | ix |
| LIST OF TABLES | xiii |
| NOMENCLATURE | xiv |
| SECTION | |
| 1. INTRODUCTION | 1 |
| 1.1. DIESEL ENGINE AND EMISSIONS..... | 1 |
| 1.2. STRATEGIES USED BY MANUFACTURERS TO REDUCE EMISSIONS | 2 |
| 1.3. GENERAL SCR SYSTEM CHEMISTRY AND REACTIONS..... | 4 |
| 1.4. UREA-SCR TECHNOLOGY | 5 |
| 1.4.1. Role of Mixer..... | 6 |
| 1.4.2. Urea Decomposition and Deposit Formation. | 7 |
| 1.4.3. Chemo-Physical Processes in Urea-SCR System..... | 8 |
| 1.4.3.1. Spray atomization | 9 |
| 1.4.3.2. Droplet evaporation | 9 |
| 1.4.3.3. Spray wall interaction | 10 |
| 1.4.3.4. Liquid film formation and transport. | 12 |
| 1.4.3.5. Reaction chemistry | 12 |
| 1.5. RESEARCH OBJECTIVE AND APPROACH..... | 13 |

| | |
|--|----|
| 2. UREA DEPOSIT STUDY IN AN OPEN SYSTEM | 15 |
| 2.1. LITERATURE REVIEW | 15 |
| 2.2. EXPERIMENTAL SETUP AND ANALYTIC METHODS | 17 |
| 2.2.1. Liquid Temperature and Phase Change. | 17 |
| 2.2.2. Open Vessel Heating. | 18 |
| 2.2.3. Chemical Analysis. | 19 |
| 2.3. RESULTS AND DISCUSSIONS | 19 |
| 2.3.1. Liquid Temperature and Phase Change | 19 |
| 2.3.2. Open Vessel Heating Results | 20 |
| 2.3.3. Chemical Characterization of Samples | 23 |
| 2.3.4. TGA of DEF and Pure Urea | 25 |
| 2.4. INFERENCE | 29 |
| 3. UREA DEPOSIT STUDY IN CLOSED SYSTEM | 30 |
| 3.1. EFFECT OF PRESSURE ON UREA DEPOSITS | 30 |
| 3.2. EXPERIMENTAL SETUP AND ANALYTICAL METHODS | 33 |
| 3.3. RESULTS AND DISCUSSIONS | 35 |
| 3.3.1. Open System Validation | 35 |
| 3.3.2. Closed System Results | 35 |
| 3.4. INFERENCE | 42 |
| 4. SINGLE DROPLET AND LIQUID FILM EXPERIMENT | 43 |
| 4.1. LITERATURE REVIEW | 43 |
| 4.2. EXPERIMENTAL SETUP | 45 |
| 4.2.1. Single Droplet Experiment. | 45 |

| | |
|---|----|
| 4.2.2. Liquid Film Temperature Measurement. | 46 |
| 4.2.3. Gravity-Driven Liquid Film. | 47 |
| 4.2.4. Stagnant Film Experiment. | 49 |
| 4.3. RESULTS AND DISCUSSIONS | 50 |
| 4.3.1. Single Droplet Experiment | 50 |
| 4.3.2. Gravity Driven Liquid Film..... | 52 |
| 4.3.3. Stagnant Film Test Results..... | 55 |
| 4.4. INFERENCE | 60 |
| 5. EXPERIMENT ON A HOT GAS TEST BENCH..... | 61 |
| 5.1. LITERATURE REVIEW..... | 61 |
| 5.2. EXPERIMENTAL SETUP | 62 |
| 5.2.1. Optic Box Design..... | 63 |
| 5.2.2. Flow Characterization..... | 65 |
| 5.2.3. Flow Velocity Measurement..... | 69 |
| 5.2.4. Test Repeatability. | 70 |
| 5.3. RESULTS AND DISCUSSION | 71 |
| 5.3.1. Local Deposit Forming Temperatures | 72 |
| 5.3.2. Leidenfrost Effect and Deposit Forming Regime..... | 74 |
| 5.3.3. Critical Injection Rate (CIR)..... | 75 |
| 5.3.4. Effect of Gas Flow Rate..... | 76 |
| 5.4. INFERENCE | 81 |
| 6. DEPOSIT CHARACTERIZATION | 82 |
| 6.1. ANALYTICAL METHODOLOGY | 82 |

| | |
|---|-----|
| 6.2. C-13 NMR (CARBON-13 NUCLEAR MAGNETIC RESONANCE) | 82 |
| 6.3. FTIR (FOURIER TRANSFORM INFRARED SPECTROSCOPY)..... | 84 |
| 6.4. THERMOGRAVITOMETRIC ANALYSIS (TGA) | 86 |
| 6.5. ESI-MS (ELECTRON SPRAY IONIZATION-MASS SPECTROMETRY) . | 87 |
| 6.6. LIQUID CHROMATOGRAPHY(LC) | 89 |
| 6.6.1. Amide Column..... | 89 |
| 6.6.2. HSS-T3 and C18 Dual Column Setup | 90 |
| 6.6.3. HILIC Column..... | 93 |
| 6.7. AMMONIUM CARBAMATE CHARACTERIZATION | 97 |
| 6.7.1. Thermogravimetric Analysis | 98 |
| 6.7.2. Gas Chromatography-Mass Spectroscopy (GC-MS) | 99 |
| 6.8. INFERENCE | 101 |
| 7. CONCLUSION | 103 |
| 8. FUTURE WORK | 105 |
| REFERENCES..... | 106 |
| VITA | 113 |

LIST OF ILLUSTRATIONS

| | Page |
|---|------|
| Figure 1.1 Diesel Emission Control Technologies Implemented | 2 |
| Figure 1.2 Layout of Urea-SCR System in Diesel Engines..... | 5 |
| Figure 1.3 DEF Refill Nozzle in New Diesel Vehicles | 6 |
| Figure 1.4 Chemo-Physical Process Inside a Mixer Leading to Deposit | 8 |
| Figure 1.5 Vapor Pressure of DEF Solution | 10 |
| Figure 2.1 Beaker Filled with DEF placed on a Heated Plate | 18 |
| Figure 2.2 Open Vessel Heating Setup | 19 |
| Figure 2.3 Liquid Temperature Change with Time for Three Plate Temperatures | 20 |
| Figure 2.4 Weight Change and Liquid Temperature Measurement | 21 |
| Figure 2.5 Samples Extracted at Different Temperature | 22 |
| Figure 2.6. Rate of Weight Loss in Deposit Decomposition Region..... | 23 |
| Figure 2.7 Chemical Quantitation using LC-MRM for Open Heating System | 24 |
| Figure 2.8 TGA of DEF and Pure Urea At 20°C/Min | 25 |
| Figure 2.9 Pure Urea Heated at Different Heating Rate | 26 |
| Figure 2.10 Time Scale of Deposit Formation and Deposit Decomposition | 27 |
| Figure 2.11 Products of Urea Decomposition Heated At 10°C/Min | 28 |
| Figure 3.1 Future Regulation Limit on NO _x Emissions | 30 |
| Figure 3.2 High Temperature High Pressure Reactor System | 34 |
| Figure 3.3 Test Procedure for Pressurized System | 34 |
| Figure 3.4 Temperature Plot with Time and Final Deposit Residue | 35 |

| | |
|---|----|
| Figure 3.5 Temperature Plot at Higher Pressure..... | 36 |
| Figure 3.6 Effect of Pressure on Deposit Weight and Residence Time..... | 37 |
| Figure 3.7 Deposit Residue from Pressurized System..... | 38 |
| Figure 3.8. Liquid Sampled at 50psia | 39 |
| Figure 3.9. Liquid Sampled at 100psia | 40 |
| Figure 4.1 Boiling Curve of Water. | 44 |
| Figure 4.2 Single Droplet Impingement | 46 |
| Figure 4.3 Emissivity Calibration using IR Camera..... | 47 |
| Figure 4.4 Test Plate Dimensions | 48 |
| Figure 4.5 Experimental Setup for Gravity-Driven Flow..... | 49 |
| Figure 4.6 Stagnant Liquid Film Experiment Setup | 50 |
| Figure 4.7 Single Droplet Impingement Results..... | 51 |
| Figure 4.8 Deposits on Painted vs Non-Painted Surface | 52 |
| Figure 4.9 Deposit Initiation in Gravity Driven Liquid Film. | 53 |
| Figure 4.10 Low Temperature Zone | 56 |
| Figure 4.11 Medium Temperature Zone..... | 57 |
| Figure 4.12 Stagnant Film Test with Temperature Measurement using IR Camera | 58 |
| Figure 4.13 IR Film Temperature Measurement and Solidification Point | 59 |
| Figure 5.1 Truck Setup With DPF, DOC, Optic Box and SCR..... | 63 |
| Figure 5.2 Optic Box Design | 64 |
| Figure 5.3 Thermocouple Position..... | 65 |
| Figure 5.4 Recirculation Eddies Inside the Channel..... | 66 |
| Figure 5.5 Modified Inlet Design to Reduce Recirculation..... | 66 |

| | |
|---|----|
| Figure 5.6 Streamlines Indicating Low Recirculation with Perforated Plate | 67 |
| Figure 5.7 Inlet Velocity Contour Plot | 68 |
| Figure 5.8 Final Optic Box Design | 68 |
| Figure 5.9 Pitot Tube Calibration Results..... | 69 |
| Figure 5.10 Test Repeatability | 71 |
| Figure 5.11 Deposit Growth with Time | 72 |
| Figure 5.12 Deposit Initiating Temperatures | 73 |
| Figure 5.13 Deposit Weight and Images Generated at Different Operating Conditions.. | 73 |
| Figure 5.14 Leidenfrost Threshold | 75 |
| Figure 5.15 Critical Injection Rate for 800kg/hr | 76 |
| Figure 5.16 Deposit Mitigating Mechanism at High Exhaust Flow Rate..... | 77 |
| Figure 5.17 Deposit Initiation and Growth in Wall Film Regime | 80 |
| Figure 6.1 C-13 NMR Spectra of Deposit Sample | 83 |
| Figure 6.2 C-13 Standard Compound Peak | 83 |
| Figure 6.3 FTIR Spectra of Deposit Sample..... | 84 |
| Figure 6.4 FTIR Spectra of Standard Compounds..... | 85 |
| Figure 6.5 Comparison of Deposit Sample Peak with Standard Compounds | 85 |
| Figure 6.6. TGA Analysis of Deposit Sample and Standard Compounds..... | 86 |
| Figure 6.7. ESI-MS Spectra of Deposit Sample | 87 |
| Figure 6.8 Peak Height Quantitation of Three Compounds | 88 |
| Figure 6.9. Amide Column: Peak Separation and Retention Time..... | 90 |
| Figure 6.10 Standard Curves for Dual Column Setup | 91 |
| Figure 6.11 Compound Separation and Retention for Dual Column..... | 92 |

| | |
|--|-----|
| Figure 6.12 Standard Curves for HILIC Column | 94 |
| Figure 6.13 Cross-Talk Phenomenon in HILIC Column | 95 |
| Figure 6.14 Ammonium Carbamate Test Samples..... | 98 |
| Figure 6.15 TGA Curves of Ammonium Carbamate Samples. | 99 |
| Figure 6.16 Peak Retention Time | 100 |
| Figure 6.17 Predicted Retention Time..... | 100 |
| Figure 6.18 GC-MS Peaks | 101 |

LIST OF TABLES

| | Page |
|--|------|
| Table 1.1 European Emission Regulation between 2000-2014 | 2 |
| Table 1.2 Different Strategies to Control Diesel Emissions | 3 |
| Table 2.1 Summary of Urea Thermal Decomposition Chemical Reactions..... | 16 |
| Table 2.2 Rate of Weight Loss in Different Regions..... | 22 |
| Table 2.3 Solubility of Deposit Compounds in Water..... | 29 |
| Table 3.1 Effect of Pressure on Urea Conversion..... | 38 |
| Table 3.2 Chemical Mass Composition of Samples from 100psia Experiment | 41 |
| Table 4.1 Time Required for the Liquid Film to Reach the End of Plate..... | 54 |
| Table 4.2 Time and Location of Deposit Initiation from IR Camera | 55 |
| Table 4.3 Solidification Time for Stagnant Liquid Film | 57 |
| Table 4.4 Chemical Mass Composition | 59 |
| Table 5.1 Pitot Tube Calculations..... | 70 |
| Table 5.2 Deposit Weight for Different Gas Flow Rate | 79 |
| Table 5.3 Reynolds Number | 80 |
| Table 6.1 LC-MRM Transition | 94 |

NOMENCLATURE

| Symbol | Description |
|--------|------------------------------|
| ICE | Internal Combustion Engine |
| PM | Particulate Matter |
| EGR | Exhaust Gas Recirculation |
| DPF | Diesel Particulate Filter |
| DEF | Diesel Exhaust Fluid |
| SCR | Selective Catalyst Reduction |
| CYA | Cyanuric Acid |
| CFD | Computational Fluid Dynamics |
| UWS | Urea Water Solution |
| TGA | Thermogravimetric Analysis |
| ESI | Electron Spray Ionization |
| LC | Liquid Chromatography |
| MRM | Multiple Reaction Monitoring |
| DFT | Density Functional Theory |
| IR | Infrared |
| CIR | Critical Injection Rate |
| FTIR | Fourier Transform Infrared |
| NMR | Nuclear Magnetic Resonance |
| MS | Mass Spectroscopy |

1. INTRODUCTION

1.1. DIESEL ENGINE AND EMISSIONS

From large stationary generators to automobiles, internal combustion engines (ICE) have made tremendous impact on human life. Diesel engine provides a combination of high thermal efficiency and low carbon di-oxide emissions compared to the gasoline engine. The difference between the diesel and gasoline engine lies in the way the fuel is burnt. Gasoline being volatile, readily mixes with air and a spark is enough to initiate combustion. On the other hand, diesel, does not mix well with air. However, atomized diesel sprayed onto hot compressed air generates spontaneous combustion. Since diesel engine compresses only the air and not the air-fuel mixture, compression ratio achieved is high without any risk of self-ignition which helps it to achieve high thermal efficiency. However, a major problem that lies with diesel engines is the NO_x and particulate matter emissions.

Tail pipe has basically two pollutants which are formed in opposite conditions: NO_x (NO, NO₂, N₂O, N₂O₃, N₂O₅) and particulate matter (PM). While running a lean fuel mixture can lead to high combustion and produce elevated NO_x emissions, a rich fuel mixture can lead to a less efficient combustion forming soot (black smoke seen when applied a sudden high-pressure gas pedal). NO_x and PM can deteriorate human health as well as surrounding environment.

During the past few decades, to preserve the quality of air, US Environmental Protection Agency and European Emission Board have taken stringent actions on cutting down diesel emissions. Table 1.1 [1] below displays the acceptable limits stated by

European Emission Standards. The numbers suggest that companies had to reduce eighty percent NO_x and ninety percent PM emissions during the 2000-2015 period.

Table 1.1 European Emission Regulation between 2000-2014

| Year | CO(g/km) | NO _x (g/km) | PM(g/km) |
|------|----------|------------------------|----------|
| 2000 | 0.64 | 0.5 | 0.05 |
| 2005 | 0.5 | 0.25 | 0.025 |
| 2011 | 0.5 | 0.18 | 0.005 |
| 2014 | 0.5 | 0.08 | 0.005 |

1.2. STRATEGIES USED BY MANUFACTURERS TO REDUCE EMISSIONS

Figure 1.1 and Table 1.2 briefly describes the strategies adopted by various manufacturers to comply with emission standards at various stages.

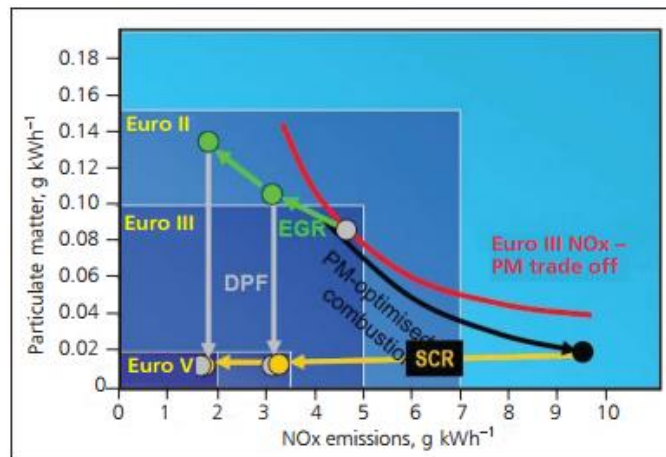


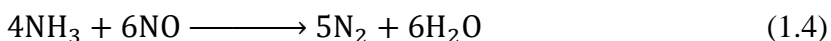
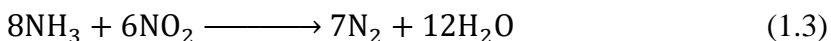
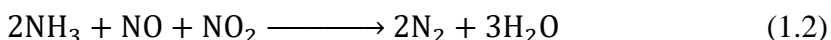
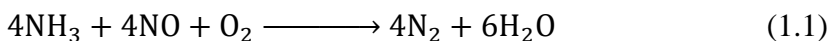
Figure 1.1 Diesel Emission Control Technologies Implemented
(Strategies adopted by various manufacturers to comply with emission standards at various stages. SCR is the current technology used to reduce 90% NO_x in commercial vehicles)

Table 1.2 Different Strategies to Control Diesel Emissions

| Technology | Working Principle | Advantages | Drawbacks |
|---|---|--|---|
| EGR(Exhaust Gas Recirculation) | Designed to reduce NOx emissions. Recycles the exhaust gases back to the engine. Air fuel mixture is replaced with inert gases to reduce combustion. | No additional structural components are needed. | Less efficient, leads to low fuel efficiency. More fuel goes unburnt producing more particulate matter. |
| DPF (Diesel Particulate Filter) | Designed to cut PM emissions. Screen Filters traps the soot. DPF gets plugged quickly. To clear the filter, engine is run on regeneration mode where fuel is burnt to provide high temperature at DPF to burn all PM. | Absorbs and reduces the overall particulate matter coming out of the tail pipe. | To be on regeneration mode, car must be running on a highway which is not always possible and most of the time regeneration is not complete. In long run DPF must be cleaned or replaced. |
| Lean-Trap NOx | Designed to trap NOx during lean fuel mode. When the trap fills, engine runs on a regeneration mode where rich fuel mixture is used. NOx is catalytically converted to N ₂ during regeneration. | 70-80% NOx conversion efficiency for low capacity engines. | Less storage capacity. Trap can get over-filled during long highway drive. |
| DEF-SCR (Diesel Exhaust Fluid-Selective Catalyst Reduction) | Injects a reductant (urea solution) through a special catalyst into the exhaust stream to reduce NOx to nitrogen. | 95 % NOx conversion efficiency and does not affect the engine performance unlike other technologies. | Urea crystallization and deposits which leads to plugging the channel. Additional urea refill transportation and infrastructure must be built. |

1.3. GENERAL SCR SYSTEM CHEMISTRY AND REACTIONS

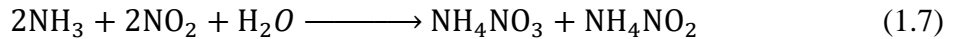
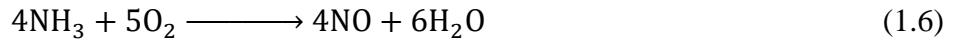
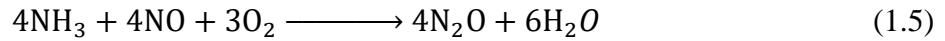
In diesel exhaust system, NO_x is generally 95% NO [2]. In SCR systems, NO and NH₃ are reacted on a catalyst surface following Langmuir-Hinshelwood Mechanism [3]. The most common catalyst used are V₂O₅/TiO₂. A set of reactions occurring inside SCR system is shown below:



Due to the presence of higher NO in exhaust system, Reaction (1.1) is considered as a standard SCR reaction and it is a fast reaction. Reaction (1.2) is faster than reaction (1.1) which is an important conversion reaction at low SCR temperatures. For this reason, NO₂ concentration is sometimes deliberately increased to maintain the 50-50 stoichiometry. [4] Reaction (1.3) and (1.4) are slow and sometimes excess NO₂ can go unreacted.

Temperature of diesel exhaust is generally between 300-500 °C [5]. At temperatures above 400 °C, undesirable reactions with oxygen can cause secondary emissions. It can either form Nitrous oxide as per reaction (1.5) or complete oxidation of ammonia can occur to form nitrogen oxide (reaction (1.6)).

At very low temperature (below 200 °C) ammonium nitrate is formed which gets deposited on the pores of catalyst (reaction (1.7)) [6].



1.4. UREA-SCR TECHNOLOGY

SCR systems have been used in stationary sources like boilers and heavy marine vessels to reduce NO_x emissions for a long time. Application of SCR is extended to diesel automobiles where it works in conjunction with DEF (Diesel Exhaust Fluid) which is ammonia based. DEF is injected just before the catalytic converter where ammonia in DEF reacts with NO_x and reduces it to nitrogen and water [7]. Ammonia is not directly used in the SCR-system as it is difficult to store. Urea is a good source of ammonia which is nontoxic, clean, odorless, and less corrosive. Figure 1.2 shows a layout of the overall exhaust system. It is composed of urea storage system, urea supply system and catalytic converters.

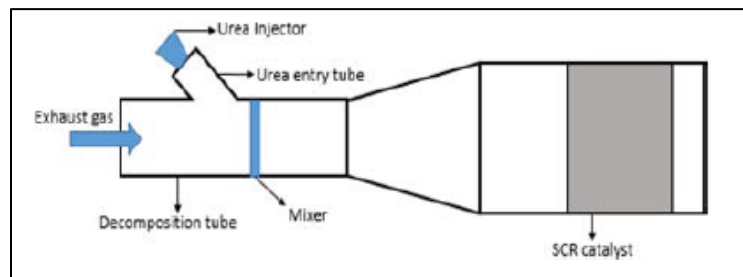


Figure 1.2 Layout of Urea-SCR System in Diesel Engines
(DEF is injected just before the catalytic converter where ammonia in DEF reacts with NO_x and reduces it to nitrogen and water)

DEF is typically a 32.5% concentration urea solution which is also known as AdBlue in Europe, marketing term used by automobile industry. At this concentration,

lowest freezing point ($-11\text{ }^{\circ}\text{C}$) of urea is achieved below which it crystallizes. For this reason, engine recirculating water heats urea tank. Further reduction in freezing point can be achieved by using other sources of ammonia. For example, solid urea and ammonium salts can go up to $-30\text{ }^{\circ}\text{C}$ freezing point [5].

DEF levels are monitored and must be refilled. The engine will limit performance and end up not starting when DEF is empty. Figure 1.3 [8] shows new diesel vehicles equipped with DEF tank where the nozzle is adjacent to fuel tank nozzle for easy refill.



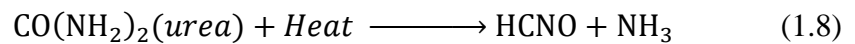
Figure 1.3 DEF Refill Nozzle in New Diesel Vehicles
(DEF tank is adjacent to fuel tank nozzle for easy refill)

1.4.1. Role of Mixer. Spray droplets from commercial doser are a combination of small and large droplets. Smaller droplets evaporate during the flight through exhaust gases whereas the larger droplets due to its inertia would impinge the exhaust wall. To facilitate better mixing and evaporation of droplets, a mixer was introduced before the SCR catalyst. For good NO_x conversion, a uniformly distributed ammonia concentration must be achieved within the catalyst inlet surface [9]. High turbulence for mixing would induce higher back pressure. Effectiveness of a mixer is quantified by uniformity of ammonia

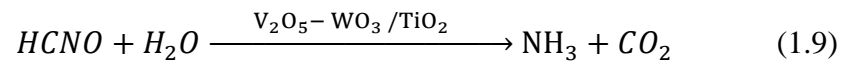
concentration and velocity in front of the catalyst and the back pressure it induces. Studies were conducted to investigate the mixer performance on different mixer designs but none of the studies have concluded a single best design.

1.4.2. Urea Decomposition and Deposit Formation. A significant challenge in urea injection is related to its complex decomposition chemistry leading to formation of undesired deposits in the exhaust unit. Ideally, one molecule of urea should convert into two molecules of ammonia (urea thermolysis and hydrolysis).

a) Thermolysis: Urea when sprayed on hot exhaust gas, decomposes to isocyanic acid (ICA) and ammonia.



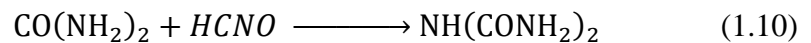
Hydrolysis: Isocyanic acid reacts with water to form Ammonia



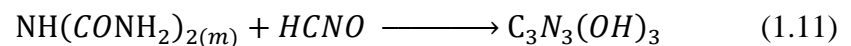
The reaction proceeds through an intermediate isocyanic acid. Isocyanic acid is very reactive and initiates secondary deposit reactions.

Deposit Forming Reactions:

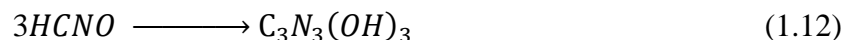
1. Urea reacts with isocyanic acid and forms Biuret



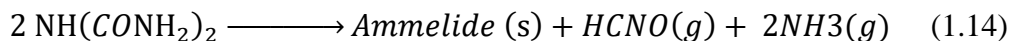
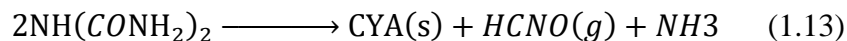
2. Biuret reacts with isocyanic acid to form cyanuric acid (CYA)



3. Trimerization of isocyanic acid to form CYA



4. Formation of ammelide and CYA from biuret



1.4.3. Chemo-Physical Processes in Urea-SCR System.

The mixer and SCR are a complex system in which the process is not transparent to follow the critical steps involved in deposit initiation and growth. To develop a better mixer, there is a need to have a good understanding of the physical and chemical processes inside the mixer. Figure 1.4 summarizes the important chemo-physical process inside a mixer.

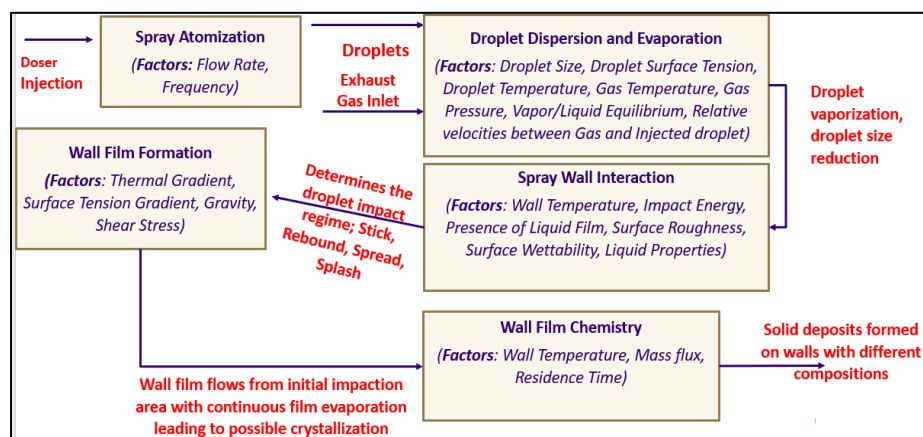


Figure 1.4 Chemo-Physical Process Inside a Mixer Leading to Deposit (Summarizes the important chemo-physical process inside a mixer-a) spray atomization b) droplet evaporation c) spray-wall interaction d) wall film formation e) wall film chemistry)

Computational Fluid Dynamics (CFD) is an important tool that guides SCR product development. Complex chemo-physical process in the system leads to challenges in modeling. During the past few decades, significant research has been done on engine fuel deposits where various models have been validated and adapted to CFD codes [10]. Most of these models have been developed for diesel and water spray. Improving accuracy of

current CFD model by calibrating the critical aspects which are unique to urea-water solution and SCR system has been the current approach [11].

1.4.3.1. Spray atomization. CFD codes have in-built primary spray break up models where the injection velocity and droplet size are determined based on orifice diameter, nozzle gap, cone angle and injection pressure but sometimes these models are not considered due to inaccurate prediction. In that case spray properties are defined as boundary conditions which is represented by parcels of randomly chosen diameters with spray mass fractions assigned to each parcel to maintain experimentally measured size distribution using laser diffraction. [11]

1.4.3.2. Droplet evaporation. Uncertainty exists in literature on the physical state of UWS droplet decomposition. This is a challenge in modeling as well as in general understanding of deposit forming mechanism. Different modeling approaches have been adapted in the literature for urea water droplet decomposition. Most models consider water evaporation as first step followed by urea melting and final step as decomposition. Some models include presence of gaseous urea before thermolysis.

According to Moltner et al. [12] the maximum residence time for 50 μm droplet to travel 0.5m through exhaust gases is 0.04s for a given operating condition. For a 50 μm pure water droplet, Moltner's model predicts at least 0.15s to completely evaporate. The evaporation rate of UWS droplet will be even lower because of lowering vapor pressure of urea (Figure 1.5). Hence droplets do not have enough residence time in gas phase to completely evaporate. Grout et.al [13] in his experiments showed if all heat is transferred to a droplet of 150 μm then it must travel with exhaust gases about 3m to completely

evaporate under low load conditions. Since the usual length of exhaust pipe is less than 45cm, all droplets will hit the wall surface.

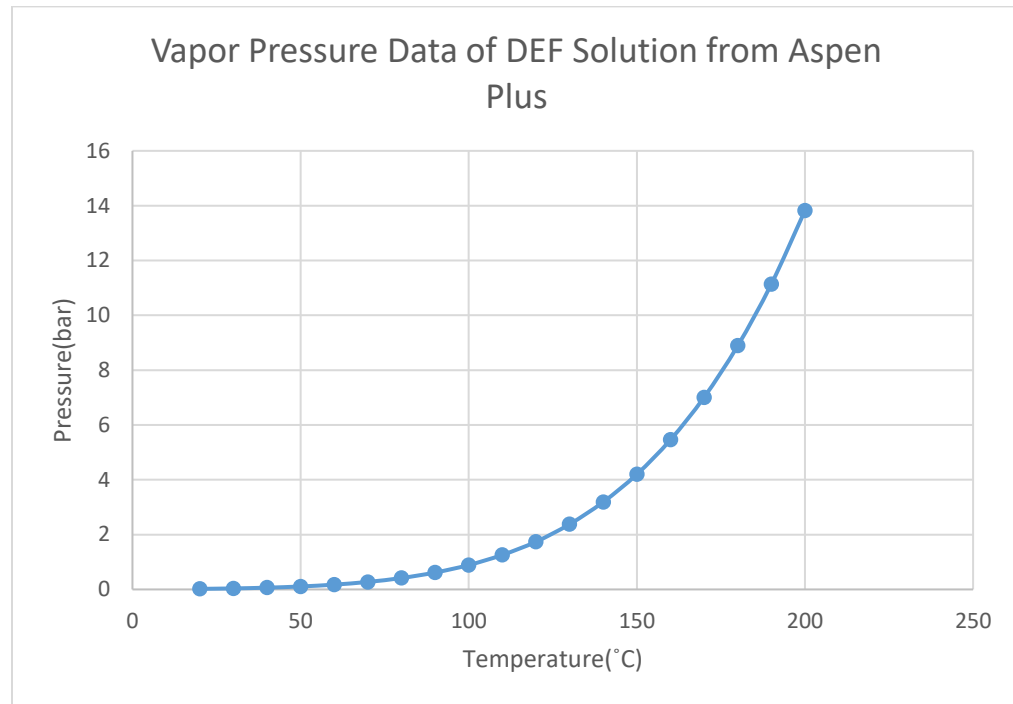


Figure 1.5 Vapor Pressure of DEF Solution

1.4.3.3. Spray wall interaction. When droplet hits the wall, heat is transported to the droplet by conduction. Thermolysis reaction of urea is an endothermic reaction [14]. When this occurs on the wall surface, there is a drop in wall temperature. If a drop hits the same spot as before and if the surface has not been given enough time to heat up, liquid wall film starts depositing. Depending on the wall temperature, impact energy, liquid film presence, surface roughness, contact angle and liquid properties, a droplet impinging on the wall can either stick, bounce, deposit, or break-up [15] [16]. Figure 1.4 shows detailed understanding of various impingement regime which was developed based on single

droplet experiment. Bai-Gosman model is adapted to the current Star CCM+ code [10].

The alternate spray interaction model which many researches have considered is the Kuhnke model [17] [18] [19]. This model has different droplet stability criteria compared to the Weber number in Bai-Gosman model.

The matrix was developed based on wall temperature (T_w) and Weber number. Important impingement regime is distinguished based on rebound temperature (T^*_s) and sliding temperature (T^*_L) that are linked to boiling temperature (T_{sat}) and Leidenfrost temperature (T_L) by an empirical factor.

$$T^*_s = B^*_s \cdot T_{sat}$$

$$T^*_L = B^*_L \cdot T_L$$

Critical Weber number relate to the droplet stability limit that marks the onset of splash effect which are defined based on droplet Laplace number. The empirical factors are related to the wall surface roughness and liquid film thickness.

$$We_s = A_w \cdot La^{-0.18} \text{ [Wet Walls]}$$

$$We_a = A(rs) \cdot La^{-0.18} \text{ [Dry Walls]}$$

Bai-Gosman model has been validated for diesel spray injection application. The boundary number (We_a , We_s , T^*_s , T^*_L) must be adapted for UWS and stainless steel.

Liquid film deposition temperature (T^*_s) is the temperature which separates wall wetting regime and non-wall wetting regime [11]. Compared to water, UWS has a higher tendency for wall film formation [16]. In SCR exhaust systems, temperature is generally between 300-500 °C [5] and so surface temperatures are usually higher than boiling temperature of liquid. As urea-water is a binary liquid, the heat flux and deposition temperature must be modeled dependent on liquid composition because the saturation

temperature of binary liquid varies with concentration [16]. There is no consensus on B^* 's values (Equation 3) in published research papers. It varies between 1.2 and 1.6 which makes the deposition temperature (T^* 's) range very broad [18]. Previous researches have indicated the dependence of experimental setup on Leidenfrost/deposition limit temperature and recommended to have a test bench that is comparable to actual exhaust systems.

1.4.3.4. Liquid film formation and transport. When temperatures fall below a critical non-wetting point, the liquid film forms but deposits do not generate because liquid film does not have enough residence time to heat up to the deposit forming temperatures due to continuous fresh incoming droplets.

Rapid evaporation of water occurs at impingement location and due to high latent heat of water, the impingement is subjected to local wall cooling. Due to continuous impingement, liquid film accumulates and progresses downstream due to gravity and turbulent gas shearing. The deposit chemical reactions are driven by the heated downstream conditions where higher temperatures exist, and residence time required for deposit initiation is far less than impingement location.

1.4.3.5. Reaction chemistry. To characterize the events accurately taking place inside a full cycle mixer test, dominant chemical reactions must be identified, kinetics must be defined and modeled. In literature, there are rigorous kinetic model developed which is based on Thermo-Gravimetric Analysis (TGA) [20] but popular approach to model the deposit formation is through empirical models that classifies risk of deposit formation based on isocyanic acid concentration, film thickness, urea concentration etc [21].

1.5. RESEARCH OBJECTIVE AND APPROACH

Primary engineering focus of commercial manufacturers is to optimize the after-treatment system that reduces the favorable conditions for deposit formation. Injector type, mounting angle, exhaust flow direction, operating load conditions are critical parameters that determines the droplet state before impingement. Significant uncertainty still exists due to turbulent gas mixing, urea droplet decomposition, spray wall interaction and the liquid film chemistry.

A systematic investigation into the mechanism of deposit formation was conducted through numerous experiments. The approach was to deconvolute the effect of transport and chemistry on urea decomposition and deposit formation.

The second section is focused around the fundamental chemistry and the time scale of urea decomposition. These tests were conducted using pure urea, urea's decomposition products including biuret, triuret, cyanuric acid, ammeline, and ammelide and urea-water solution of different concentrations including diesel exhaust fluid. These experiments investigate the effect of heating rate and temperature on the rate of deposit formation and decomposition. The change in chemical composition with temperature was characterized to understand the solidification phase change conditions.

The third section deals with the study of urea decomposition pathway and the effect of urea to ammonia conversion in a closed pressurized system. The risk of deposit formation in a heated urea nozzle was investigated by heating aqueous urea solution in a closed system maintained between 30-200psia. Liquid was sampled out at different time intervals and chemical characterization was conducted.

The fourth section is focused on the liquid film experiment. A stream of DEF liquid is introduced on a surface that is maintained at temperatures higher than saturation temperature of liquid. The local temperature for deposit initiation was monitored. These experiments represented a more practically close condition to a mixer.

The fifth section discusses the deposit test on a hot gas test bench. Deposit test was conducted using a Class 8 truck with a typical after-treatment system layout. An optic box was placed between the DPF and SCR with a spray impingement plate at the center of the box. Deposit initiating temperatures were identified independent of the operating conditions. The effect of transport processes on urea deposits was also studied.

The final section is focused on the different analytical techniques applied to characterize the deposit mixture. Characterization procedure included TGA, electrospray ionization (ESI) and liquid chromatography-multiple reaction monitoring (LC-MRM). The method development for LC-MRM has been discussed in detail.

2. UREA DEPOSIT STUDY IN AN OPEN SYSTEM

The objective was to identify the dominant reactions at different temperature regime, the time scale for solidification and decomposition reactions. The focus of this experiment was not to dive deep into reaction kinetics but to get an understanding from a practical perspective of how the heating rate and temperatures affect the rate of deposit formation and growth inside the exhaust mixer wall.

2.1. LITERATURE REVIEW

Fundamental study on urea decomposition has been investigated by several researchers. The products of urea decomposition and the application of urea in SCR systems along with the role of the hydrolysis catalyst was documented in the early works of Fang et al. [22]. A comprehensive study of urea decomposition using TGA that involved identifying all the possible chemical reactions by simultaneously characterizing the gas and solid composition was carried out by Schaber et al. [23]. The chemical reactions were categorized based on different temperature regions. The summary of Schaber et al.'s work is shown in Table 2.1. Lundstrom et al. [24] investigated the effect of surface-to-volume ratio of the vessel and the role of gas mass transfer on urea decomposition product distribution. Eichelbaum et al. [25] established the advantage of zeolite catalyst on urea decomposition using TGA/DTA. The solid residues above 500°C was characterized as heptazines using photoluminescence [25]. Liu et al [26]. demonstrated the synthesis of graphitic carbon-nitride by pyrolysis of urea without the use of catalyst. The reaction path was an extension of Schaber et al.'s [23] and Eichelbaum et.al's [25] proposed reaction

mechanism where at higher temperatures ammeline and melamine react to form melam and under excess heat melam converts to melon and finally forms graphitic nitride. In Bernhard et al.'s [27] study, gaseous urea at atmospheric pressure was measured for the first time. Sebelius et al. [28] conducted density functional theory (DFT) study of urea decomposition and byproduct formation without the presence of catalyst. Brack et al. [20] [29] proposed a detailed kinetic reaction model for thermal decomposition of urea using TGA. Tisher et al. [30] modified the same kinetics by including the phase change thermodynamics and distinguished between the process that are controlled by thermodynamic equilibrium and reactions that are kinetically controlled. DEF is a binary mixture. Urea concentration and its effect of vapor pressure on the mixture is an important criterion in the SCR [11]. In chemistry, hydrolysis of HNCO reaction has been studied in the presence of a catalyst [25]. Studies have indicated that an increase in the water vapor fraction increases the extent of HNCO hydrolysis [31]. The effect of water was investigated by Zhang et al. [32]. They concluded that water had no significant effect on the chemical transformation of urea between 100-200°C.

Table 2.1 Summary of Urea Thermal Decomposition Chemical Reactions

| Reaction Region | Process | Chemical Equation |
|-----------------|--|--|
| A. 50-160°C | <ol style="list-style-type: none"> 1. Melting point of urea is 133°C 2. Urea vaporizes between 140-152°C 3. Decomposition begins accompanied by gas evolution from melt at 152 °C | <ol style="list-style-type: none"> 1. $\text{CO}(\text{NH}_2)_2(s)(\text{urea}) \longrightarrow \text{CO}(\text{NH}_2)_2(m)$ 2. $\text{CO}(\text{NH}_2)_2(m)(\text{urea}) \longrightarrow \text{CO}(\text{NH}_2)_2(g)$ 3. $\text{CO}(\text{NH}_2)_2(m)(\text{urea}) + \text{Heat} \longrightarrow \text{HCNO}(g)(\text{isocyanic acid}) + \text{NH}_3(g)$ <p>Major Products at the End of Reaction Region A- Urea</p> |

Table 2.1 Summary of Urea Thermal Decomposition Chemical Reactions [23] (cont.)

| Reaction Region | Process | Chemical Equation |
|-----------------|--|---|
| C. 190-250°C | <ol style="list-style-type: none"> 1. Increased evolution of gases from urea melt which reflects the biuret decomposition at 193°C 2. Auto-Condensation associated with Biuret decomposition to produce CYA 3. Biuret decomposition to produce Ammelide 4. Ammeline production is observed 5. Melamine is identified at 250°C | <ol style="list-style-type: none"> 1. $\text{NH}(\text{CONH}_2)_2(\text{m}) \longrightarrow \text{CO}(\text{NH}_2)_2(\text{m}) + \text{HCNO}(\text{g})$ (Urea decomposes) 2. $2\text{NH}(\text{CONH}_2)_2(\text{m}) \longrightarrow \text{CYA}(\text{s}) + \text{HNCO}(\text{g}) + 2\text{NH}_3(\text{g})$ 3. $2\text{NH}(\text{CONH}_2)_2(\text{m}) \longrightarrow \text{Ammelide}(\text{s}) + \text{HNCO}(\text{g}) + \text{NH}_3(\text{g}) + \text{H}_2\text{O}(\text{g})$ 4. $\text{Ammelide}(\text{s}) + \text{NH}_3(\text{g}) \longrightarrow \text{Ammeline}(\text{s}) + \text{H}_2\text{O}(\text{g})$ $2\text{HNCO}(\text{g}) + \text{CO}(\text{NH}_2)_2 \longrightarrow \text{Ammeline}(\text{s}) + 2\text{H}_2\text{O}(\text{g})$ 5. $\text{Ammeline}(\text{s}) + \text{NH}_3(\text{g}) \longrightarrow \text{Melamine}(\text{s}) + \text{H}_2\text{O}(\text{g})$ <p>Major Products at the End of Reaction Region C-CYA and Ammelide Trace Products-Urea, Biuret, Ammelide and Melamine</p> |
| D. 250-380°C | <ol style="list-style-type: none"> 1. CYA begins to lose mass between 250-275 °C via sublimation with small amount of decomposition 2. At temperature greater than 275 °C, CYA and ammelide continue to decompose and sublime At 350 °C, CYA significantly decomposed and ammelide and ammeline continue to sublime | <ol style="list-style-type: none"> 3. $\text{CYA}(\text{s}) \longrightarrow 3\text{HNCO}(\text{g})$ <p>Trace Products at the End of Reaction Region D-Ammelide, Ammeline and Melamine</p> |

2.2. EXPERIMENTAL SETUP AND ANALYTIC METHODS

2.2.1. Liquid Temperature and Phase Change. A simple pool boiling test was conducted to monitor the change in liquid temperature with time to identify the phase change. A beaker filled with DEF solution was placed on a heated plate and a thermocouple was positioned inside the beaker to measure the liquid temperature as shown in Figure 2.1.



Figure 2.1 Beaker Filled with DEF placed on a Heated Plate
(Two thermocouples measured liquid temperature and surface temperature)

2.2.2. Open Vessel Heating. To quantify the rate of weight loss, 60g of urea-water mixture was heated in an open cylindrical stainless-steel vessel as shown in Figure 2.2. A pipe heater rated at 100W was wrapped around the vessel. A weighing scale having a readability of 0.1g was placed below the vessel. Insulation was placed between the vessel and the heater to protect the balance. The wall temperature was set to the maximum output of the heater which was approximately 300°C. The weight change and liquid temperature was measured with time for 3 different urea concentrations: -20%, 32.5% and 50%. The experiment is identical to the TGA. One of the advantages it has over the TGA experiment is that the solidification point could be visualized which helps to separate the time required for solidification and decomposition. Another advantage is that this experiment can directly measure the liquid temperature, which is not feasible in a TGA experiment. The drawback is that the weight change measurement is not as precise as the TGA.

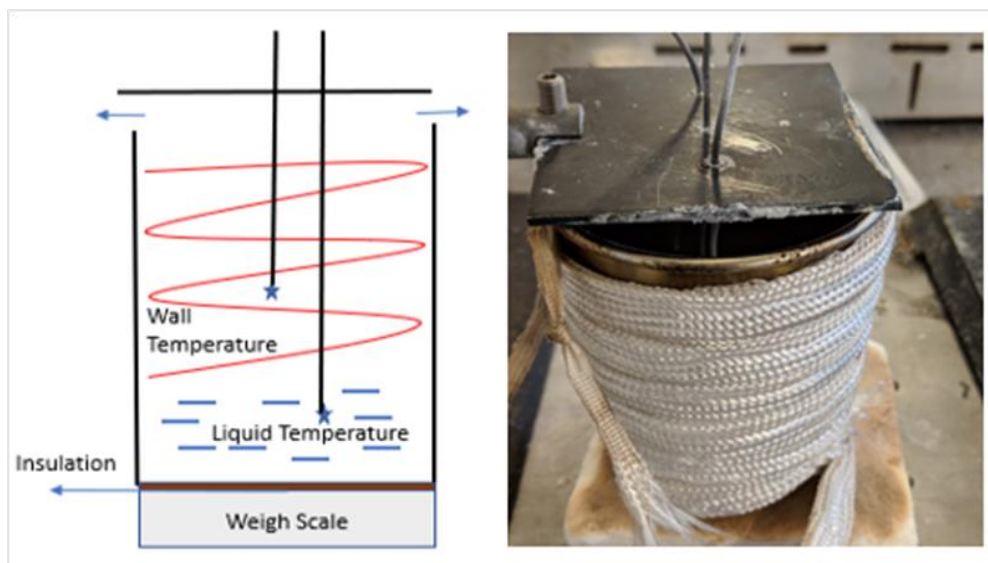


Figure 2.2 Open Vessel Heating Setup
(Two thermocouples measure the wall temperature and liquid temperature)

2.2.3. Chemical Analysis. Chemical compounds were quantified using Liquid chromatography-multiple reaction monitoring (LC-MRM). The detailed method analysis is discussed in Section 6.

2.3. RESULTS AND DISCUSSIONS

2.3.1. Liquid Temperature and Phase Change. Three experiments with different plate temperatures were conducted- 250°C, 275°C, and 325°C. Curves in Figure 2.3 denote the change in liquid temperature with time at different plate temperatures. The black solid lines indicate the time at which the liquid completely converted to solid. Increasing the plate temperature resulted in higher heating rates that expedited the solidification process. The solidification point was found to be in the temperature range that corresponded to Region 3(190-250°C) in Table 2.1. At this range, biuret decomposed to form cyanuric acid and ammelide.

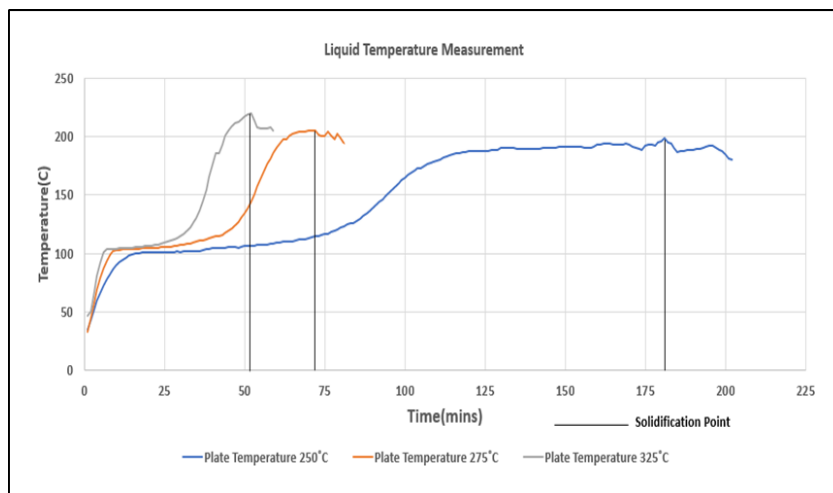


Figure 2.3 Liquid Temperature Change with Time for Three Plate Temperatures (Black solid line represents the point at which the complete solidification occurs)

2.3.2. Open Vessel Heating Results. From Figure 2.4, as the wall temperature increased; the liquid temperature steadily rose to the saturation temperature of the mixture. With an increase in urea concentration, saturation temperature of the mixture increased by few degrees. As soon as a certain amount of water evaporated, the urea decomposition was initiated, leading to a rise in liquid temperature. From Table 2.1, it was understood that in this temperature region, urea decomposed, and the dissolved isocyanic acid reacted with urea to form biuret; however, no solidification was observed. Sebelius et al. [28] had concluded that the reaction is exothermic based on DFT calculations. When the temperature reached above 200°C, the curve flattened as the mixture began to solidify. The different stages of solidification process are shown in Figure 2.5. The process of identifying the solidification point was performed based on the slope change of the liquid temperature curve and observation. Experiments were repeated, and data were recorded by two different individuals independently. The weight change was recorded every two minutes. Once the

liquid solidified, the “liquid temperature” thermocouple was positioned close to the wall temperature thermocouple to reduce weight change errors in the deposit decomposition region.

Based on the solidification point, two regions were identified: - (A) water evaporation/urea decomposition and (B) deposit decomposition. The rate of weight loss in each region was quantified. At the end of each region, the time taken, and the amount of weight loss was recorded. The rate of evaporation and decomposition was calculated by dividing the weight loss by the time required for the same. The calculations are shown in Table 2.2.

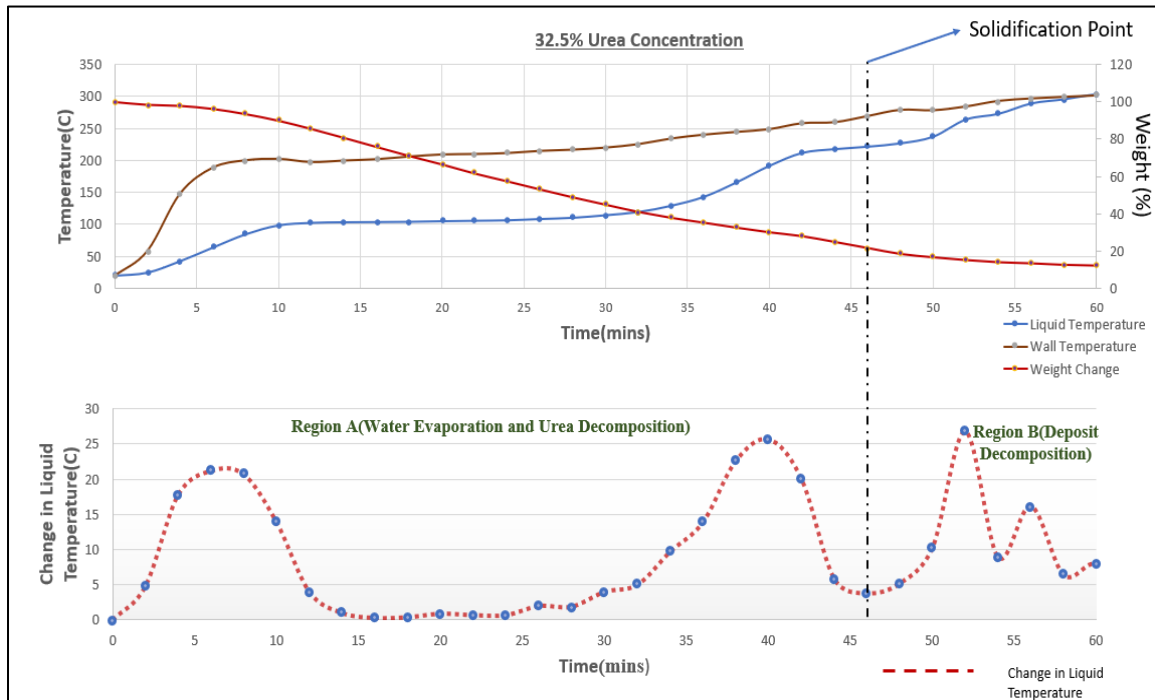


Figure 2.4 Weight Change and Liquid Temperature Measurement
(The primary y-axis represents the temperature and the secondary y-axis represents the weight change measurement. The black dashed line illustrates the time at which the liquid completely converted to solid. The green dashed line illustrates the weight percentage value when most of the water evaporated from the mixture)

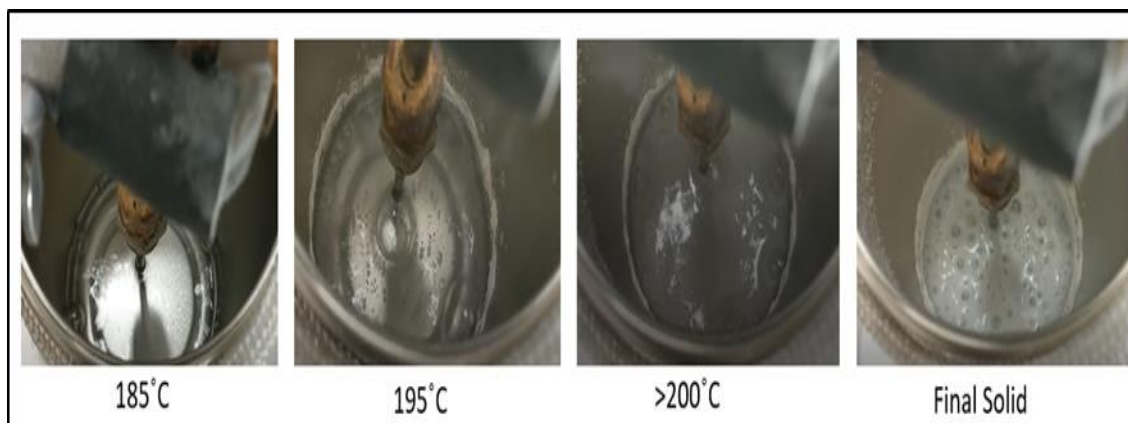


Figure 2.5 Samples Extracted at Different Temperature
(At 185°C, the liquid appeared clear with minimum gas bubble evolution. At 195°C, the gas bubble evolution was intense within the liquid. Above 200°C, the liquid was not transparent and started to solidify. With increase in the temperature, the liquid completely solidified to a white mass)

The rate of water evaporation and urea decomposition were greater than the rate of deposit decomposition. For the same heat output, with an increase in water content, more energy was required to evaporate the water which delayed the solidification process.

Table 2.2 Rate of Weight Loss in Different Regions

| Urea Concentration | Water Evaporation and Urea Decomposition (A) | | | Deposit Decomposition (B) | | |
|---------------------------------------|--|------------|--------------|---------------------------|------------|--------------|
| | Weight Loss(g) | Time(mins) | Rate (g/min) | Weight Loss(g) | Time(mins) | Rate (g/min) |
| Total Weight:60g Total Time:60mins | | | | | | |
| 20% | 53 | 52 | 1.01 | 3.6 | 8 | 0.45 |
| 32.5% | 47 | 46 | 1.02 | 5.6 | 14 | 0.40 |
| 50% | 39.4 | 40 | 0.99 | 8.3 | 20 | 0.42 |

The rates of water evaporation, urea decomposition, and deposit decomposition were in a comparable range for all urea concentrations.

The calculated average rate of deposit decomposition was 0.4 g/min. When the mixture solidified, the deposit lost significant weight during the initial period. With time, the rate slowed down. For 50% urea concentration, the sample had 20 minutes in the decomposition region (Figure 2.6).

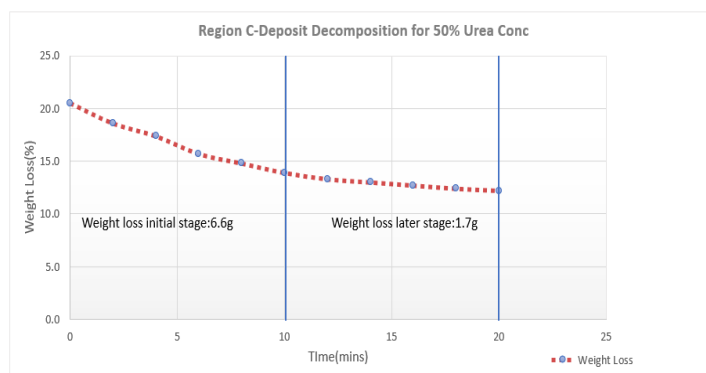


Figure 2.6. Rate of Weight Loss in Deposit Decomposition Region (Deposit decomposition region for 50% urea concentration. Sample had total 20 minutes in the decomposition region)

During the initial 10 mins, the sample mass loss was 6.6 g; in the next 10 mins, the mass loss was only 1.6g (Figure 2.6). As time progressed, the rate of decomposition eventually became stagnant. At that stage, to completely decompose the sample, temperature would have to be higher. This is discussed in the TGA experiment section.

2.3.3. Chemical Characterization of Samples. To better understand the phase change composition, an experiment was conducted where samples were extracted at different liquid temperatures and characterized for chemical composition. Four samples were extracted at different liquid temperatures; out of which, two were below 200 °C and

two were above 200 °C. The liquid chromatography column used, and the detailed method applied is discussed in Section 6.

It was observed that urea concentration dropped with increasing temperature (Figure 2.7). The triuret and biuret followed similar trends with the highest concentration in the “205°C” sample. Ammelide, melamine, CYA, and ammeline concentration increased with increasing temperature, but it was very low or absent until the “205°C” sample. The sample solidifies when there is higher quantity of biuret and CYA.

According to Schaber et al. [23], as the temperature rose above 200°C, the biuret converted to unstable urea, CYA and ammeline (Table 2.1). Biuret melts at 193°C while CYA and ammeline decomposes above 300°C. This should be the weight loss observed at the beginning of the decomposition region.

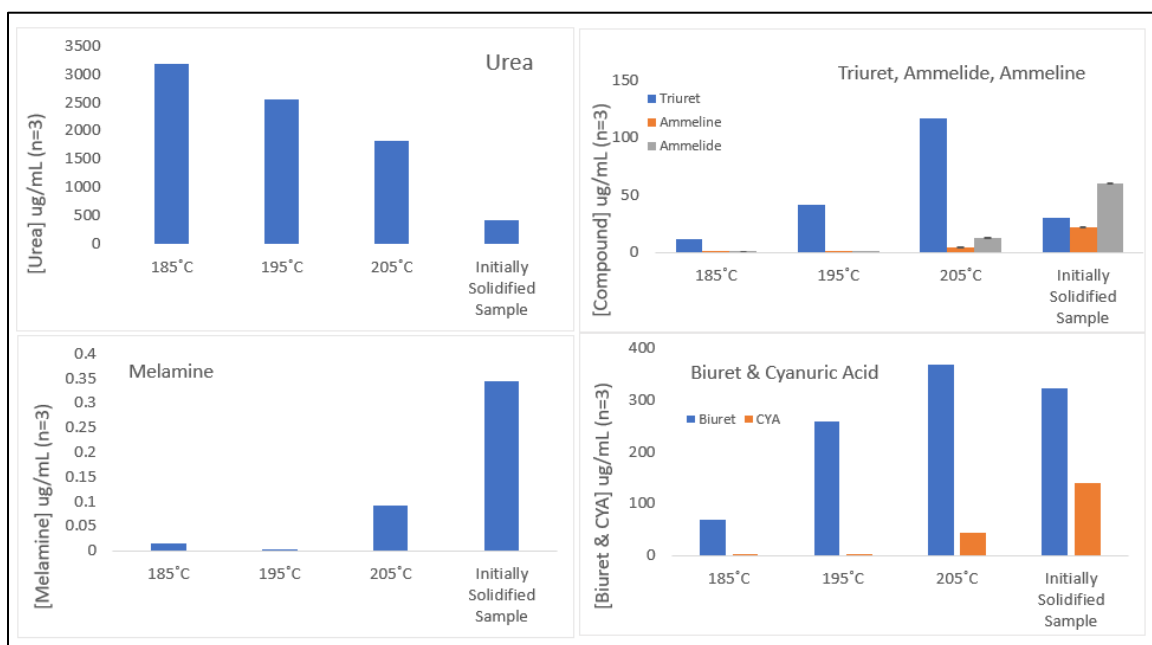


Figure 2.7 Chemical Quantitation using LC-MRM for Open Heating System (Chemical quantification using LC-MRM. Area under curve (AUC) data were generated and compounds quantified using a mixed standard curve of 7 compounds)

Recently, Tisher et al. [29] proposed a modified reaction scheme where biuret in the melt phase converted to triuret above 200°C and the triuret reacted further to form CYA and ammelide. Comparing the “initially solidified sample” and the “final deposit sample” composition, triuret concentration reduced significantly while CYA/Ammelide concentration increased. The data supports the reaction path observed by Tisher et.al [29]

2.3.4. TGA of DEF and Pure Urea. In TGA experiment, the sample was heated at a constant heating rate and the decomposition curve (weight change) was plotted against temperature shown in Figure 2.8. DEF and pure urea are heated at 20°C/min using TGA.

From Table 2.1, it is known that urea decomposition initiates around 130°C. TGA plot of DEF (Figure 2.8) indicates that more than 60% of the sample decomposed before urea decomposition temperature was reached. The saturation temperature of 32.5% urea water solution is 106°C [13] and so most of the weight loss before urea decomposition is evaporation of water. Once the urea decomposition initiated, the curve followed a similar reaction path as pure urea.

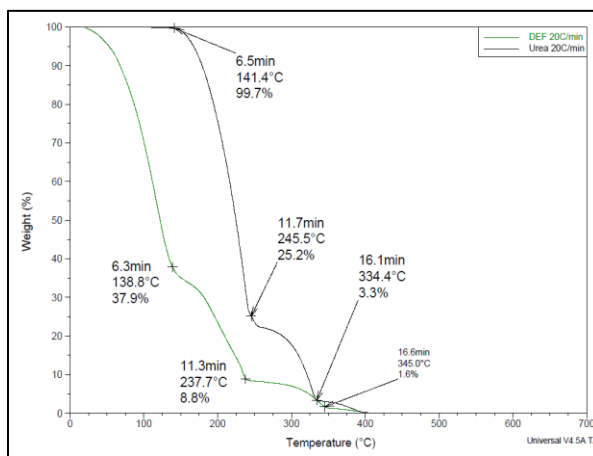


Figure 2.8 TGA of DEF and Pure Urea At 20°C/Min
(The decomposition curve (weight change) was plotted as a function of temperature)

Pure urea is subject to different heating rate: $2.5^{\circ}\text{C}/\text{min}$ to $100^{\circ}\text{C}/\text{min}$ (Figure 2.9). The objective of heating urea at different rate was to understand the time scale of deposit formation and decomposition. Schaber et al. [23] in his TGA experiment has characterized the decomposition curve of pure urea at $10^{\circ}\text{C}/\text{min}$. At $10^{\circ}\text{C}/\text{min}$, 133°C is attributed towards the initial urea decomposition point. 190°C is attributed to biuret decomposition and 250°C to CYA decomposition.

From the Figure 2.9, at low heating rate ($<10^{\circ}\text{C}/\text{min}$), biuret and cyanuric acid decomposition points are distinguishable but as we increase the heating rate ($>20^{\circ}\text{C}/\text{min}$), biuret and cyanuric acid decomposition points are convoluted.

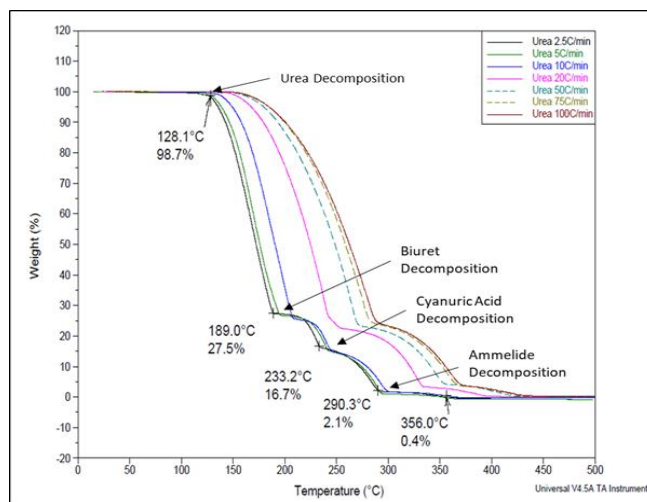


Figure 2.9 Pure Urea Heated at Different Heating Rate
(Slope shift is attributed to different decomposition reactions)

Assuming biuret decomposition to be the initial solidification point (deposit formation) as observed in the open heating system and weight percent less than one as

final decomposition point, with increase in heating rate, the deposit formation rate and overall decomposition rate increases (Figure 2.10).

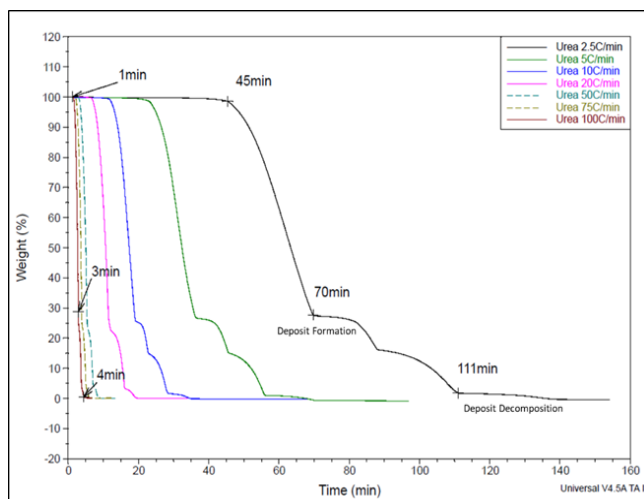


Figure 2.10 Time Scale of Deposit Formation and Deposit Decomposition
(The weight change is plotted as a function of time)

For 2.5°C/min heating rate, deposit formation time is 70 mins while the decomposition time is 111 mins. For 100°C/min heating rate, deposit formation time is 3mins while the deposit decomposes in 4 mins.

All the possible decomposition products of urea namely biuret, triuret, melamine, CYA, ammeline, ammelide are heated at 10°C/min. The decomposition time scales, and temperature are relatively high for ammelide and ammeline (Figure 2.11). Ammelide forms when biuret decomposes above 190°C but it can be decomposed only at temperatures above 500° [22] [23]. Based on the results from TGA and open vessel heating, 190-250°C is the region where deposits are initiated, and growth is accelerated.

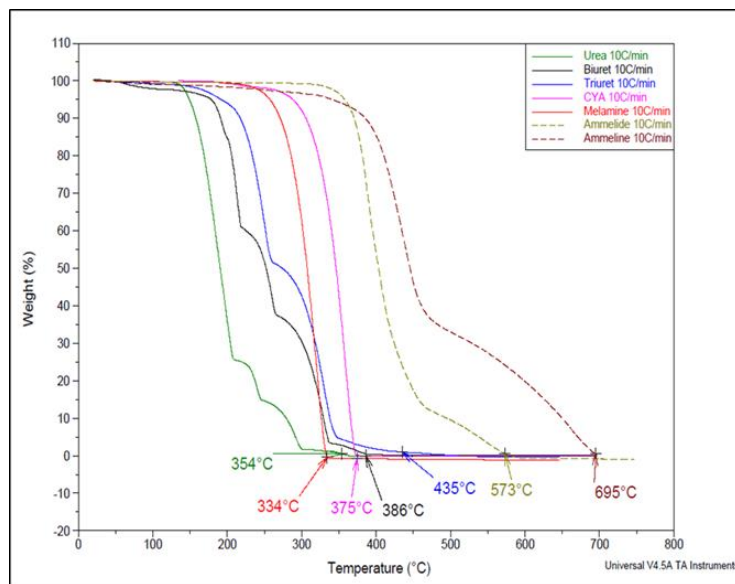


Figure 2.11 Products of Urea Decomposition Heated At 10°C/Min
(The decomposition temperatures of pure compounds are labeled)

From application perspective, inside a mixer, at high temperatures and high heating rates, spray droplets don't adhere to the surface due to Leidenfrost effect. Only at low temperatures, spray droplet sticks to the surface and forms liquid film [31]. Once a liquid film forms, deposits initiation is accelerated with increasing heating rate but would not decompose if the temperatures aren't higher than 350°C. Once the deposit initiates, the deposits can dissolve back in the incoming liquid film. Table 2.3 shows the solubility of different compounds in water. As soon as the deposit product mixture composition changes from urea-biuret-triuret to CYA- ammelide, the solubility of the mixture also reduces which eventually crystallizes out as deposit as observed in the open heating vessel experiment.

Table 2.3 Solubility of Deposit Compounds in Water

| Component | Solubility in Water |
|---------------|---------------------|
| Urea | 1079g/L |
| Biuret | 20g/L |
| Cyanuric Acid | 2g/L |
| Ammelide | 0.07g/L |
| Ammeline | 0.01g/L |

2.4. INFERENCE

Experiments were focused on the fundamental urea decomposition chemistry. Data from TGA showed the range of temperatures at which urea and its derivative compounds decomposed. Liquid temperature was measured real time, and the solidification point was identified. The effect of water on solidification time scale was investigated.

Based on liquid temperature, three regions were defined- water evaporation, urea decomposition and deposit decomposition. Rate of mass loss was quantified in all three regions for different urea concentration. With change in urea concentration, the rate of urea decomposition and deposit decomposition remained the same. With increase in urea concentration, the solidification time reduced significantly.

3. UREA DEPOSIT STUDY IN CLOSED SYSTEM

3.1. EFFECT OF PRESSURE ON UREA DEPOSITS

To meet the stringent future regulation limit (Figure 3.1), reducing NO_x emissions at low exhaust temperatures which commonly exists during cold start up and low load conditions must be addressed.

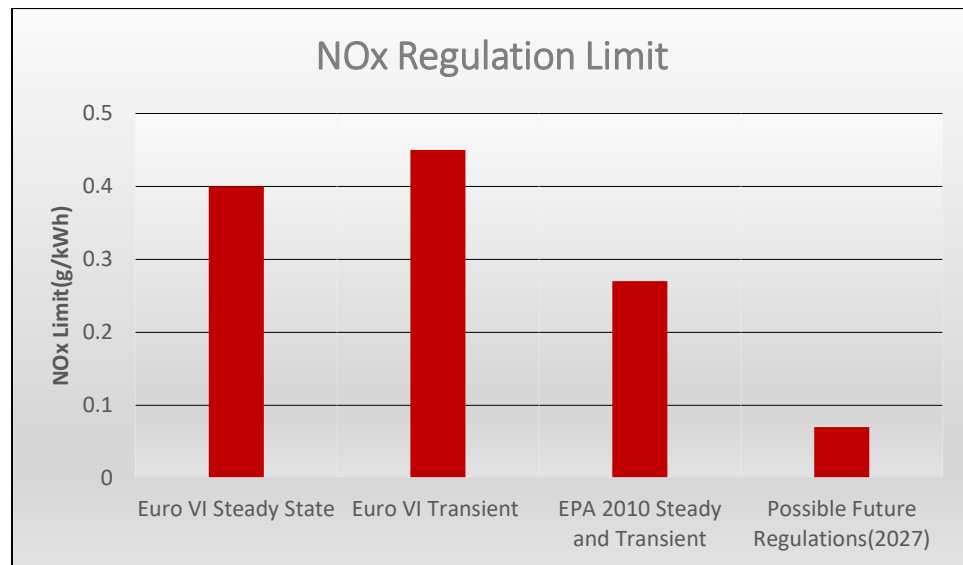


Figure 3.1 Future Regulation Limit on NO_x Emissions

In the current exhaust after-treatment system, urea is sprayed above 200°C to generate ammonia but the injection is stopped when temperatures drop below 170°C to prevent deposit formation [33]. In a heated urea nozzle, urea solution is pumped to a certain pressure and the liquid is heated above saturation temperature before spray atomization [33] [34] [35]. A patent by Pierz et al. 2007 has demonstrated that urea solution when pressurized to super-heated conditions, the solution atomized in the form of fine mist which

reduces the droplet sauter mean diameter [36]. Larrson et al. (2016) has shown that 87% reduction in droplet size compared to existing commercial injectors can be achieved through flash boiling injector [37]. Recent works have focused on understanding the spray characterization of preheated urea atomization. Vuuren et al.2013 characterized the urea solution spray from heated tip using high speed imaging and observed higher vapor fraction with increase in DEF temperature [38]. Brizi et al.2019 concluded that fully developed flash boiling along with significant improvement in spray atomization can be achieved when fluid temperature is 130°C [39].

In normal urea injectors, the generated droplets, due to the surface tension at the interface, there is a pressure difference between the inside and the outside of the droplet which increases the boiling point of the liquid. [40]. The Laplace pressure is given by:

$$\Delta P \equiv P_{inside} - P_{outside} = \gamma \frac{2}{R}$$

P_{inside} – Pressure inside droplet

$P_{outside}$ – Pressure outside droplet

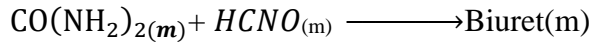
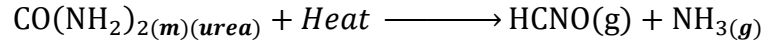
γ – Surface Tension

R-Radius of droplet

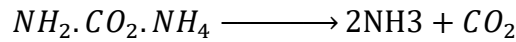
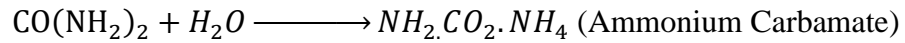
When droplet size is in nanometers, the pressure inside the droplet can be several atmospheres. Therefore, water would boil at higher temperatures inside these droplets. The effect of pressure on deposits is studied through this experiment.

The goal of this experiment is to study the effect of pressure on urea deposits by heating aqueous urea solution at different pressures. The initial sample and the final residue are weighed and compared for different pressure. The experiments investigate the risk of deposit formation in a flash boiling doser.

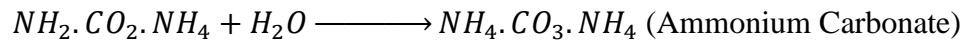
Inside a mixer, once a liquid film is generated, most of the water evaporates before the urea decomposition begins. The water vapor is also not retained in the system and the reactions proceeds through isocyanic acid intermediate initiating deposit reactions [23]:



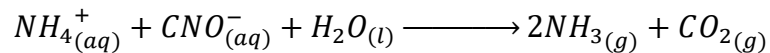
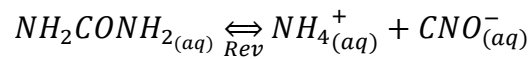
In the current test, liquid water and vapor is retained during urea decomposition by pressurizing the system. Literature suggests a different pathway where urea decomposes through an alternate intermediate ammonium carbamate in the condensed phase [42] [43].



Two step hydrolysis reaction mechanism where ammonium carbamate reacts with water to form ammonium carbonate has also been proposed [44]. Ammonium carbonate further dissociates into carbon dioxide and ammonia.



Studies have also indicated that aqueous urea is in equilibrium with ammonium cyanate which hydrolysis to yield ammonia and carbon dioxide [45].



There are several patents related to NO_x reduction in stationary boilers where ammonia is produced by heating an aqueous solution of urea at high pressures [42] [43]

[44] The urea solution is pressurized to keep the reaction products in liquid phase. Hydrolysis reaction is generally slow, and many patents includes the use of conversion catalyst to increase the reaction rate.

3.2. EXPERIMENTAL SETUP AND ANALYTICAL METHODS

In the current test, a 32.5% concentration urea-water solution (DEF) was subject to high temperature and pressure using the parr reactor as shown in Figure 3.2. There were two pressure sensors attached to the system- a mechanical pressure gauge and a transducer and two thermocouples for measuring liquid temperature and wall temperature.

50g DEF solution was weighed in the pressure vessel (Figure 3.3(a)) and was clamped to the system using a split-ring cover clamp (Figure 3.3(b)). The heater was loaded on the pressure vessel (Figure 3.3(c)) and the nitrogen line was opened to pressurize the system (Figure 3.3(d)). The reactor was heated from room temperature to 300°C. The pressure was monitored and maintained in the system by releasing excess pressure caused due to rise in temperature and vapor formation (Figure 3.3(d)). Data was recorded till the liquid temperature exceeded 225°C. The heater was immediately removed and cooled by purging excess nitrogen to eliminate the decomposition reactions. The reactor was detached from the system and weighed for final deposit mass (Figure 3.3(f)).

Chemical analysis of the samples was conducted using LC-MRM. The method and column used are discussed in Section 6.

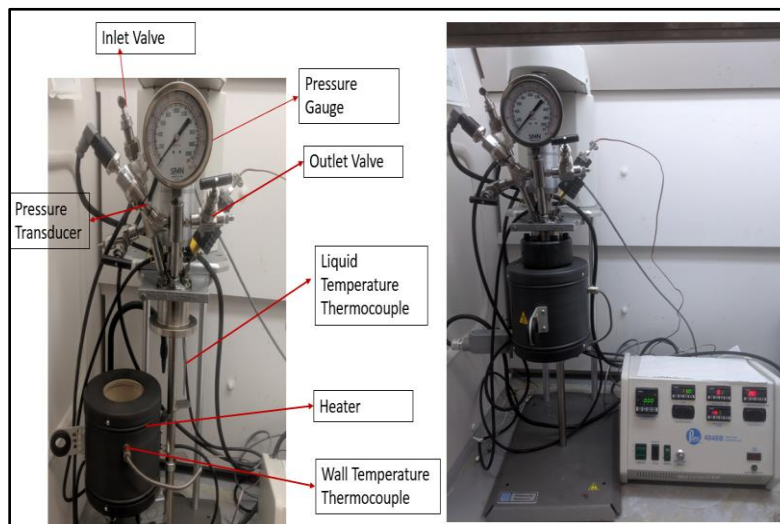


Figure 3.2 High Temperature High Pressure Reactor System
(Two pressure sensors attached to the system- a mechanical pressure gauge and a transducer and two thermocouples for measuring liquid temperature and wall temperature)



Figure 3.3 Test Procedure for Pressurized System
(a) 50g DEF solution was weighed in the pressure vessel b) Reactor clamped to the system using a split-ring cover clamp c) Heater was loaded on the pressure vessel d) Nitrogen line was opened to pressurize the system e) Data was recorded till the liquid temperature exceeded 225°C f) Reactor was detached from the system and weighed for final deposit mass)

3.3. RESULTS AND DISCUSSIONS

3.3.1. Open System Validation. The first test was conducted at atmospheric pressure. 50g of DEF liquid was heated from room temperature to 300°C. The liquid temperature and wall temperature are plotted on the primary y-axis while the pressure is plotted on the secondary y-axis. The liquid temperature curve followed the similar pattern observed in the previous experiment. The saturation temperature was around 104°C. As soon as the liquid temperature exceeded 225°C, the heater was turned off and excess nitrogen was purged to eliminate the decomposition reactions. The final deposit weight was 7.9 g (Figure 3.4).

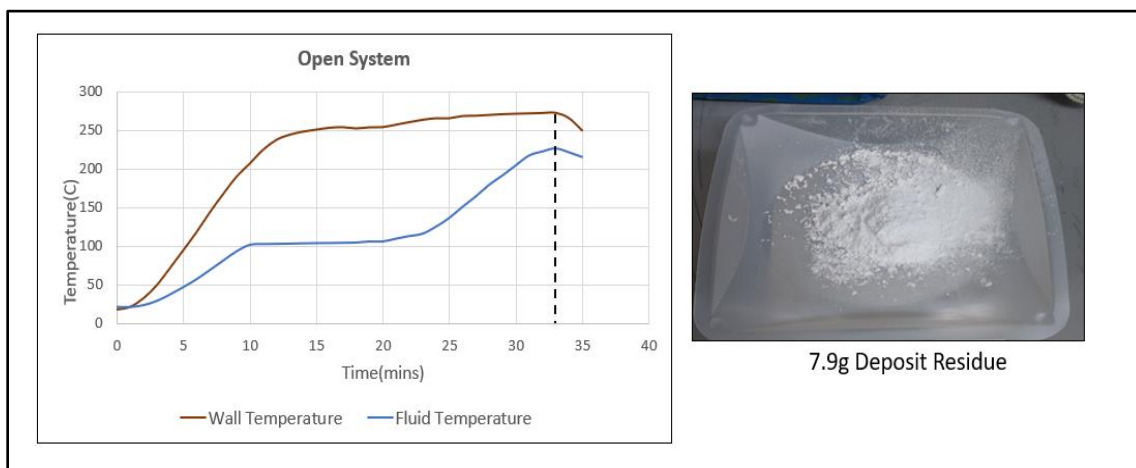


Figure 3.4 Temperature Plot with Time and Final Deposit Residue
(Test was conducted at atmospheric pressure; the liquid temperature and wall temperature was monitored as a function of time)

3.3.2. Closed System Results. Similarly, higher pressures were tested while keeping the other parameters constant. The saturation temperature of water is marked on the graph and plotted for each pressure (Figure 3.5). The point where the liquid temperature

reached 225 °C and the heater was turned off is marked on the graph. With an increase in pressure, deposit residue inside the pressure vessel at the end of the experiment reduced. Water boils at a higher temperature with an increase in pressure. As pressure increased from 0-75 psia, the saturation liquid temperature curve and the saturation temperature of water were comparable. Previously, TGA of DEF had shown that 68% of water is lost before urea decomposition temperatures are reached. Dana et al. [45] had reported that only 2.6% of mass loss is due to hydrolysis of urea in an open system, but at higher pressures, the presence of water at a wider temperature range drives the hydrolysis reaction and enhances the conversion of urea, resulting in less residual deposit inside the system.

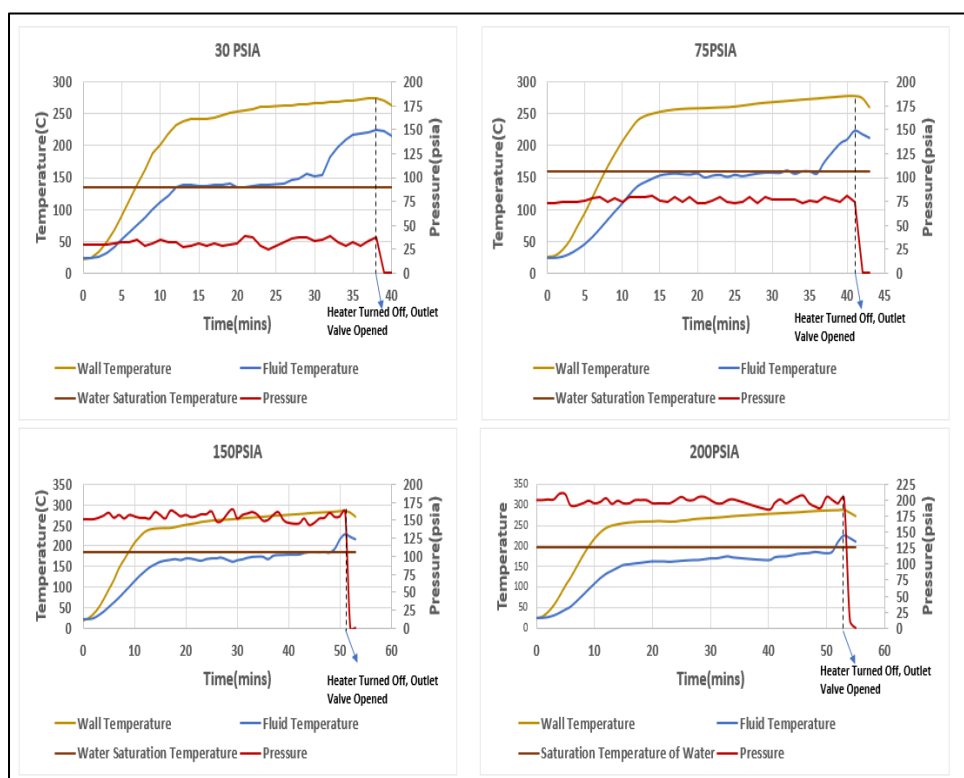


Figure 3.5 Temperature Plot at Higher Pressure

(The liquid temperature and wall temperature plotted on the primary y-axis, and the pressure on the secondary y-axis. The saturation temperature of water at corresponding pressure is represented by the solid brown line)

For very high pressures (150-200 psia), the saturation temperature of the liquid remained significantly lower than the saturation temperature of water. In the presence of more water, urea completely hydrolyzed to ammonia through ammonium carbamate or carbonate intermediate. The reaction is highly endothermic which might have shifted the saturation temperature of the mixture to lower temperature [41].

Figure 3.6 shows the effect of pressure on the deposit residue and the residence time for the reaction to complete.

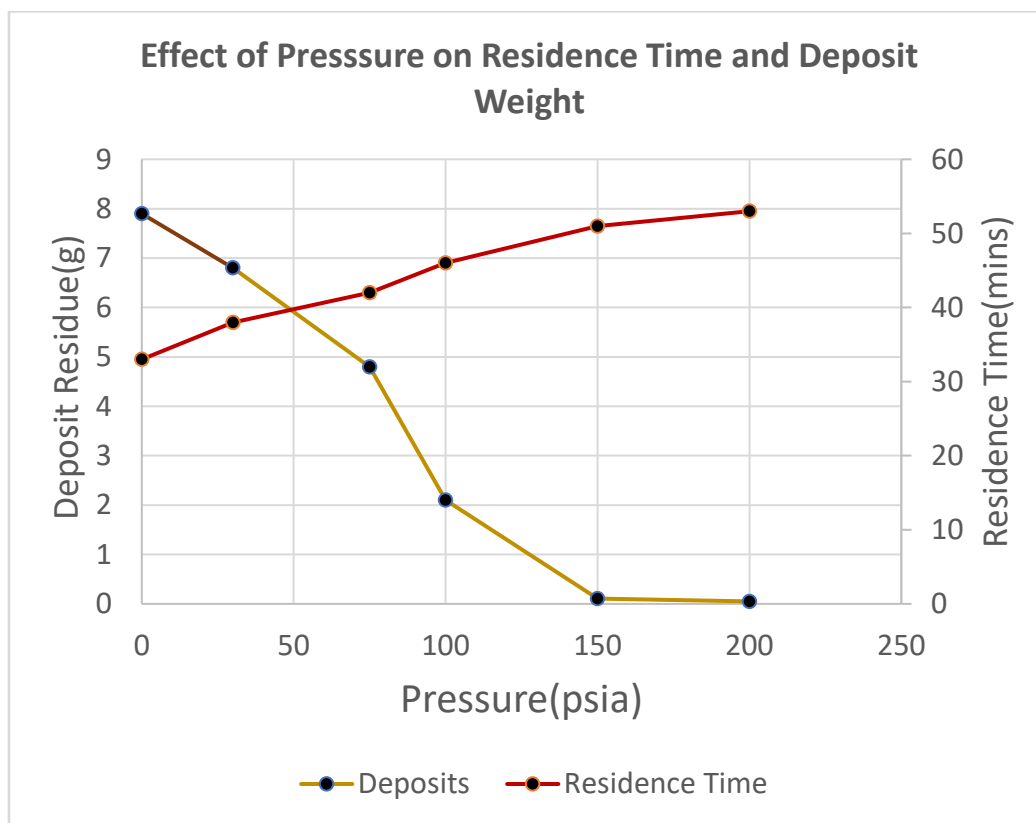


Figure 3.6 Effect of Pressure on Deposit Weight and Residence Time
(The deposit weight is plotted on the primary y-axis, and the residence time on the secondary y-axis)

Literature has reported that urea decomposes to isocyanic acid in more alkaline conditions [42] and that urea is stabilized in the presence of water [46]. Dana et al. [45] observed that the endothermic effects associated with biuret decomposition were not observed at higher pressures, and concluded that a minor amount of biuret might have formed in the presence of water. Hence, with an increase in pressure, more water drove the hydrolysis reaction which increased the conversion of urea into the gas phase and leaves less deposit residue (Table 3.1). A non-catalyzed urea hydrolysis reaction is a slow reaction. As we increased the extent of the hydrolysis reaction by retaining more water at higher pressure, the residence time for the reaction to complete also increased. Figure 3.7 shows the deposit residue that was present at the end of the reaction cycle.

Table 3.1 Effect of Pressure on Urea Conversion

| Pressure(psi) | Initial DEF(g)(A) | Amount of Urea(g)(B) $=0.325 \times A$ | Final Deposit(g)(C) | Conversion (%) $D=(B-A) \times 100/B$ |
|---------------|-------------------|---|---------------------|--|
| 14.6 | 50 | 16.25 | 7.9 | 51. |
| 30 | 49.9 | 16.21 | 6.8 | 58.0 |
| 75 | 50.7 | 16.47 | 4.8 | 70.8 |
| 150 | 50.5 | 16.41 | 0.11 | 99.3 |
| 200 | 50.7 | 16.47 | 0.05 | 99.6 |

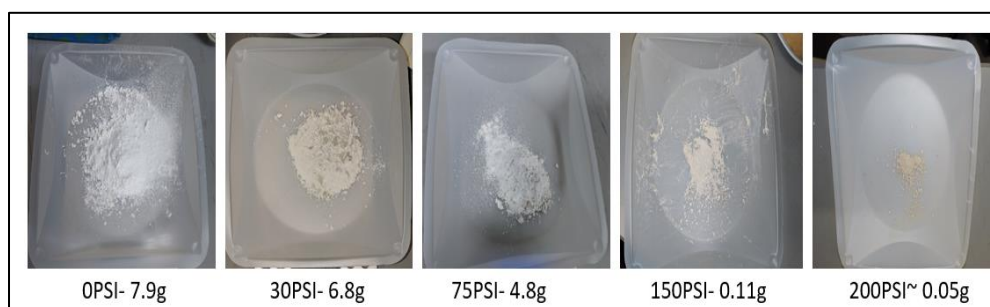


Figure 3.7 Deposit Residue from Pressurized System

The goal of this experiment was to understand the risk of deposit formation inside a heated nozzle. Urea heated nozzles operate at relatively lower pressures (3-8 bar). Two experiments were conducted at two different pressures where liquid was sampled out at different time intervals to evaluate the deposit formation risk. The pressure vessel was filled with DEF and pressurized to 50psia and 100psia. In both experiments, the wall temperature was set at 300 °C.

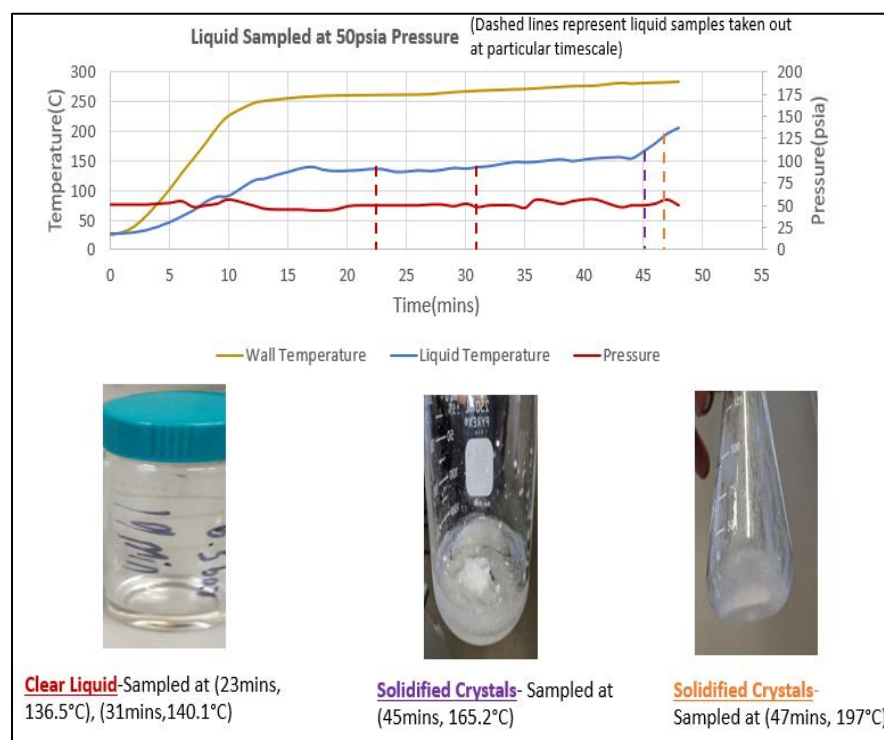


Figure 3.8. Liquid Sampled At 50psia

(a) Samples extracted at saturation temperature was clear liquid b) Samples extracted above saturation temperature had solid crystals c) Samples extracted close to 200°C, most of the liquid solidified inside the reactor and very less sample was retrieved)

At 50 psia, 4 samples were extracted, and at 100 psia, 5 samples were extracted and analyzed. Dashed lines in Figure 3.8 and 3.9 indicates the time and the liquid temperatures

at which each the sample was taken out. Samples extracted at the saturation point of the mixture were clear liquid and remained stable without any phase change for both experiments. A sample extracted at 165 °C and 50psia was a combination of liquid and solid crystals. Not many samples were retrieved at temperatures above 190 °C at 50 psia because almost all the liquid had solidified inside the reactor.

Sample extracted at 179 °C and 100 psia was in liquid state but it was viscous. At 100 psia, a liquid sample extracted at 209 °C solidified as soon as it was cooled to room temperature. The characterization of these samples was conducted to understand the chemical composition.

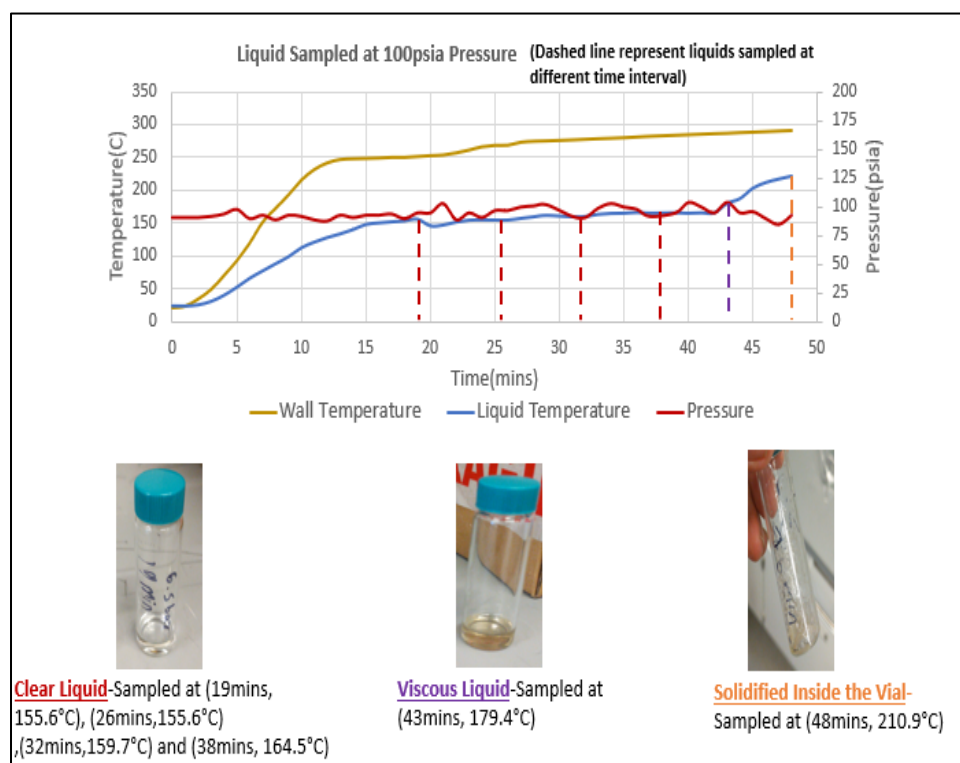


Figure 3.9. Liquid Sampled At 100psia

(a) Samples extracted at saturation temperature was clear liquid b) Samples extracted above saturation temperature was viscous liquid c) Samples extracted above 200 °C solidified inside the vial)

Three samples from the 100 psia experiment were chemically quantified by optimized LC-MRM methods in formic acid solvents (Table 3.2).

Liquid sampled after 32 mins at 160°C had mostly urea. Less than 10 percent of the sample was biuret. Liquid extracted after 42 mins at 180 °C had significant amount of biuret along with urea. As temperatures increased above 210°C, the urea and biuret relative concentration remained the same. However, other compounds like triuret, CYA, ammelide and ammeline were only present in trace amount for all samples.

Table 3.2 Chemical Mass Composition of Samples from 100psia Experiment

| Mass Composition (%) | | | | | | | |
|----------------------|------|---------|----------|----------|----------|--------|-----|
| Sample | Urea | Triuret | Ammeline | Ammelide | Melamine | Biuret | CYA |
| 160°C | 91.9 | 0.0 | 0.0 | 0.0 | 0.0 | 8.1 | 0.0 |
| 180°C | 71.9 | 0.4 | 0.0 | 0.0 | 0.0 | 27.6 | 0.1 |
| 210°C | 73.6 | 0.3 | 0.0 | 0.0 | 0.0 | 26.0 | 0.1 |

Vuuren et al. [39] reported that the temperature control at higher temperatures was less stable for heated urea injectors. The Pierz et al. [37] patent recommended to pre-heat aqueous urea to 200°C at 50psi. From the previous experiments, we clearly observe that there is a high risk of crystallization if urea solution is heated to elevated temperatures.

However, the risk of CYA and ammelide formation was low. At lower pressures, it was best to operate below the saturation temperature of water at the corresponding pressure.

Future work would focus on simultaneously measuring the gas composition and detecting the presence of ammonium carbamate/carbonate in liquid samples to characterize the reaction path in a pressurized system.

3.4. INFERENCE

The risk of deposit formation in heated urea nozzle was investigated by heating DEF solution in a closed system at different pressures. At higher pressures, the risk of deposit formation was reduced. In open system, most of the water evaporated before urea decomposition initiates. At higher pressures, due to the presence of water at wider temperature range, urea underwent hydrolysis and the deposit residual weight decreased. Non-catalyzed liquid phase hydrolysis reaction is slow, and hence at higher pressures, the residence time required to complete the reaction in the presence of water was higher. Liquid was sampled at different time intervals and chemical characterization was conducted. Excess heating especially at lower pressures can lead to deposit formation inside the heated urea nozzle. Operating below the saturation temperature of water at corresponding pressures would reduce the risk of deposit formation.

4. SINGLE DROPLET AND LIQUID FILM EXPERIMENT

In open vessel heating and TGA experiment, the samples were heated starting from room temperature to deposit forming temperature and finally to deposit decomposition temperature. In the current experiment, the DEF is introduced directly on a surface temperature higher than the saturated fluid temperature.

4.1. LITERATURE REVIEW

In typical SCR systems, the surface temperatures are above the boiling temperature of the liquid and it is important to understand the different boiling regimes. Figure 4.1 [47] describes the boiling curve of water as a function of excess temperature which is the difference between the wall temperature and liquid saturation temperature. At very high surface temperatures, vapor blanket forms between the surface and the droplet. The minimum heat flux is at the Leidenfrost point. A droplet impinging a surface can either stick or rebound which is dependent on surface temperature, droplet size, droplet velocity, liquid physical properties and the substrate properties [10]. Droplet impinging on wall dissipates kinetic energy and deforms the droplet while the surface tension stabilizes the droplet [15]. The dimensionless number that characterizes this effect is the Weber number. Wiranata et al. [48] studied the effect of surface temperature and Weber number to spreading ratio and concluded that the spreading is shaped better at lower Weber numbers.

Effect of surface properties on Leidenfrost effect has been studied and concluded that on a polished level, surface roughness had negligible influence on the LFP [49] but

when surfaces were modified at nano-level, extraordinary shifts in Leidenfrost temperatures as high as 175°C was observed [50]

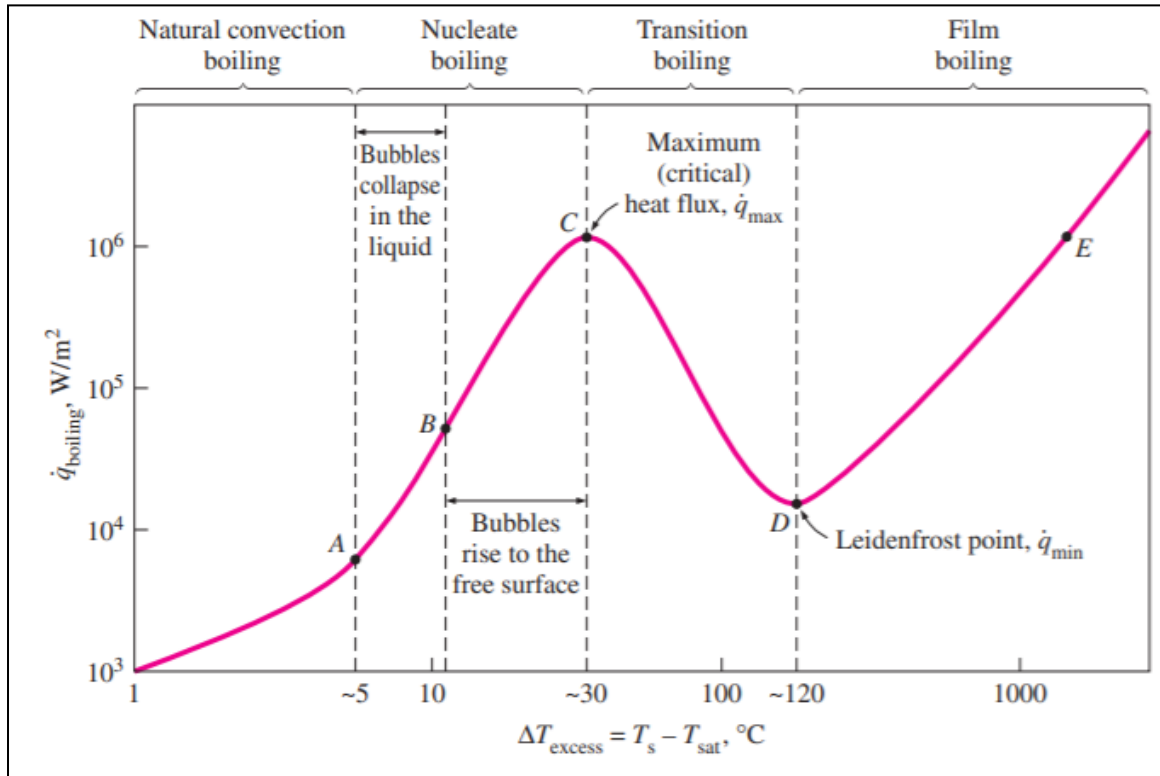


Figure 4.1 Boiling Curve of Water
(Heat transfer is plotted as a function of excess temperature - difference between the wall temperature and liquid saturation temperature)

The effect of droplet diameter, impact velocity and substrate temperature on single droplet of aqueous urea solution was conducted by Bornhorst et.al [51]. The study found that urea solute has strong influence on droplet disintegration. The effect of surface roughness on post-droplet impingement condition has been studied by various researchers. With increase in surface roughness, critical weber number for droplet adhesion reduces [10]. Therefore, with increase in surface roughness, less droplets convert to liquid film at

a certain temperature which helps to reduce deposit formation. Modifying DEF solution by adding surfactants to reduce deposits have been demonstrated and patented by many researches [52] [53], but little is known about modifying surface properties to mitigate deposits inside the mixer.

In exhaust spray systems, a liquid film is formed when the surface temperature falls below a critical temperature where droplets adhere to surface [10]. Deposits do not generate at the impingement location unlike the single droplet experiment due to continuous impingement that lead to local wall cooling making the surface unsuitable for accelerated deposit reactions. As liquid film moves from initial impingement area to a region of higher temperatures, water evaporation along with deposit initiation is expected. Shear stress and gravity plays an important role in transport of liquid dynamics. The effect of liquid film flow rate and temperature are studied using a gravity driven liquid film.

In a moving film, fresh incoming DEF changes the chemistry and surface temperature on the plate. A dynamic film essentially doesn't capture the local conditions for deposit formation. Therefore, an experiment was conducted in which the film is stagnant, and the urea concentration is fixed. The experiment helps to identify the local temperature and the time scale required for solidification.

4.2. EXPERIMENTAL SETUP

4.2.1. Single Droplet Experiment. In general substrate studies, high speed videography was used to study the contact angle for impacting droplets to determine the splash and deposition threshold. In this experiment, the wall wetting, droplet break up, deposit formation and time scale was evaluated for different surface temperatures. The

injector was placed at a fixed height and same diameter droplet was generated through an injector with a stainless-steel needle (Figure 4.2). The test was conducted with surface temperatures between 180-280°C with 10°C interval. The surface conditions and the time scale for deposit formation were recorded for each experiment.

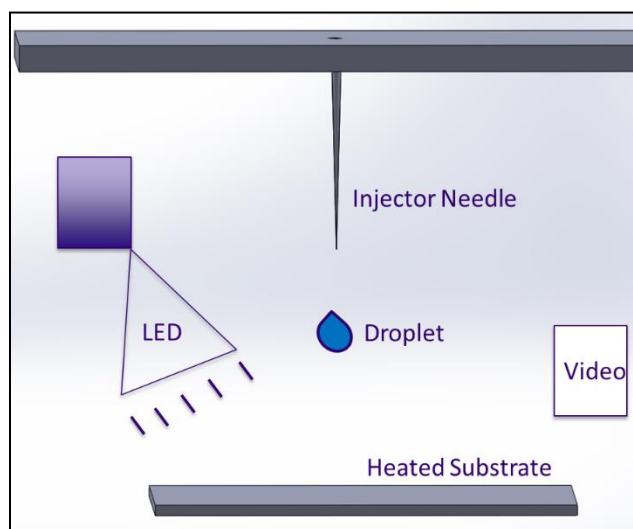


Figure 4.2 Single Droplet Impingement
(Injector was placed at a fixed height and droplet was generated using a stainless-steel needle)

4.2.2. Liquid Film Temperature Measurement. Using the thermocouples to measure thin liquid film temperature was a challenge. A non-intrusive technique like an IR camera was adopted to monitor the liquid temperature. Application of IR camera had its own challenges. Emissivity is an important material property that had to be calibrated. Emissivity of water was well established in literature with a value of 0.98. In stagnant film test, as water vaporized, and urea concentration increased, emissivity changed. To capture the change in film temperature, emissivity was calibrated by heating DEF in a stainless-steel pan. Urea emissivity value was found by varying emissivity in camera until liquid

temperature matched thermocouple temperature. Figure 4.3 clearly depicts the influence of emissivity on temperature.

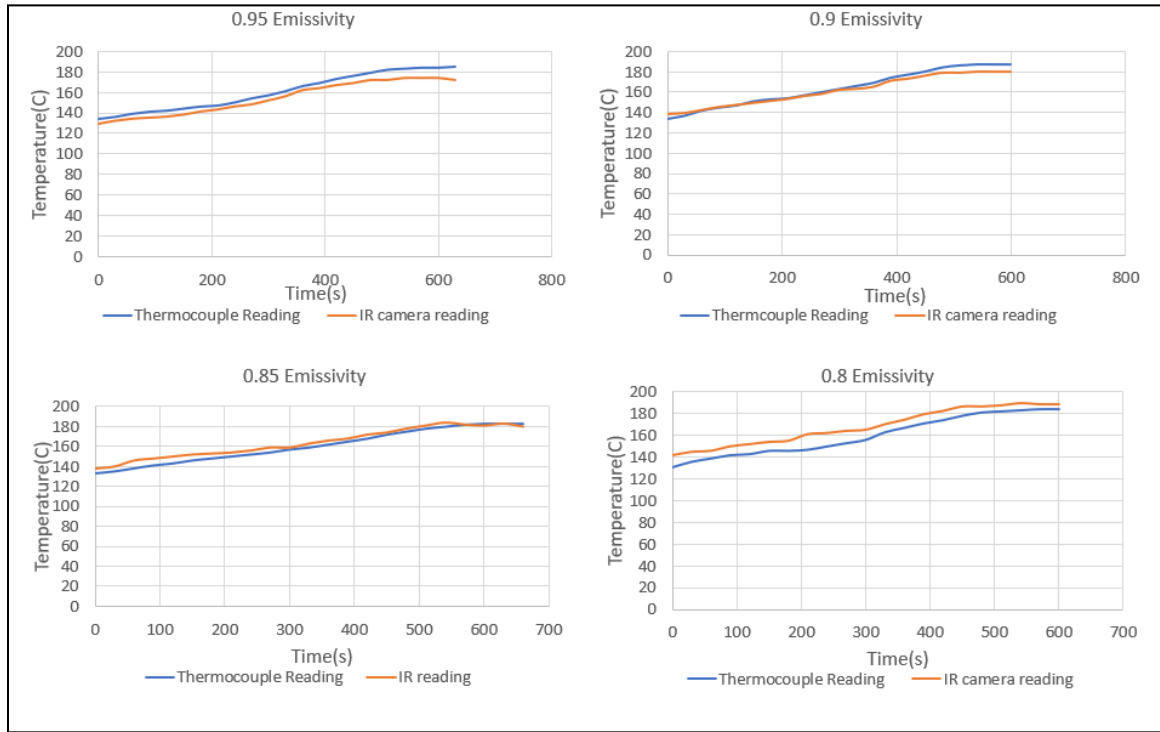


Figure 4.3 Emissivity Calibration using IR Camera
(Urea emissivity value was found to be 0.9 by varying emissivity in camera and by matching the liquid temperature with thermocouple measurements)

The emissivity at 0.95 under predicted the temperature at all the data points. Emissivity at 0.8 overpredicted the temperature at all the data points. Both 0.9 and 0.85 values of emissivity value predicted liquid temperature accurate but 0.9 was used for film test as it was the best estimate for mixture of urea and water.

4.2.3. Gravity-driven Liquid Film. A test plate with 23"x12" was placed at a 11° angle on an optic table using four threaded mounting post (Figure 4.4). A ceramic heater was used to heat the plate from beneath. The ceramic heater was placed 6"

downstream of the injection location. The challenge was to create a thin uniform film that was identical to the one in the exhaust system. Forming a film from spray was not a controlled process. Lan et.al [55] used a porous plug which when flushed with the test surface formed a uniform liquid film on the surface. The same approach was used to facilitate the liquid film formation in this test. Lan's et.al [54] had measured the liquid film thickness and found to be between 200-600 μm based on different surface tension, flow rate and angle of the plate. An IR camera was used to identify the time and location of deposit initiation based on change in liquid temperature and visual observation (Figure 4.5).

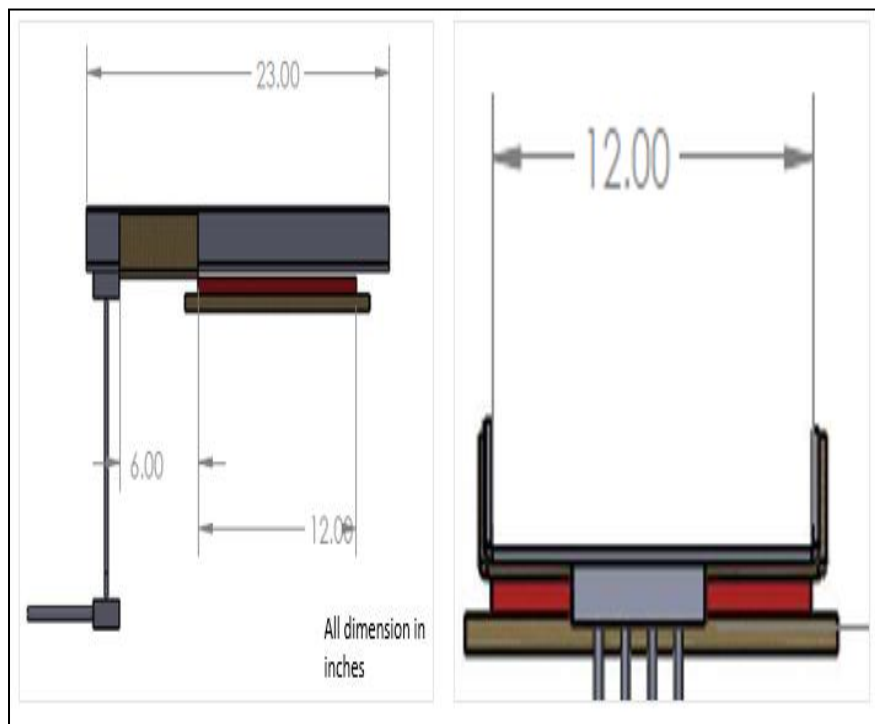


Figure 4.4 Test Plate Dimensions

(A test plate with 23"x12" was placed at an angle. Ceramic heater was used to heat the plate from beneath)

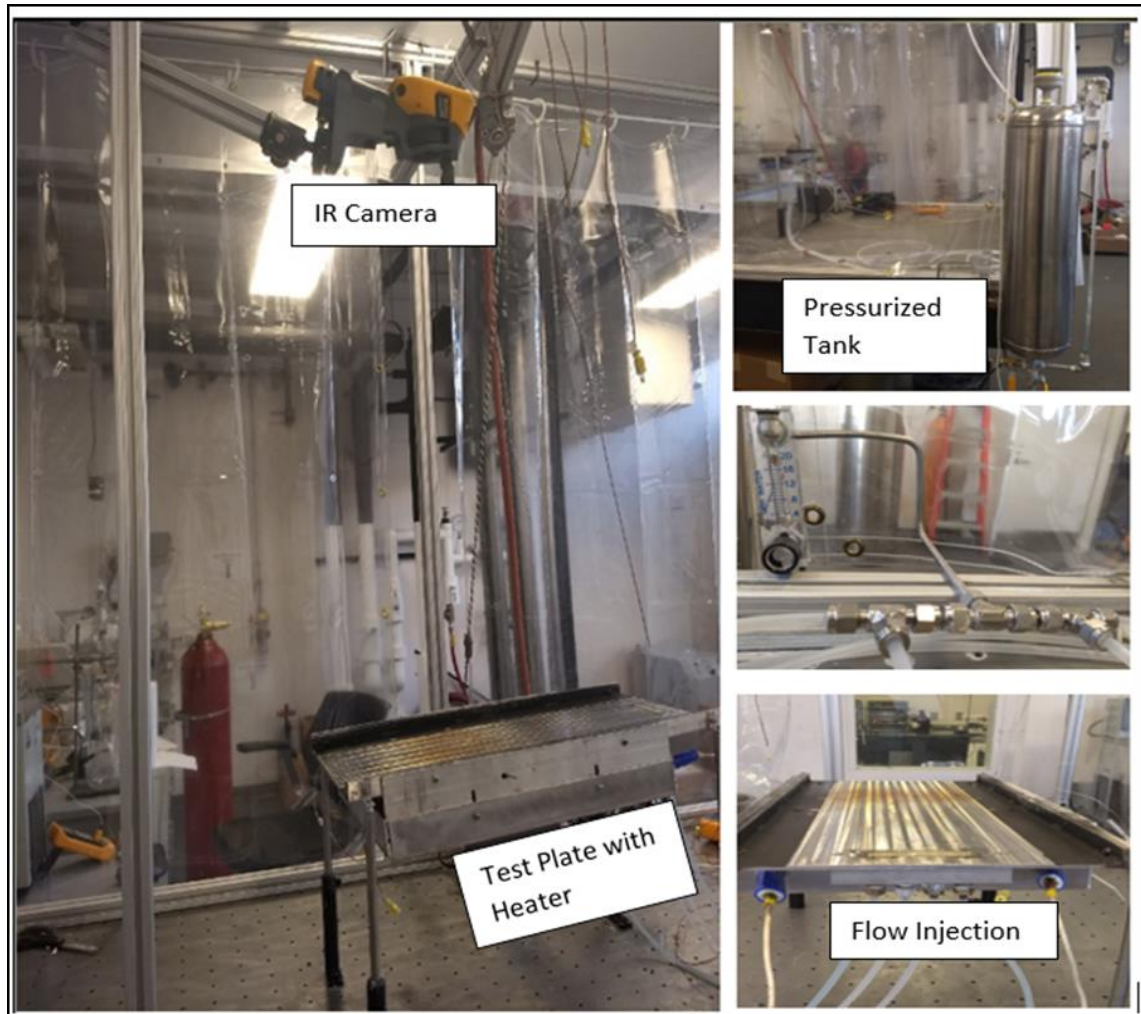


Figure 4.5 Experimental Setup for Gravity-Driven Flow
(IR camera was used to identify the time and location of deposit initiation. Porous plug was used to form a uniform liquid film on the surface)

4.2.4. Stagnant Film Experiment. A liquid film was introduced from the top using a burette on a heated stainless-steel plate (Figure 4.6). For a fixed temperature, 1mL of DEF was introduced on the heated plate. The temperature was recorded real time using a data-acquisition system. Video of the solidification process was shot on a 240fps camera. Three different temperature zones were considered- Low temperature(180-220°C), Medium temperature(240-280°C) and high temperature(300-325°C).



Figure 4.6 Stagnant Liquid Film Experiment Setup
(Liquid film was introduced from the top using a burette on a heated stainless-steel plate)

For each experiment, from the video, three different images were presented -initial, intermediate and final stage. The time required for solidification was recorded.

4.3. RESULTS AND DISCUSSIONS

4.3.1. Single Droplet Experiment. At low surface temperatures(180-240°C), droplet adhered to the surface and generated deposits. At higher temperatures (>240°C), droplet did not adhere to surface but shattered into smaller droplets and did not form deposit. With increase in temperature, the droplet evaporation time and the deposit initiation time reduced (Figure 4.7).





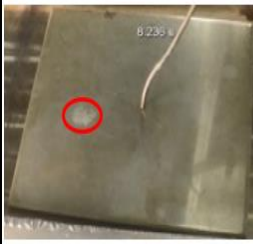
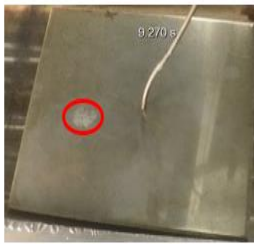
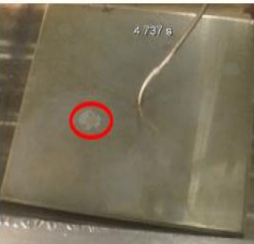

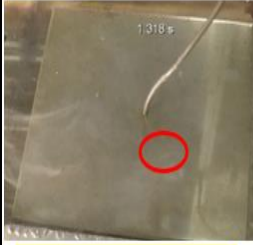
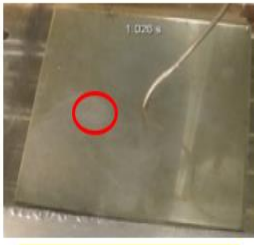
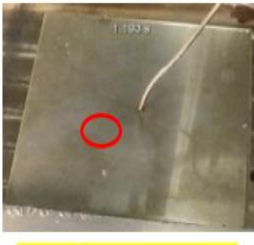
| 180°C | 190°C | 200°C | 210°C |
|--|--|---|---|
|  |  |  |  |
| Wet Wall, Time:126s | Wet Wall, Time: 70s | Wet Wall, Time: 39s | Droplet Breakup/Wet Wall, Time: 20s |
| 220°C | 230°C | 240°C | 250°C |
|  |  |  |  |
| Droplet Breakup/Wet Wall, Time:7s | Droplet Breakup/Wet Wall, Time:4s | Droplet Breakup/Wet Wall, Time:3s | Droplet Breakup ,No Deposit |
| 260°C | 270°C | 280°C | |
|  |  |  | |
| Droplet Breakup ,No Deposit | Droplet Breakup ,No Deposit | Droplet Breakup ,No Deposit | |

Figure 4.7 Single Droplet Impingement
(Droplet condition and time required for solidification was recorded)

Droplets of different size were sprayed on a painted surface. Even the smallest diameter droplet adhered to the surface and converted to deposit. The same droplets sprayed on the non-painted surface did not generate deposits (Figure 4.8). This indicated that if droplets get adhered to the surface, deposits will generate even at high temperature irrespective of the size of droplet or thickness of liquid film further indicating that deposit reactions are surface based.

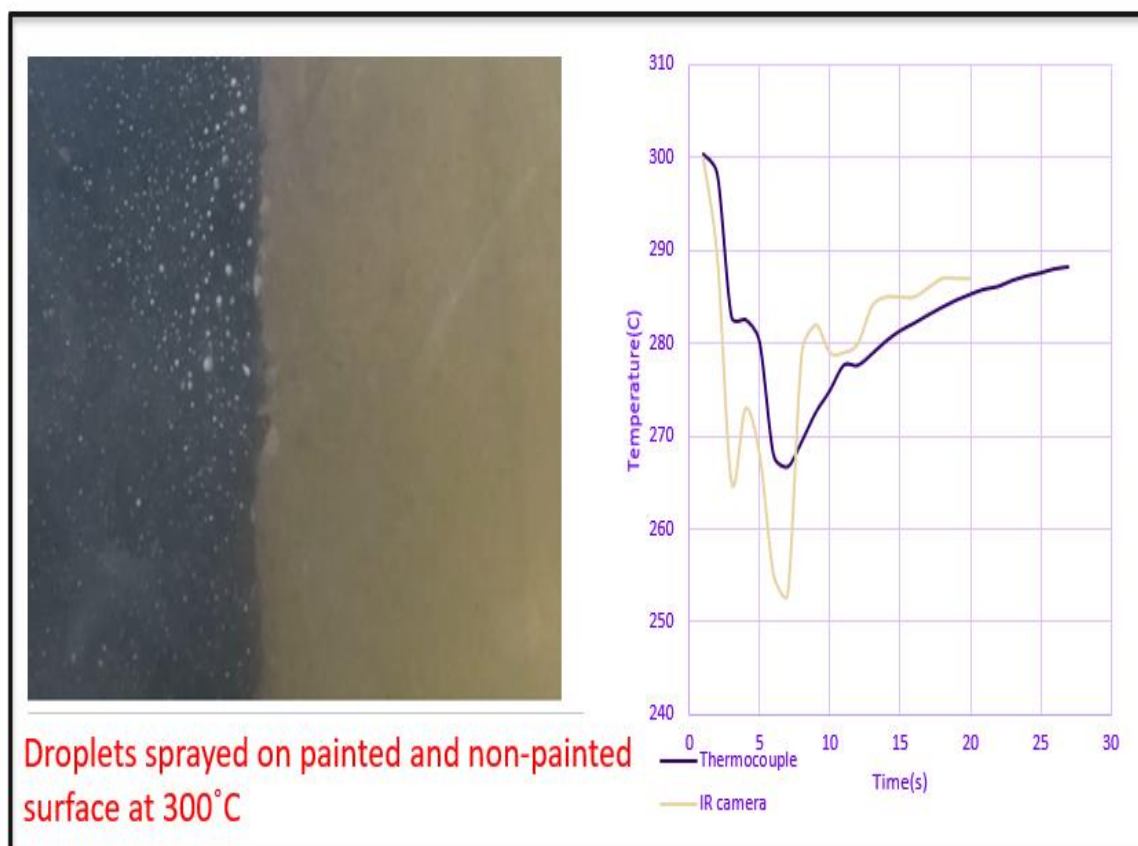


Figure 4.8 Deposits on Painted vs Non-Painted Surface
(Painted side: Droplet adhered to the surface and converted to deposit. Non-painted side:
Did not generate deposits)

4.3.2. Gravity Driven Liquid Film Results. Three flowrates 0.2, 0.4, 0.8 gal/hr. and four temperatures -200, 220, 260 and 260°C were tested. From the video, the time between the liquid ejection from the porous filter and the deposit initiation was recorded (Figure 4.9). The location of deposit initiation and the time for the liquid film to reach the end of the plate was recorded. One of the limitations in this study was that the shearing effect of exhaust gas was not considered that can possibly entrain a part of liquid back to the gas phase. This is discussed in the next section where the effect of gas flow rate on deposit initiation and growth are studied.

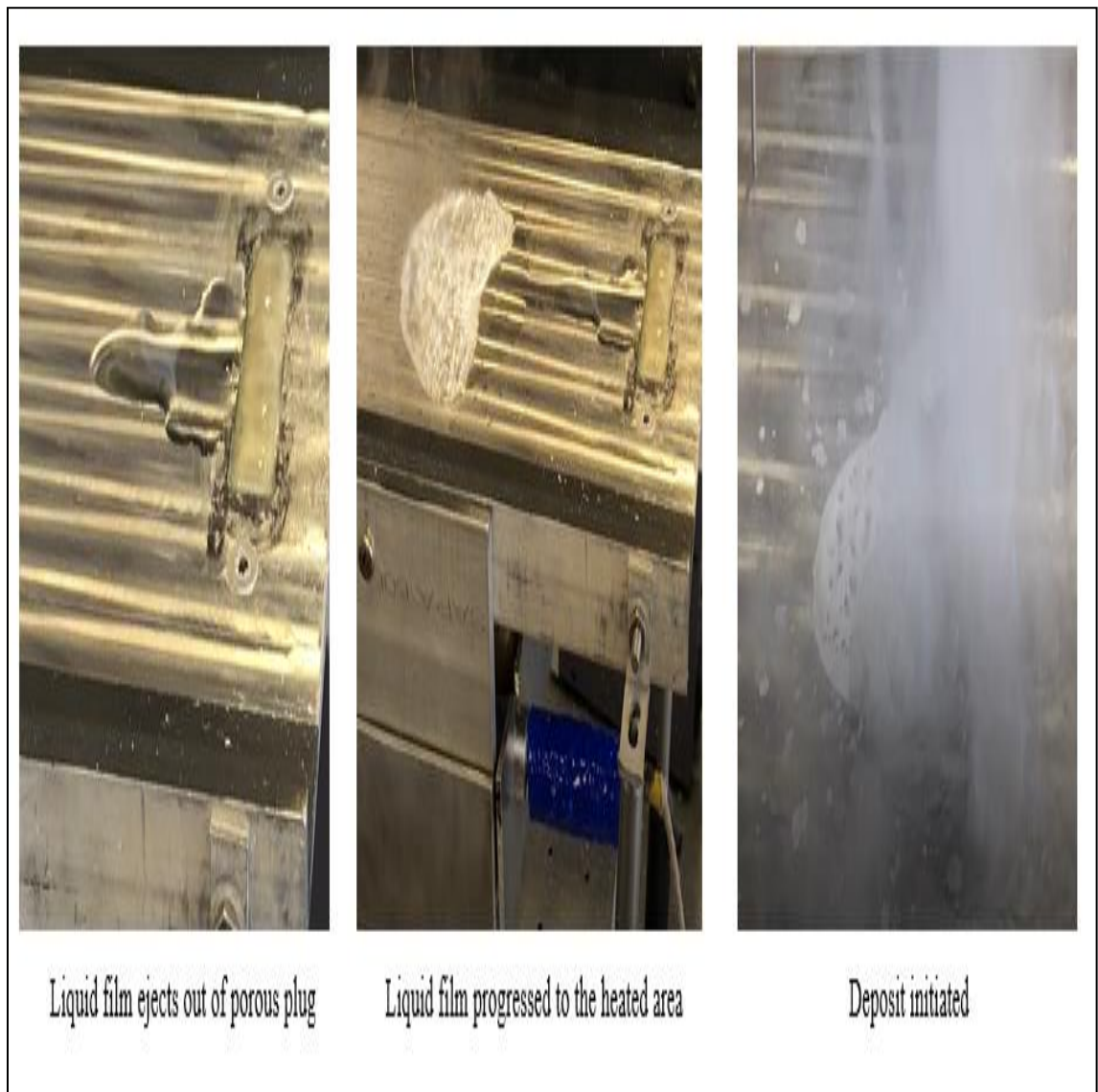


Figure 4.9 Deposit Initiation in Gravity Driven Liquid Film

At 200°C, no deposits were formed for all three flow rates indicating that temperatures were low for deposits to initiate. At 220°C, 0.2 gal/hr generated deposit while 0.4 and 0.8gal/hr. did not generate any deposit. At 240 and 260°C, deposits were generated at all flow rates. The liquid film did not solidify at high flow rates and low temperature.

Once the film was formed, higher the inherent energy content in the wall, more was the heat transferred to the film, higher was the risk of deposit.

Table 4.1 Time Required for the Liquid Film to Reach the End of Plate

| Flow Rate | Temperature | Plate Condition | Time for the Film to Reach the End of Plate |
|------------------|--------------------|------------------------|--|
| <i>gal/hr</i> | <i>°C</i> | | <i>Seconds</i> |
| 0.2 | 200 | No Deposit | 128 |
| | 220 | No Deposit | 360 |
| | 240 | Deposit | 1033 |
| | 260 | Deposit | 801 |
| | | | |
| 0.4 | 200 | No Deposit | 76 |
| | 220 | No Deposit | 77 |
| | 240 | Deposit | 232 |
| | 260 | Deposit | 360 |
| | | | |
| 0.8 | 200 | No Deposit | 67 |
| | 220 | No Deposit | 82 |
| | 240 | Deposit | 140 |
| | 260 | Deposit | 260 |

The time required for the liquid film to reach the end of the plate was recorded for all operating conditions. The time data in Table 4.1 observed high values when deposits initiated indicating that it dammed the incoming liquid flow and allowed higher residence time for the film to undergo reactions.

The trend showed that with lower flow rate and higher temperature, deposit reactions were accelerated, and the location of deposit shifted upstream (Table 4.2). Once the deposit initiated, it restricted the incoming film flow and it was subjected to more

residence time. Initial solidification location was extremely important in predicting the overall deposit content in a test bench as it can alter the residence time of incoming liquid film.

Table 4.2 Time and Location of Deposit Initiation from IR Camera

| Flow Rate | Temperature | Total time for deposit initiation | Location of Initial Deposit |
|------------------|--------------------|--|------------------------------------|
| <i>gal/hr</i> | <i>°C</i> | <i>Seconds</i> | |
| 0.2 | 220 | 39 | Center of T1&T2 |
| | 240 | 31 | Closer to T1 |
| | 260 | 28 | At T1 |
| | | | |
| 0.4 | 240 | 28 | Center of T1&T2 |
| | 260 | 25 | Closer to T1 |
| | | | |
| 0.8 | 240 | 19 | Center of T1&T2 |
| | 260 | 20 | Closer to T1 |

4.3.3. Stagnant Film Test Results. At 180°C, all three stages did not show any gas evolution inside the film (Figure 4.10). The solidification process was a mostly physical phenomenon of crystallization. At 220°C, initial stages did not have any gas bubble evolution inside the film. In the intermediate stage, gas bubble evolution was visible around the corner of the liquid film as marked in Figure 4.10. At the final stage, there were distinctly two different type of deposits formed. For experiments conducted between 260°- 280°C, the gas evolution inside the film was intense right from the initial stage till the final solidification (Figure 4.11). Deposit formation was accelerated in this region and solidification was due to chemical reactions. The time scale of deposit initiation was

recorded (Table 4.3). At low temperatures, the time required for solidification was very high.

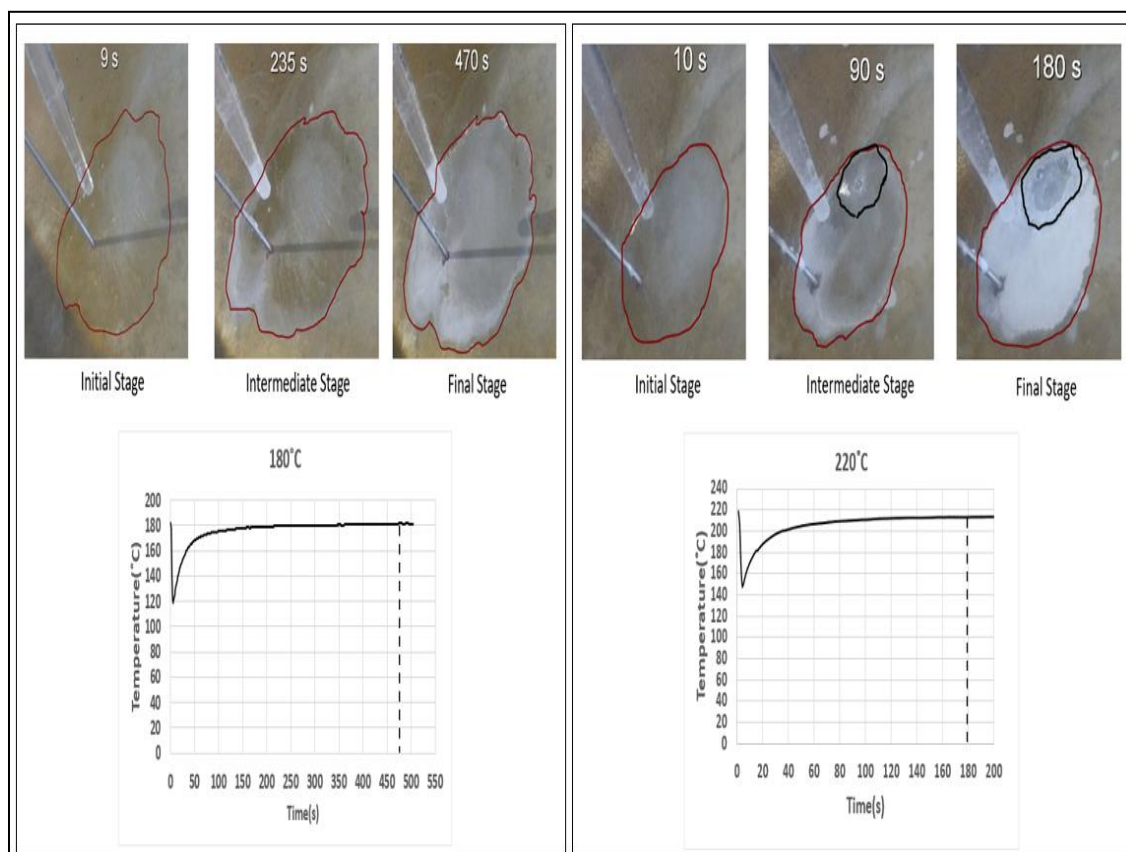


Figure 4.10 Low Temperature Zone

(At 180°C, all three stages did not show any gas evolution inside the film. At 220°C, initial stages did not have any gas evolution inside the film. In the intermediate stage, gas bubble evolution was visible around the corner of the liquid film)

The liquid film above 300°C, formed a vapor layer between the liquid and the plate. This is called Leidenfrost phenomena. At 300° C, very small amount of liquid wetted the surface which generated deposit and at 320°C, entire film was on Leidenfrost State. However, liquid film moved away from the initial impingement region and formed deposits where temperatures were lower. The time scale for deposit initiation decreased with increase in surface temperature (Table 4.3).

Table 4.3 Solidification Time for Stagnant Liquid Film

| Temperature(°C) | Solidification Time(s) |
|-----------------|------------------------|
| 180 | 470 |
| 220 | 209 |
| 260 | 63 |
| 280 | 35 |
| 300 | 13 |

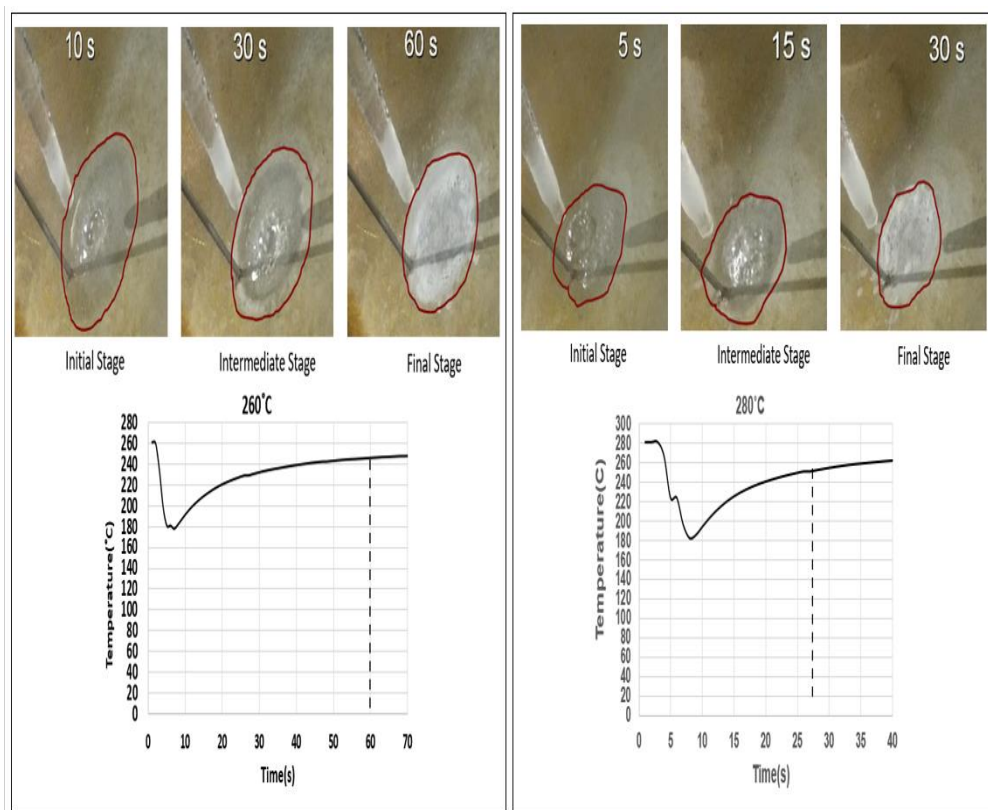


Figure 4.11 Medium Temperature Zone
(Gas evolution inside the film was intense right from the initial stage till the final solidification)

A stagnant film test was repeated with an IR camera monitoring the liquid temperature. In Figure 4.12, 1ml liquid was introduced over a 240°C heated plate. The IR

camera recorded the real time liquid temperature. As the gas bubbles evolved from the liquid film, there existed a temperature distribution within the film. To get an accurate value, at every time frame, an average of many data points is taken within the central location of the film as shown in Figure 4.12 (b) and plotted against time (Figure 4.13). The thermocouple recorded the plate temperature value is also plotted on the same graph. The experiment was repeated for various combination of plate temperature and DEF volume.

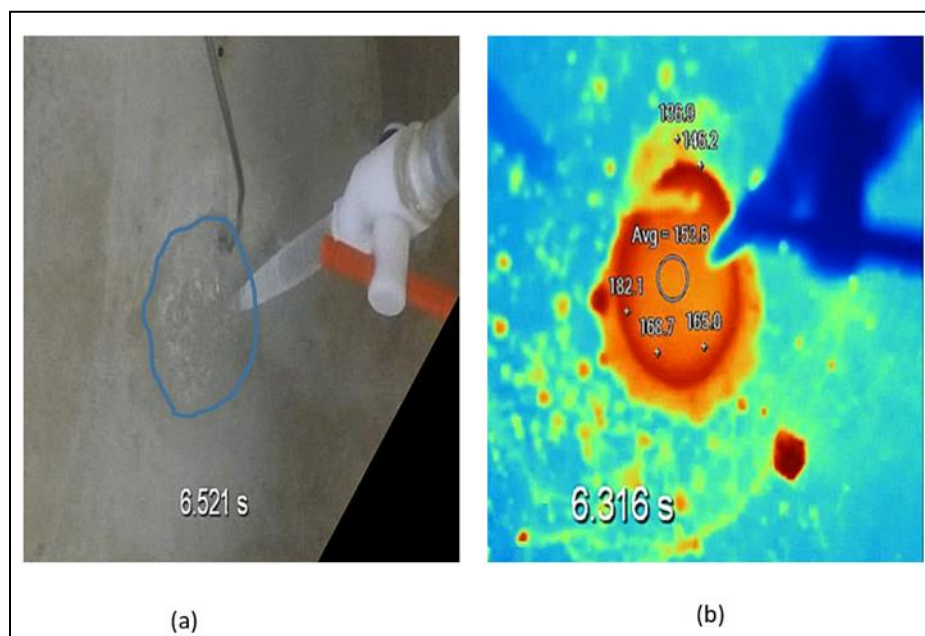


Figure 4.12 Stagnant Film Test with Temperature Measurement using IR Camera (IR camera recorded the real time liquid temperature. Average of many data points is taken within the central location of the film)

In Figure 4.13, the curves represent the liquid temperature measured by the IR camera for different experiments. Unlike the previous pool boiling beaker experiment, where we could see the water evaporation trend clearly, here the vaporization of water was instantaneous and could not be captured. However, the trend for urea decomposition and

the final solidification point (dashed lines) was captured fairly accurate. The region of solidification was in 200°C range. This data was in line with the experiment measured by thermocouple in the pool boiling experiment.

Chemical Characterization of Stagnant Liquid Film Samples: The deposit sample was analyzed using LC-MRM method to quantify the deposit composition (Table 4.4). The method has been discussed in the Section 6.

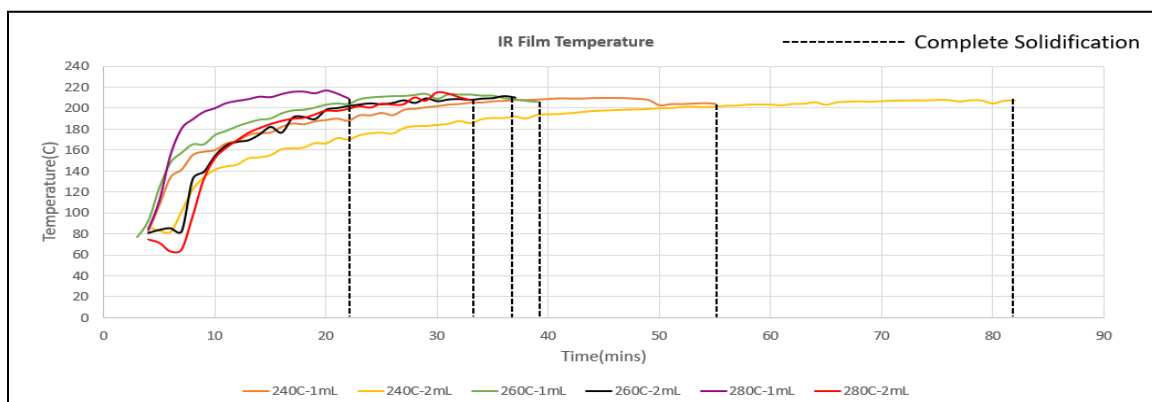


Figure 4.13 IR Film Temperature Measurement and Solidification Point
(Curves represent the liquid temperature measured by the IR camera for different experiments)

Table 4.4 Chemical Mass Composition

| | Mass Composition (%) | | | | | | |
|--------|----------------------|---------|----------|----------|----------|--------|------|
| Sample | Urea | Triuret | Ammelide | Ammeline | Melamine | Biuret | CYA |
| 180°C | 15.3 | 3.1 | 1.2 | 0.1 | 0.0 | 73.5 | 6.7 |
| 220°C | 11.5 | 1.6 | 7.8 | 1.5 | 0.1 | 54.6 | 23.0 |
| 260°C | 9.8 | 1.1 | 13.8 | 4.3 | 0.2 | 27.5 | 43.2 |
| 280°C | 3.4 | 0.5 | 15.4 | 5.2 | 0.3 | 18.3 | 56.9 |

At 180°C, the deposit sample largely composed of biuret and urea. With increase in temperature, the samples contained higher amount of cyanuric acid, ammeline and ammelide. The decrease in biuret composition and increase in CYA and ammeline indicated that CYA and ammeline are formed when biuret decomposes above 200°C.

4.4. INFERENCE

Experiments on a single droplet indicated that at higher temperatures, droplet breaks and do not adhere to the surface. This prevented the deposit formation. Within the wetting regime, as the temperature increased, water evaporation and deposit generation were accelerated. Similar trend was observed in liquid film experiments. The liquid film did not solidify at high flow rates and low temperatures. Once the film was formed, higher the inherent energy in the wall, more was the heat transferred to the film, higher was the risk of deposit generation. Once the deposit initiated, it restricted the film flow. The incoming film flow was subject to more residence time which was similar to the liquid film accumulation on corners and edges.

5. EXPERIMENT ON A HOT GAS TEST BENCH

This section investigates the effect of transport on urea deposits. A series of experiments were carried on the test bench to study the following:

A. Deposit Initiating Local Surface Temperature –Post Impingement:

Deposit initiating local surface temperatures were identified independent of operating parameters-exhaust flow rate, exhaust gas temperature, DEF flow rate.

B. Critical Injection Rate:(CIR)

For different gas flowrate and temperature, safe DEF injection rate is identified.

C. The Effect of Gas Flow Rate on Deposit Formation and Growth:

Effect of gas flow rate on deposit formation is studied in 2 different regime-a) wall film regime- a condition where significant liquid film exist at given operating conditions and b) boundary regime- a condition where deposits just initiate but accelerated growth does not exist.

5.1. LITERATURE REVIEW

Previous researchers have concluded that high exhaust mass flow rate and exhaust temperature significantly reduced deposit formation [54] [55] [56] [57] [58]. Roppertz et al. 2017 recommended temperatures above 300°C to eliminate deposits [55]. Wall cooling occurred due to spray impingement. When the wall temperature was high, droplet either did not adhere to the surface [10]. When wall temperature was low, droplet wets the wall and forms a liquid film [10] [59]. Liquid film was a precursor for deposit formation [31]. Low exhaust temperature decreased the surface temperature below a critical point where

droplets deposited as liquid film as observed in the previous section. Higher temperatures mitigated deposits because it prevented liquid film formation and decomposed the generated deposits (temperatures $>500^{\circ}\text{C}$). However, deposits formed at higher temperatures are chemically different from deposits formed at lower temperatures [31] [30] [60]. Recent work of Born horst et al. 2019 suggested that higher gas temperature formed deposits that required high temperatures to decompose [30]. Deposit study conducted by Scott et al. 2016 based on different gas temperatures concluded that the amount of deposits formed at higher temperatures were less but at higher temperatures amount of heptazine content in the deposit increased which required extremely high temperatures to completely decompose [60]. Not many studies have explicitly focused on the effect of flow transport on urea deposits. Previous research demonstrated that urea particles trapped in the recirculation zone, initiated deposits on the tip of the spray injector [61]. Same work also concluded that increase in local gas velocity inside the mixer reduced the risk of deposit formation. Zheng et al. 2010 found that with increase in exhaust flow rate, the urea injection rate increased without causing wall-wetting [62]. Ku et al. 2015 concluded that increasing the gas flow, increased the overall convective heat and mass transfer rate which increased the efficiency of urea droplet conversion and reduced deposit formation. [63]. Specific mechanism by which higher gas flow rate mitigates deposit formation cited from different literature is discussed in the results section.

5.2. EXPERIMENTAL SETUP

The current test was conducted outdoor on a class 8 truck along with a gas burner. An initial flow test was conducted to calibrate the engine speed with intake airflow. A

flowmeter was installed between the engine filter and compression inlet. Flowrates were measured for different RPMs. The measured values matched with the estimated airflow values. The velocity of exhaust gas was measured using a pitot tube. The after-treatment included a Diesel Oxidation Catalyst (DOC) and Diesel Particulate Filter (DPF). During initial testing, a cloud of thick white smoke(ammonia) was being released through the exhaust. A SCR was placed downstream of optic box to treat the exhaust air as shown in Figure 5.1.



Figure 5.1 Truck Setup With DPF, DOC, Optic Box and SCR

5.2.1. Optic Box Design. An optic box was positioned between the DPF and SCR which represented the mixer. The box made of stainless steel 316 was 30" long and had a square opening with 6"x 6" cross section as shown in Figure 5.2. A 3-hole Bosch injector at 11° angle was placed 5" from the optic box inlet. A constant injection with frequency of 1Hz was used. The injection was actively cooled by a flowing water system.

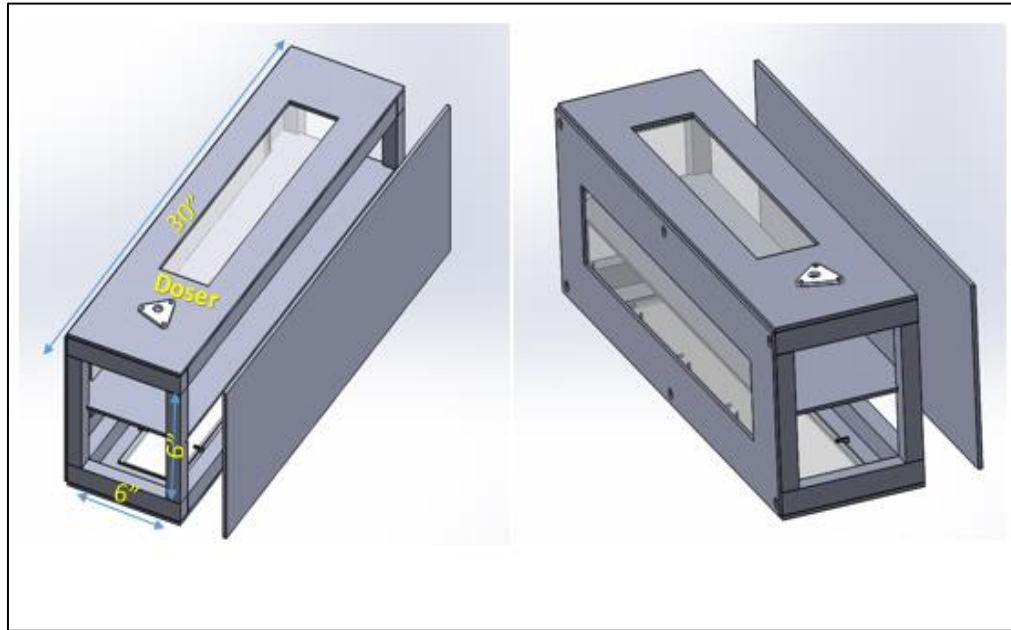


Figure 5.2 Optic Box Design
(Bosch injector at 11° angle was placed 5" from the optic box inlet. Quartz windows on three sides)

Many commercial mixers have gas flow on the top and bottom part of the impinging surface. A horizontal plate with 28" x 7.5" x 0.1" was placed in between the box. Provisions were made where the plate can be placed at 3 different height positions. The plate was introduced at half the height of the box for this test. During the initial shake down test, the plates remained flat at the heating stage but exhibited buckling behavior as soon as DEF injection was initiated. It was the result of thermal gradients through the thickness of the plate. To prevent the bending, metal braces of 1" x 0.1" cross section was welded on the non-impingement side of the plate as shown in the Figure 5.3. Thermocouples were positioned on the bottom side of the plate as shown in Figure 5.3.

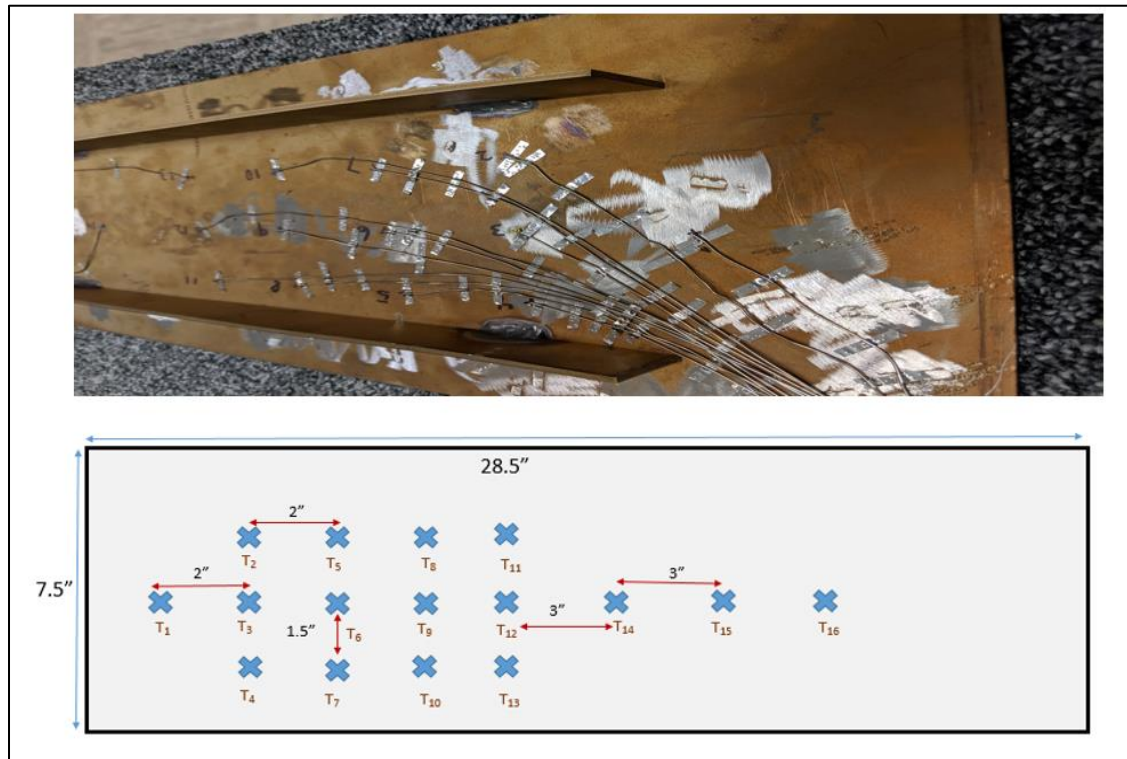


Figure 5.3 Thermocouple Position
(Metal braces attached along the length of the plate and sixteen thermocouple position on the non-impingement side of the plate)

5.2.2. Flow Characterization. Literature had reported that urea particles trapped in recirculation zone lead to deposits in different parts of the exhaust system like the injector tip or the walls of the box [64]. Our goal was to produce deposits only on the surface of the impingement plate and eliminate any recirculation zone in the direct path of spray. Change in cross sectional area from the outlet of DPF to the inlet of optic box sharply defined the recirculation zone in the design. Efficient transition sections had to be employed to avoid recirculation in the system. The design optimization was carried out using computational fluid dynamics (CFD). A sheet metal with circular opening was placed on the inlet of the optic box. The CFD results showed high recirculation around on the corners of the test box (Figure 5.4).

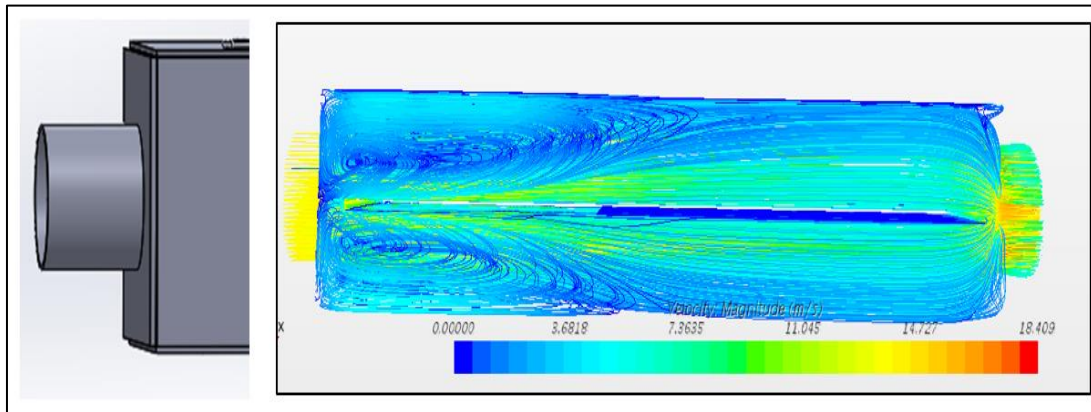


Figure 5.4 Recirculation Eddies Inside the Channel
(Sheet metal with circular opening was placed on the inlet of the optic box, high recirculation around on the corners of the test box)

A duct bend with smooth transition from circular to square channel reduced the intensity of recirculation but the flow was not completely unidirectional inside the box (Figure 5.5).

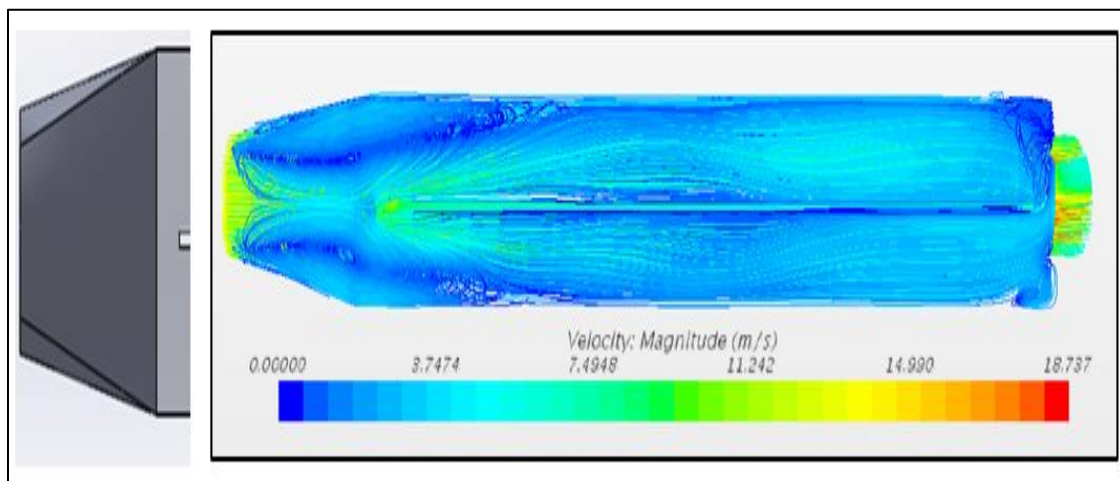


Figure 5.5 Modified Inlet Design to Reduce Recirculation
(Smooth transition from circular to square channel reduced recirculation eddies)

A solid plate containing uniformly distributed circular holes was positioned at the entrance of the box to further reduce the recirculation eddies. The porous plate was tested for both inlet design (Figure 5.6).

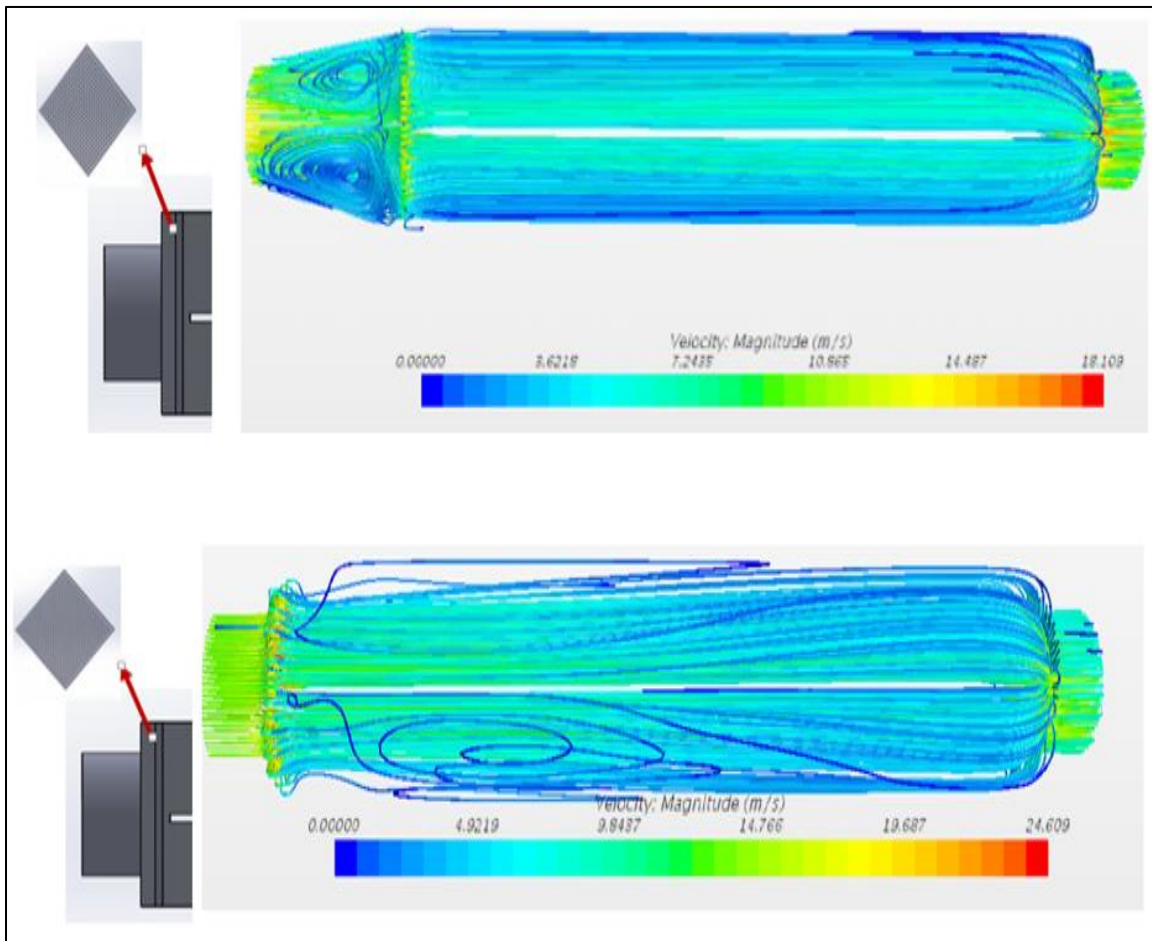


Figure 5.6 Streamlines Indicating Low Recirculation with Perforated Plate

A smooth uniform bend transition from a circular to square channel along with the porous plate eliminated the recirculation inside the box. The contour plots indicated that velocity was not homogenous across the inlet cross section of the box (Figure 5.7).

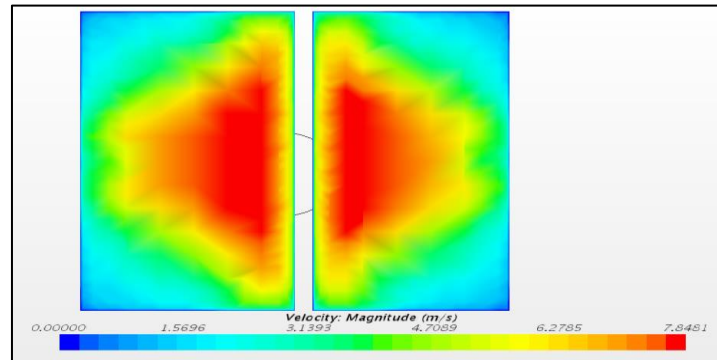


Figure 5.7 Inlet Velocity Contour Plot
(Velocity was not homogenous across the inlet cross section of the box)

The length of the square inlet was increased by 12” to make the flow more uniform.

Figure 5.8 shows that the contour and streamlines of the final design. The streamlines indicated that no recirculation eddies were present in the test setup.

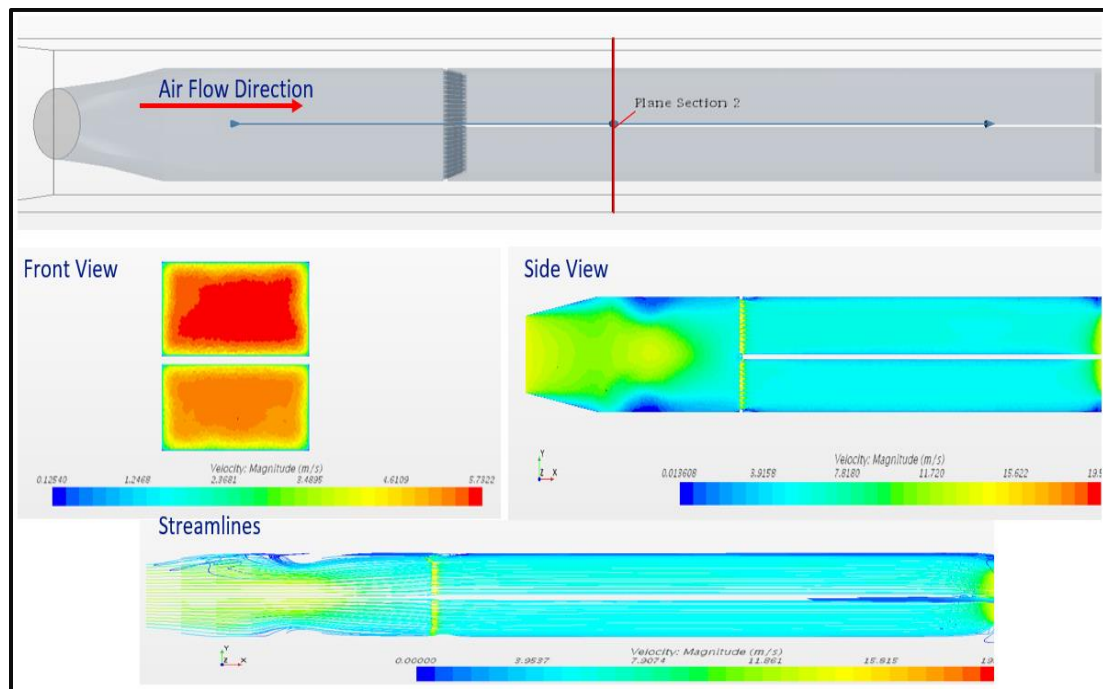


Figure 5.8 Final Optic Box Design
(Increased Inlet Length to Improve the Inlet Velocity Uniformity)

5.2.3. Flow Velocity Measurement. The velocity of the exhaust gas inside the channel was measured by determining the differential pressure using a pitot tube. Pitot tube was mounted on the center of the duct with the opening of the tip facing the airflow. The pitot tube was calibrated on an air flow test stand for a set of different flowrates and are compared against the readings from pitot tube. Velocity measurements from pitot tube had less than 10% error (Figure 5.9). The calculations are presented in Table 5.1.

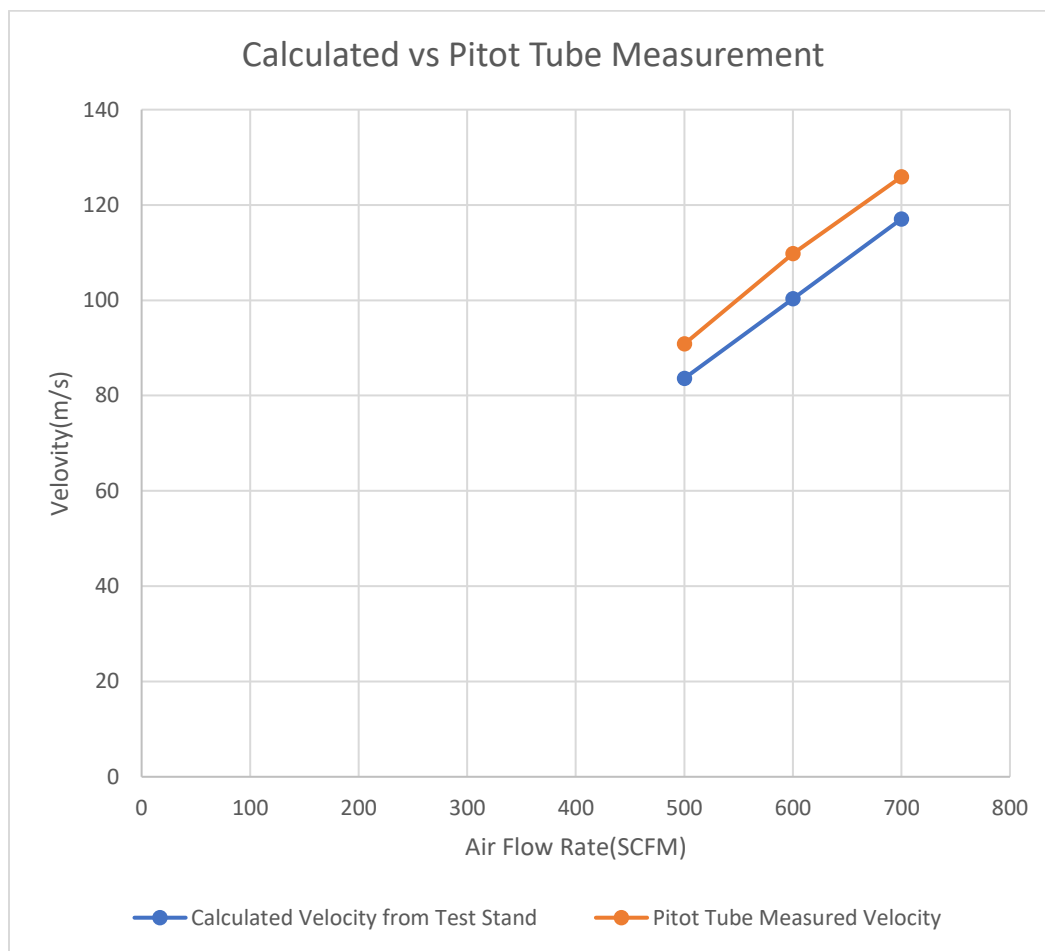


Figure 5.9 Pitot Tube Calibration Results
(Velocity measurements from pitot tube had less than 10% error)

Table 5.1 Pitot Tube Calculations

| | |
|---------------------------------------|--|
| $P_T = P_S + P_D$ | P_T : Total Pressure P_S : Static Pressure P_D : Dynamic Pressure ρ : Density v : Fluid Velocity (Assuming Air) A_c : Cross – Sectional Area \dot{V} : Volumetric Flow Rate |
| $P_D = P_T - P_S$ | |
| $P_D = \frac{1}{2} \rho v^2$ | |
| $v = \sqrt{\frac{2P_T - 2P_S}{\rho}}$ | |
| $\dot{V} = A_c v$ | |

5.2.4. Test Repeatability. To ensure the best possible measurement accuracy and consistent results, performing test repeatability was essential. Since the test was conducted outdoor, multiple tests were conducted to investigate the effect of ambient conditions like temperature and humidity. The tests were conducted with an exhaust temperature of 300°C, exhaust flow rate of 400kg/hr. and DEF flow rate of 80mg/s. The first test was conducted at 10°C ambient temperature and 44% humidity. The same operating point was repeated the next day at 2°C ambient temperature and 70% humidity. Figure 5.10 shows the comparison between the temperature profile of the two tests. The impingement temperature profile for both the tests are similar. The temperature profile near the location where deposits initiate was also identical.

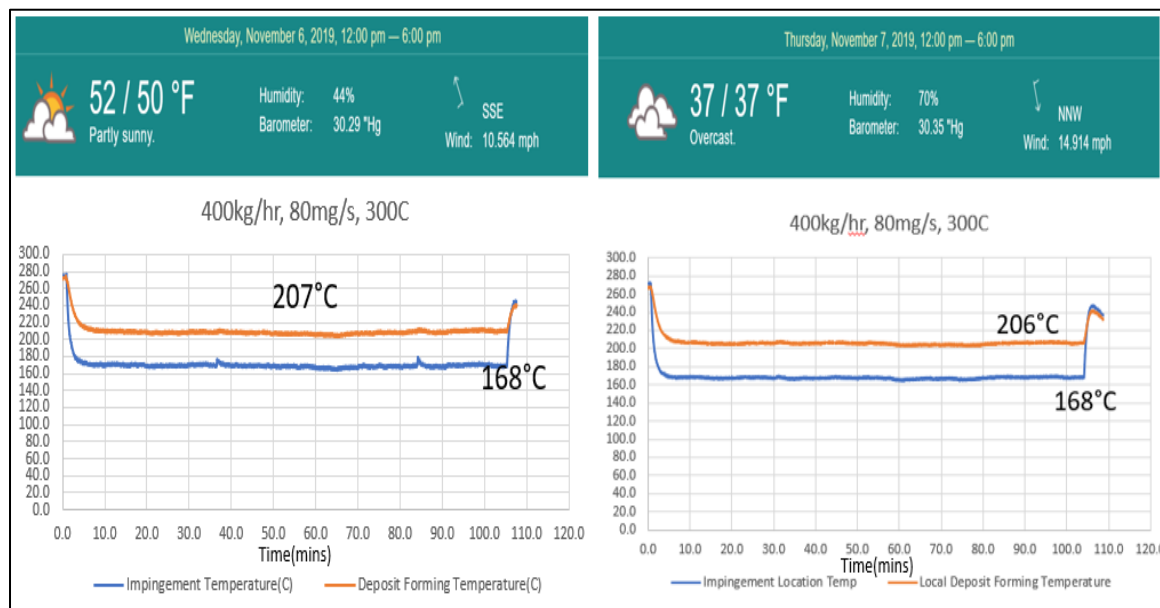


Figure 5.10 Test Repeatability

(Test repeatability to ensure the effect of ambient conditions on test results. Temperature profiles are identical and indicate that the experiment is indeed repeatable and precise)

The first test produced 23mg deposit while the second test produced 60mg after 100 minutes. There was no significant difference in terms of deposit growth. Operating conditions where deposits don't initiate were also tested for repeatability. The experiment confirmed that the temperature profiles are identical and did not form any deposits in both tests. The results indicate that the experiment is indeed repeatable and precise.

5.3. RESULTS AND DISCUSSION

The first objective was to study the local deposit initiating temperatures. Deposit initiation point was monitored through videography and matched with the corresponding thermocouple reading. If deposits initiated between 2 thermocouples, an average of both temperature readings were considered (Figure 5.11).

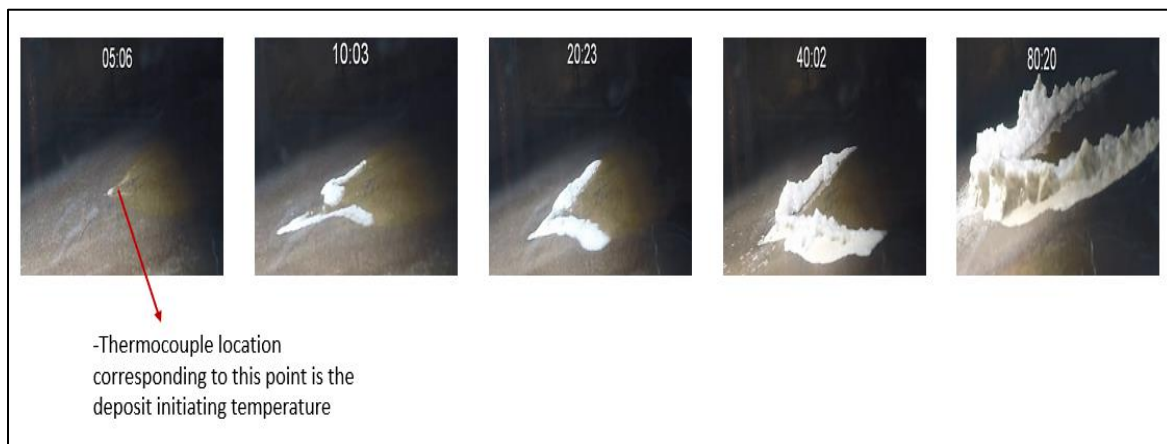


Figure 5.11 Deposit Growth with Time
(Thermocouple location indicating the deposit initiating temperature and the growth rate of deposit with time)

5.3.1. Local Deposit Forming Temperatures 19 different operating points (OP)

with couple of repeat experiments were tested to investigate the deposit forming local surface temperatures. 2 different exhaust operating temperatures-300 and 350°C and 2 different exhaust flow rates were considered-400 and 800kg/hr. For each operating condition, different DEF flow rates were tested. Each test was run for 100mins. The results are plotted in Figure 5.12.

It was observed that deposit initiating temperature lied between 197-215°C for all tested operating conditions. At high DEF flow rate(500mg/s), deposits did not initiate but plate had excess liquid film with average post impingement surface temperature around 177°C. At high exhaust temperature and low DEF flow rate, the plate was in Leidenfrost condition. The average steady state post impingement temperature was above 300°C. Impingement temperatures were lower than deposit initiating temperatures. The final deposit images are shown in Figure 5.13.

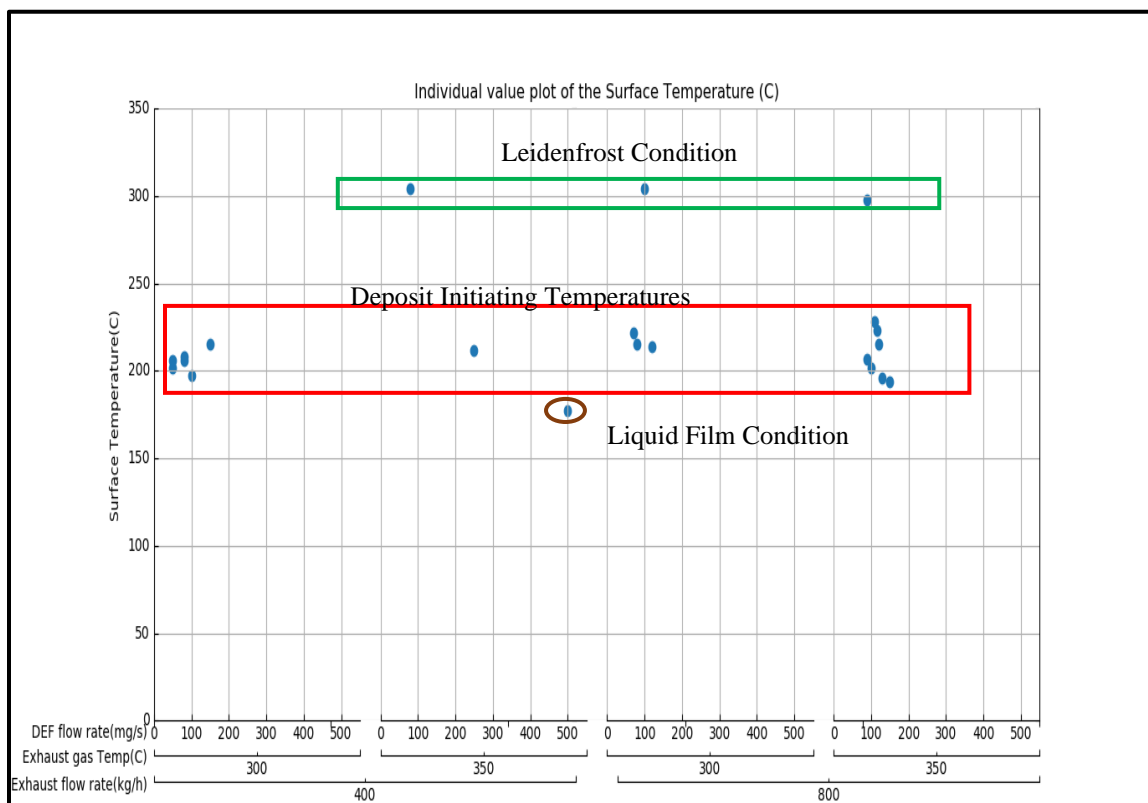


Figure 5.12 Deposit Initiating Temperatures
(Deposit initiating temperature lied between 197-215°C for all tested operating conditions)

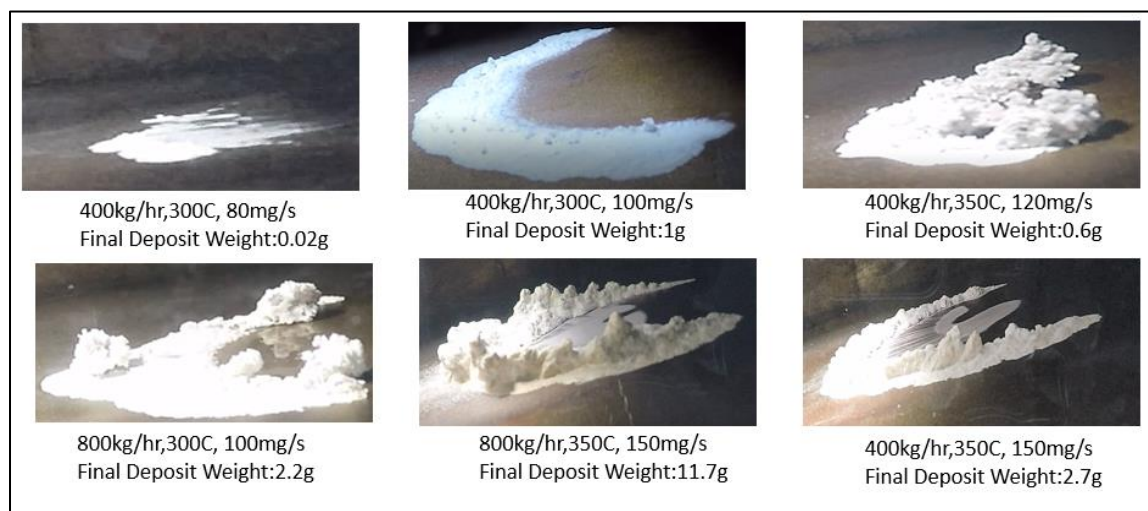


Figure 5.13 Deposit Weight and Images Generated at Different Operating Conditions

5.3.2. Leidenfrost Effect and Deposit Forming Regime. Previous liquid film experiments observed deposit formation between 220-280°C. In the current test, for all operating points, deposits did not initiate in that temperature range. The reason has been cited in multiple literature that liquid film was a precursor for deposit formation [19] [31]. When spray droplets impinge on the surface between 220-280°C, it did not form liquid film. Uncertainty exists in terms of predicting the liquid forming critical temperature since it is dependent on the exhaust system layout and geometric features [11]. In the current test setup, the liquid film forming temperature was below 190°C. Deposits did not initiate on the impingement area due to continuous liquid impingement locally cooling the surface below the deposit forming temperature. Deposits initiated when the liquid film was transported to higher temperature.

A test was conducted at high exhaust temperature(400°C) and high exhaust flow rate(800kg/hr.). DEF flow rate was increased from 125mg/s to 250mg/s with 25mg/s increment. Each test was run for 15 mins. The objective was to see if deposits form outside the temperature region mentioned in the previous section. From 120-225mg/s, the surface temperature did not significantly drop and remained constant for 15 mins, plate condition remained dry. All the droplets were in Leidenfrost condition. When the flow rate was increased to 240mg/s, there was an initial temperature drop after which the temperature became stable. After 12 mins, there was a sharp temperature drop to 200°C forming liquid film and later deposits (Figure 5.14).

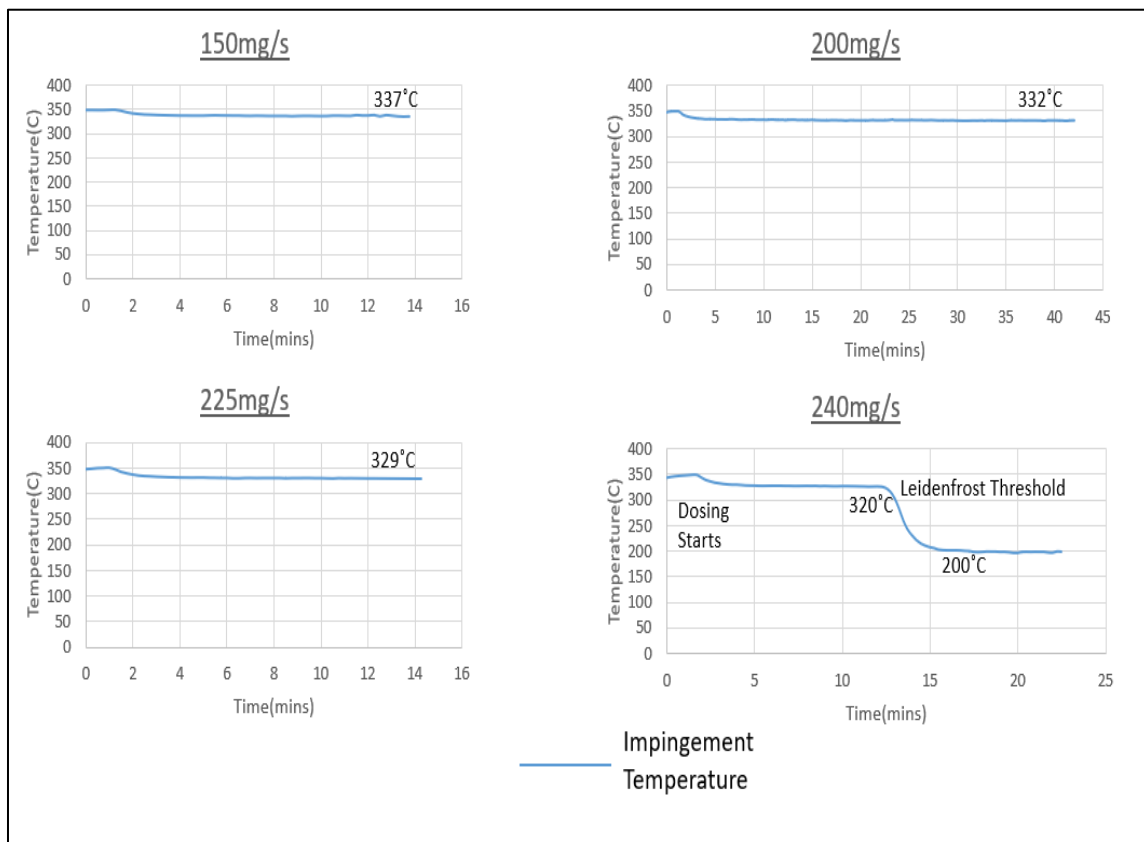


Figure 5.14 Leidenfrost Threshold
(Impingement temperature profile for 400°C gas temperature and 400kg/hr gas flow rate)

5.3.3. Critical Injection Rate (CIR). Critical injection rate is the amount of DEF that can be injected at given operating conditions without the formation of deposits. For a given exhaust flow rate, the safe injection DEF flow rate is plotted against temperature ((Figure 5.15). The red line on the graph captured the trend for CIR with temperature for 800kg/hr gas flow rate. At 300°C, the maximum injection of DEF was 70mg/s, at 350°C, the maximum injection of DEF was 120mg/s and at 400°C, the maximum injection was 237.5mg/s. With increase in temperature, the CIR increased significantly.



Figure 5.15 Critical Injection Rate for 800kg/hr
(Safe injection rate for different gas temperature at 800kg/hr gas flowrate)

5.3.4. Effect of Gas Flow Rate Transport plays a significant role in urea deposits. As stated earlier, literature suggested that higher exhaust flow rates help in deposit mitigation. Figure 5.16 illustrates the work from different literature that established various mechanisms by which higher gas flow rate reduced the risk of deposit formation.

To study the effect of transport, two gas flow rates were tested-400kg/hr and 800kg/hr. The study was conducted in two different regimes:

- a) **Boundary Regime:** For a fixed temperature and gas flow rate, the DEF flow rate is just adequate to initiate liquid film and deposits. The DEF flow rate is less than 1.3 times of CIR.
- b) **Wall Film Regime:** For a fixed temperature and gas flow rate, DEF flow rate would generate significant amount of liquid film and have deposit growth. DEF flow rate is 1.3 times more than the CIR.

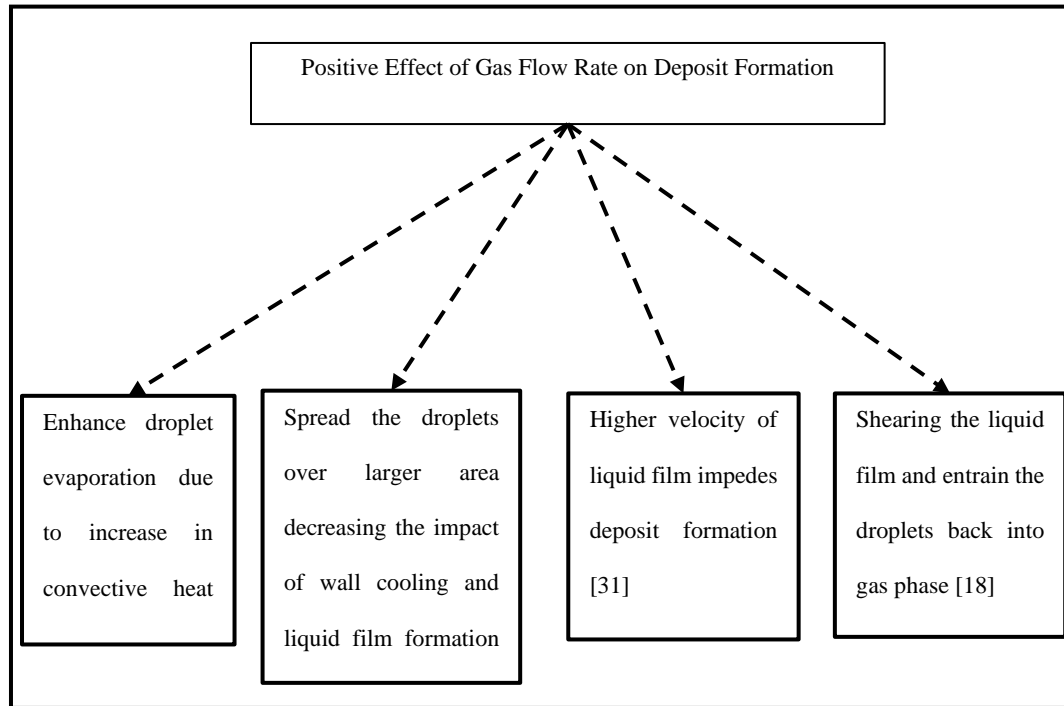


Figure 5.16 Deposit Mitigating Mechanism at High Exhaust Flow Rate
(Mechanism through which higher gas flow rate mitigates deposit formation reported in literature)

The reason to pick two different regimes was to deconvolute the effect of gas flow rate on deposit formation. The boundary regime does not generate significant wall film. Keeping the same gas temperature and DEF flow rate fixed, the effect of increasing gas flow rate would directly affect the wall film formation specifically droplet evaporation and spreading of impinging droplet mass. In the wall film regime, significant amount of wall film exists. Keeping the same gas temperature and DEF flow rate fixed, increasing gas flow rate would directly affect the post wall film formation specifically film velocity and shearing of liquid film that entrains the droplets back into gas phase.

For a fixed gas temperature and low gas flow rate, 100 mins deposit test was conducted with less than 130% CIR (boundary regime) and greater than 130% CIR (wall

film regime). For the same temperature and DEF flow rate, the exhaust flow rate was increased to 800kg/hr and tested for the same duration. The deposit weight was compared between the two experiments. To reduce experimental errors, an experiment was repeated the next day, where for the same conditions, higher gas flow rate was tested first followed by lower gas flow rate. The results are presented in Table 5.2

From Table 5.2, it was observed that for 300°C boundary regime, deposits were mitigated, and the CIR increased by 28.5% when exhaust flow was doubled. For 350°C boundary regime, the CIR increased by 9% when exhaust flow was doubled. The results are in line with the previous research [62]. However, in the wall film regime, increasing the exhaust flow rate accelerated the deposit growth rate. For 350°C, the CIR was computed as 110mg/s. To be in the wall film regime, a test was run at 150mg/s which is 36% more than the CIR. For 400kg/hr, the deposit mass after 100 mins was 2700mg and for 800 kg/hr the deposit mass increased to 11700mg. From video, it was observed that in the wall film regime, liquid film was transported quickly across the plate at higher exhaust flow rates. The literature suggested that increase in film velocity would lower the residence time for deposit reactions which in turn impede deposit formation. This might be true in some exhaust layouts and mixer designs. In the current test setup, higher exhaust flow rate stripped the liquid film to higher temperature regions on the plate where deposit reactions were accelerated. The tapering effect of high exhaust flow rate seen in Figure 5.17 was due to stripping of liquid film. Once the deposit initiated, the incoming liquid film solidified at an enhanced rate. During low exhaust flow rate, the liquid film did not taper but initiated deposits around the edges of the film. This effect of gas flow rate was seen only in the wall film regime. The time stamp shown in Figure 5.17, clearly indicated that with increasing

gas flow rate, the deposit initiated earlier, and the reason is the higher flow transported the liquid film to higher temperature region where deposit reactions were accelerated.

Table 5.2 Deposit Weight for Different Gas Flow Rate

| Regime | Gas Temperature | CIR | DEF Flow Rate | Gas Flow Rate | Deposit Weight |
|---------------|------------------------|------------|----------------------|----------------------|-----------------------|
| Wall Film | 300°C | 70mg/s | 100mg/s | 400kg/hr | 1000mg |
| | 300°C | 90mg/s | 100mg/s | 800kg/hr | 2200mg |
| | | | | | |
| Boundary | 300°C | 70mg/s | 80mg/s | 400kg/hr | 60mg |
| | 300°C | 90mg/s | 80mg/s | 800kg/hr | No Deposit |
| | | | | | |
| Boundary | 350°C | 110mg/s | 120mg/s | 400kg/hr | 400mg |
| | 350°C | 120mg/s | 120mg/s | 800kg/hr | No Deposit |
| | | | | | |
| Wall Film | 350°C | 110mg/s | 150mg/s | 400kg/hr | 2700mg |
| | 350°C | 120mg/s | 150mg/s | 800kg/hr | 11700mg |

Shearing of liquid film due to higher local velocity was one of the mechanisms suggested in the literature to help deposit mitigation. This experiment couldn't verify the stated mechanism and the reason could be the lower range of gas velocity this experiment was tested. The local velocity measured with pitot tube were comparable with the CFD calculations. The gas velocity was lower than the Munnannur's et al.'s work [61]. The

comparison of Reynold's number is shown in Table 5.3. Modifying the geometry to achieve higher gas velocity would help to shear the liquid film to mitigate deposits.

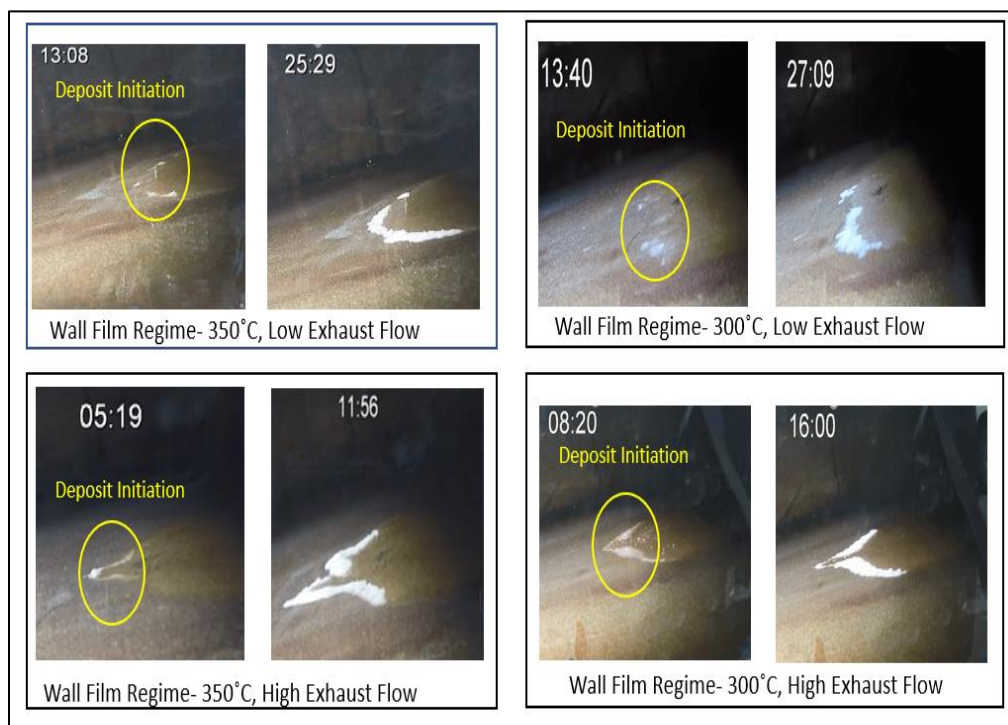


Figure 5.17 Deposit Initiation and Growth in Wall Film Regime
(With increasing gas flow rate, the deposit initiated earlier. The higher flow transported the liquid film to higher temperature region where deposit reactions were accelerated)

Table 5.3 Reynolds Number

| Exhaust Flow Rate(kg/hr) | Velocity(m/s) | Area(m ²) | Density(kg/m ³) | Viscosity (*10 ⁻⁵ Pa.s) | Reynolds Number |
|--------------------------|---------------|-----------------------|-----------------------------|------------------------------------|-----------------|
| 400 | 5.37 | 0.0049 | 0.58 | 3.06 | 498.74 |
| 800 | 10.7 | 0.0049 | 0.58 | 3.06 | 993.77 |

5.4. INFERENCE

An outdoor deposit test was conducted on a Class 8 truck with a typical after-treatment system layout. An optic box was placed between the DPF and SCR with an impingement plate in the center of the box. Deposit initiating temperatures were identified independent of operating conditions. The temperature band was within a 30°C range and the temperatures were in line with the temperature range observed in previous experiments where biuret decomposition initiated. Extreme conditions were tested to generate deposits outside the temperature range. Critical injection rate of DEF was identified for different temperatures for a fixed exhaust flow rate. With increase in gas temperature, the critical injection rate increased significantly. The effect of gas flow rate on deposits was investigated. At DEF flow rates less than 1.3 times CIR, the increase in gas flow rate mitigated deposits but when DEF flowrates were greater than 1.3 times CIR, the amount of deposits generated were higher with increase in flow rate.

6. DEPOSIT CHARACTERIZATION

6.1. ANALYTICAL METHODOLOGY

Nature of deposits change with different exhaust conditions. At low exhaust temperatures, literatures have reported that the main components of deposits are urea and biuret [31] [30]. At high exhaust temperatures, deposits mainly consist of triazanes-ammelide, cyanuric acid, ammeline and heptazines-melem, melon. As discussed in Section 2, depending on the deposit composition, the solubility and decomposition time scales vary. It was very important to quantify the deposit composition in order develop a reaction model that can accurately characterize various stages of deposit formation and decomposition.

Physical state of deposits are solids. It is a mixture of different compounds with varying chemical and physical properties. Components of deposit mixture can be partially predicted based on reaction chemistry as shown in Table 2.1. Certain components in deposits are not very soluble in common solvents. Compounds like melam and melon are not soluble in any solvents [33] [60]. Analytical methods like solid state C-13 NMR, FTIR, and TGA has the advantage of analyzing the sample in solid state. This chapter discusses a set of analytical methods used to characterize the deposit composition and the most accurate method is recommended.

6.2. C-13 NMR (CARBON-13 NUCLEAR MAGNETIC RESONANCE)

In NMR, a magnetic field is applied to nuclei and the amount of energy required to resonate various nuclei is measured. Nuclei in different environments (adjacent bonds and molecules) requires different energy to bring the nuclei in resonance. In C-13 NMR,

different carbon types are measured. A spectrum was obtained for each sample as shown in Figure 6.1. Peaks in the spectra are assigned to different type of carbon based on its environment which are unique to a particular compound as seen in Figure 6.2.

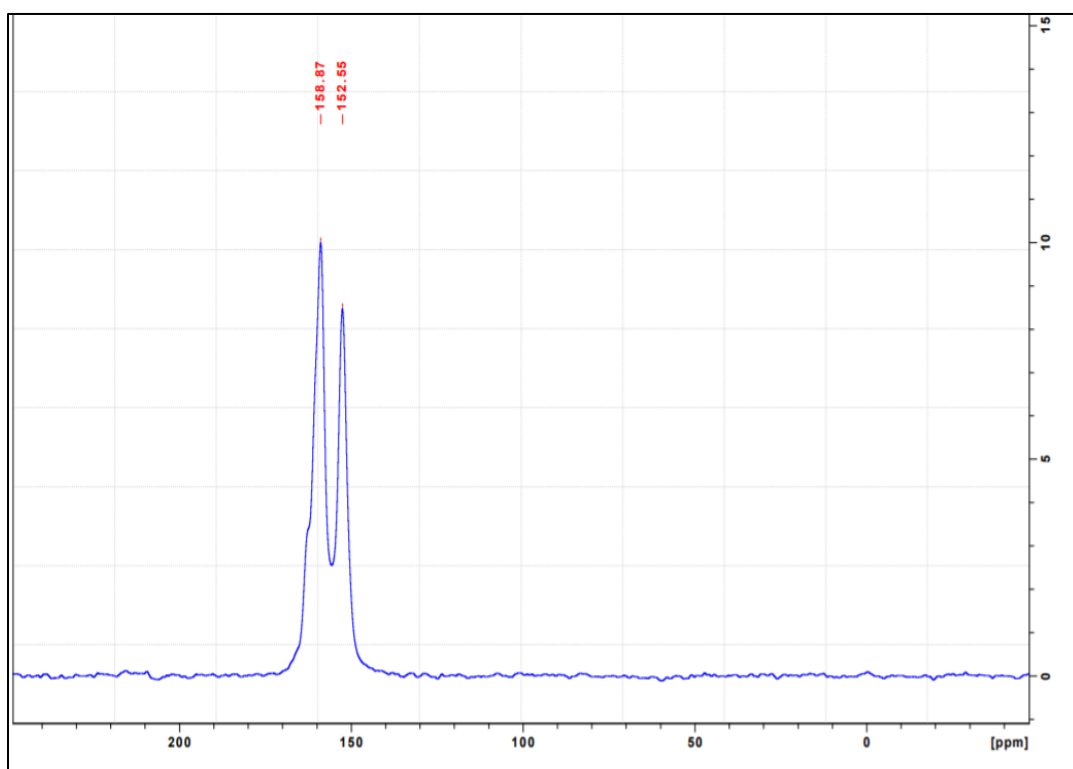


Figure 6.1 C-13 NMR Spectra of Deposit Sample
(Peaks in the spectra are assigned to different type of carbon based on its environment)

| No. | Compound | ¹³ C NMR Chemical shifts |
|-----|---------------|-------------------------------------|
| 1 | Cyanuric acid | 173 |
| 2 | Urea | 161 |
| 3 | Biuret | 153 |
| 4 | Triuret | 150; 153 |
| 5 | Melamine | 179 |
| 6 | Ammeline | 175; 180 |
| 7 | Ammelide | 176; 175 |

Figure 6.2 C-13 Standard Compound Peak

In Figure 6.1, the resonance peak at 158 is attributed to urea and the peak at 152 to Biuret/Triuret. The curves were very broad, and resolution of the peaks were low. The challenge of using C-13 NMR was that the analysis required considerable amount of sample unlike TGA and FTIR. Short duration of deposit test would generally yield low deposits which was not sufficient to obtain enough resolution in a C-13 NMR analysis. Hence, further work to improve the resolution was not considered.

6.3. FTIR (FOURIER TRANSFORM INFRARED SPECTROSCOPY)

Infrared light when shined on a molecule absorbed energy that caused bonds to stretch. In Figure 6.3, a spectrum was obtained where the peaks correspond to the frequency of IR radiation absorbed by the molecule. The y-axis denoted the percentage of transmission. If the value of transmittance was less than 100%, it suggested that the molecule had absorbed infrared resulting in stretching vibration. Different functional group and chemical bonds have different absorption frequency range.

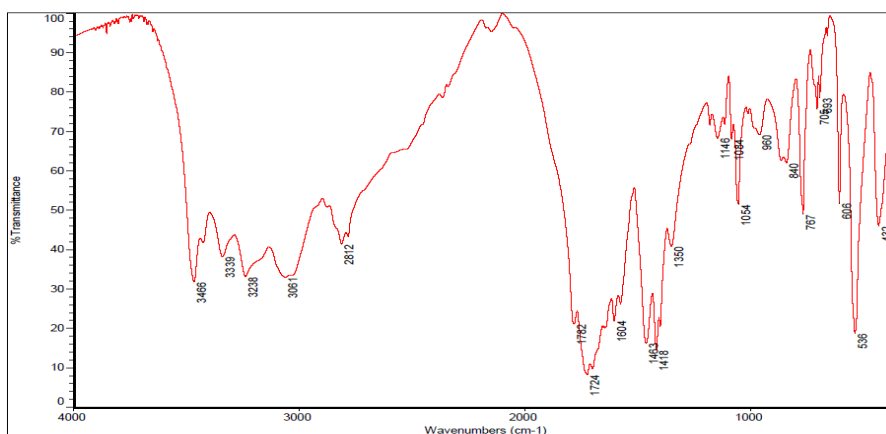


Figure 6.3 FTIR Spectra of Deposit Sample
(Peaks correspond to the frequency of IR radiation absorbed by the molecule)

Weeks et.al [68] published an IR spectrum for urea, biuret, CYA, ammeline, and melamine (Figure 6.4).

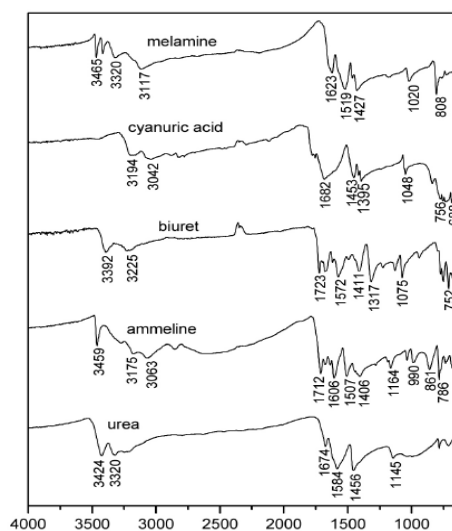


Figure 6.4 FTIR Spectra of Standard Compounds

Unique peaks of a compound were matched with deposit sample peaks to identify the components present in the deposit as shown in Figure 6.5.

| Urea Deposit Peaks | Pure Component Wave Number | | | | |
|--------------------|----------------------------|---------------|--------|----------|------|
| | Melamine | Cyanuric Acid | Biuret | Ammeline | Urea |
| 3466 | | | | | |
| 3339 | | | | | |
| 3238 | | | | | |
| 3061 | | | | | |
| 2812 | | | | | |
| 1782 | | | | | |
| 1724 | | | | | |
| 1604 | | | | | |
| 1463 | | | | | |
| 1418 | | | | | |
| 1350 | | | | | |
| 1148 | | | | | |
| 1050 | | | | | |

Figure 6.5 Comparison of Deposit Sample Peak with Standard Compounds

Based on the peaks, it was evident that the deposit samples contain melamine, cyanuric acid, biuret, ammeline and urea.

6.4. THERMOGRAVITOMETRIC ANALYSIS (TGA)

TGA was used to characterize the compounds in a sample by measuring the change in weight as a function of temperature. This is one of the analytical methods that is widely used to characterize the deposit samples. The deposit samples from gravity driven liquid film and pure compounds were heated at the same rate. All samples had three step decomposition, and the curves followed the biuret and triuret curves (Figure 6.6).

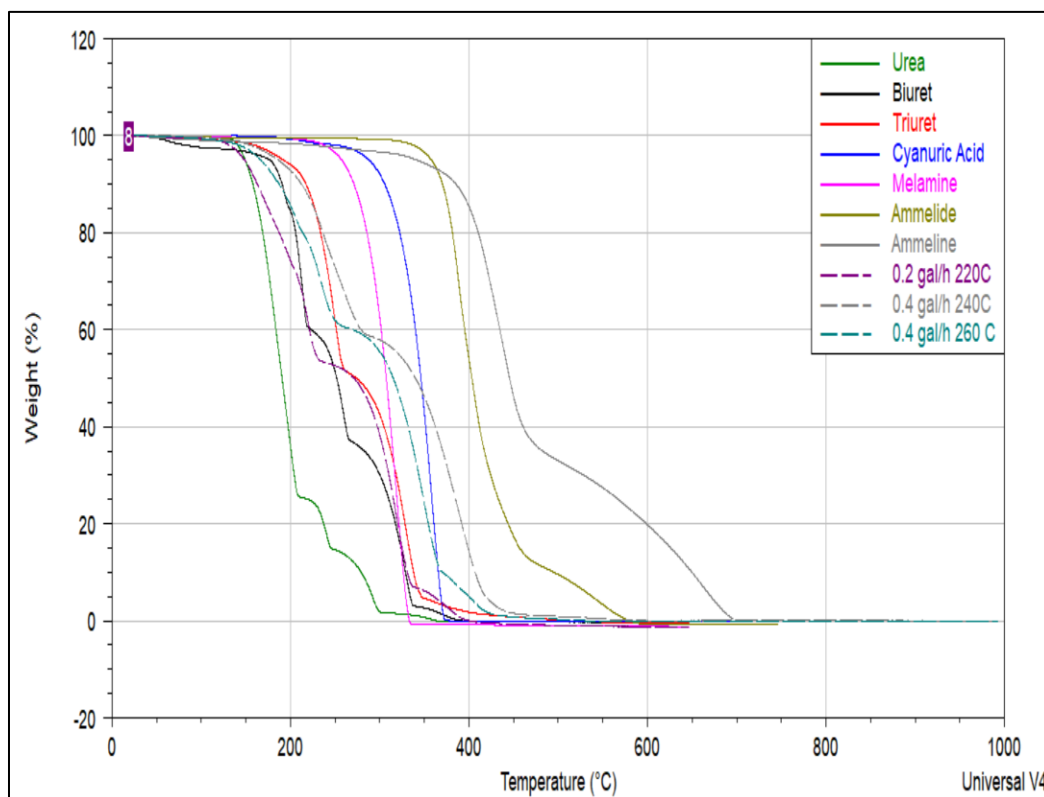


Figure 6.6. TGA Analysis of Deposit Sample and Standard Compounds
(Deposit samples from gravity driven liquid film and pure compounds were heated at 10°C/min)

6.5. ESI-MS (ELECTRON SPRAY IONIZATION-MASS SPECTROMETRY)

The sample was injected into a capillary where a high voltage was applied. A characteristic jet was created at the outlet causing the sample to be ejected as charged droplet(ion) which was then sent to mass spectrometer (MS). MS has 2 parts-an electric field and magnetic field. An electric field accelerated the charged droplet and a magnetic field deflected the ions off their path. When an ion is accelerated in electric field, it tends to move in a straight-line. The momentum is proportional to the mass of the ion. However, in MS the ions are deflected by electromagnets. The amount of force ions experience from the magnet was proportional to its charge. The path of the ion was a result of its mass to charge ratio. The detector records different charge to mass ratio as shown in Figure 6.7. The y-axis represents the relative intensity.

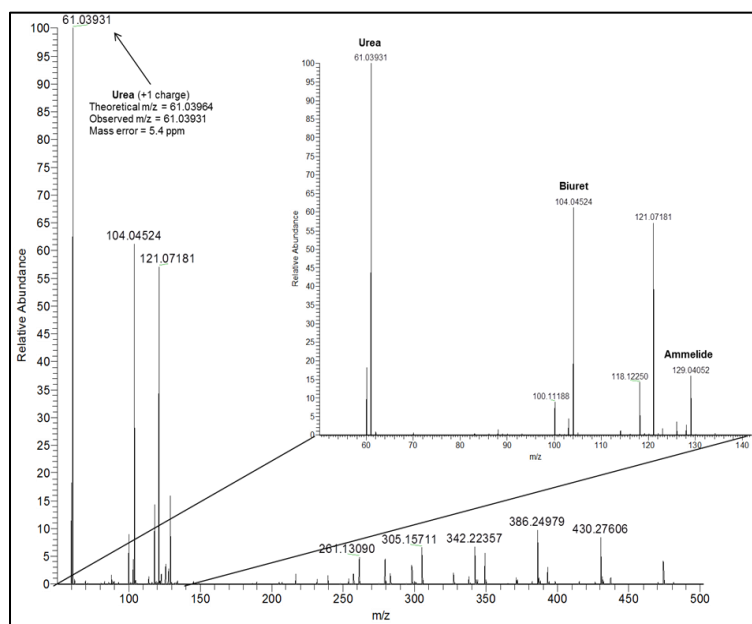


Figure 6.7. ESI-MS Spectra of Deposit Sample
(The samples were loaded into separate static nanospray ECONO 12 tips (Proxeon) and analyzed by nano-electrospray ionization in positive-ion and negative-ion modes on a ThermoScientific LTQ Orbitrap XL mass spectrometer)

The solid samples were dissolved in ethanol (at 16mg/mL). The stocks were heated to 56°C and sonicated for 10min (each). The sample was centrifuged, an aliquot of the supernatant removed, and mixed 1:5 with 99% acetonitrile/1% formic acid (or 99.9% acetonitrile, 0.1% ammonium hydroxide for negative-ion mode).

The samples were loaded into separate static nanospray ECONO 12 tips (Proxeon) and analyzed by nano-electrospray ionization in positive-ion and negative-ion modes on a ThermoScientific LTQ Orbitrap XL mass spectrometer. Typical flow rates from these tips were estimated to be 50nL/min. FTMS data were collected in the Orbitrap (60,000 resolving power, 50-250 m/z, 1 micro scan, maximum inject time of 500ms. CYA standard peak (130.02 m/z) was not observed in positive-ion mode, but the compound peak (128.00 m/z) was observed in negative-ion mode. The results are presented in Figure 6.8.

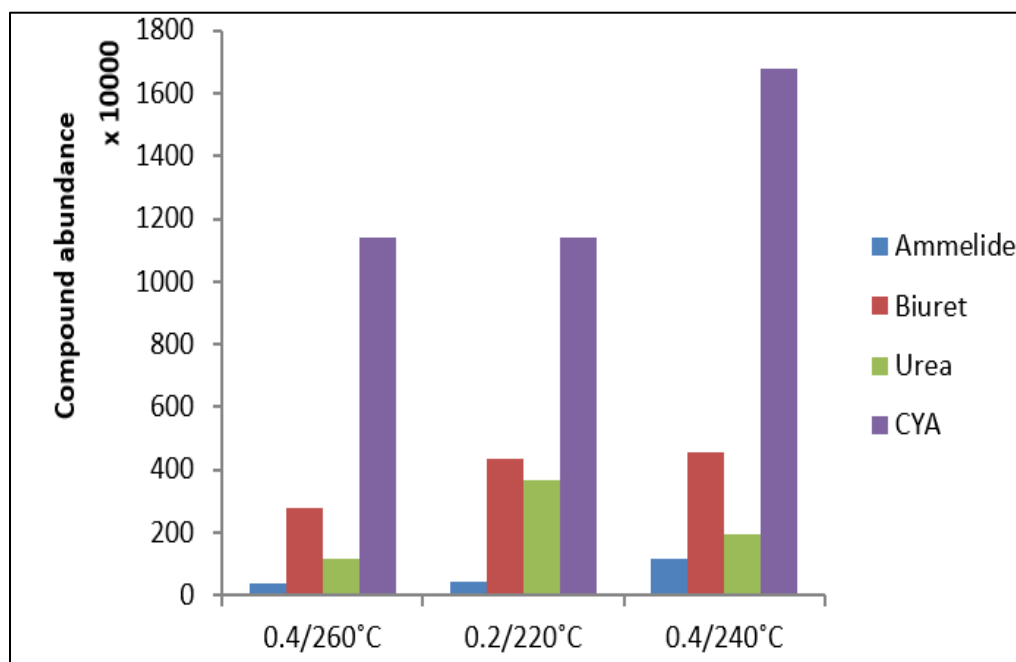


Figure 6.8 Peak Height Quantitation of Three Compounds (Urea, Biuret, CYA and Ammelide relative concentration was computed for gravity-driven liquid film experiment using ESI-MS)

6.6. LIQUID CHROMATOGRAPHY(LC)

MS is a very accurate and sensitive technique. Since deposits is a mixture, coupling MS with LC was a good way to separate the mixture and get accurate quantitation values. In a LC-MS system, if the LC unit is connected directly to the MS, the liquid mobile phase would vaporize, resulting in large amounts of gas being introduced into the MS unit. This would decrease the vacuum and prevent the target ions from reaching the detector. Therefore, a key issue for LC-MS is how to get rid of the mobile phase. ESI was used as an interface.

Three columns were tested to determine if we can observe, retain, separate and quantify the compounds: urea, biuret, triuret, melamine, cyanuric acid ammelide and ammeline.

6.6.1. Amide Column. Stocks of each compound were made as follows: ammelide, 1mg/mL in DMSO; cyanuric acid, 5mg/mL in DMSO; biuret, 27mg/mL in water; urea 1.5mg/mL in water; triuret, 1.25mg/mL in water; and melamine 2.61mg/mL in water. A mixed standard of 100ng/mL of each compound was loaded onto an amide column and eluted with a gradient of acetonitrile. Compound peaks were integrated using default methods to generate AUC (area under curve).

Clear signal for triuret (RT=1.44min), ammelide (RT=1.59min), and melamine (RT=2.12min) were observed (Figure 6.9). No signal for biuret, cyanuric acid, or urea was observed at this concentration. Amide column was not suitable for separating the deposit mixtures.

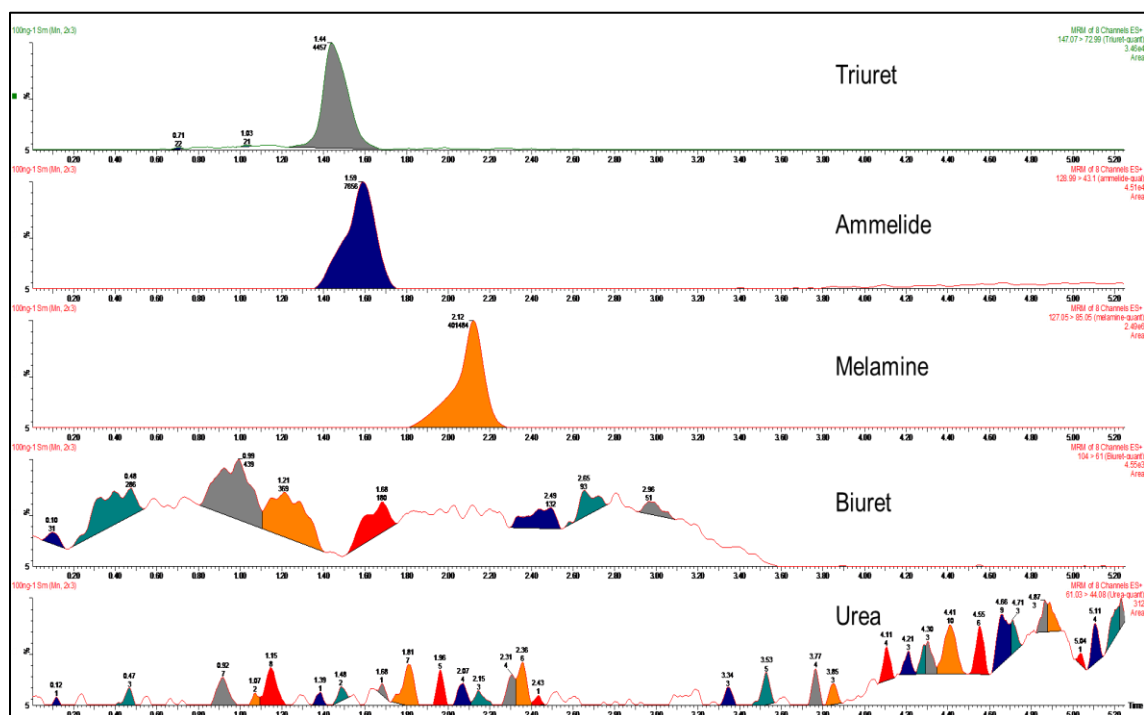


Figure 6.9. Amide Column: Peak Separation and Retention Time
(No signal for biuret, cyanuric acid, or urea was observed)

6.6.2. HSS-T3 and C18 dual Column Setup. Stocks of each compound were made similar to the amide column. Standards were made by serial dilution as follows: all 6 compounds were mixed at 500ng/mL final concentration diluted into 30ng/mL tolbutamide internal standard (IS) in 50% acetonitrile, 0.1% formic acid. All compounds showed linear responses from 0 to 500ng/mL (Figure 6.10). Linearity for melamine was lower than the others ($R^2=0.98$) suggesting signal started to saturate at 500ng/mL.

Samples (10uL injection) were separated using an Acquity H-class UPLC (Waters) on a dual column set-up comprising Waters HSS-T3 column (1.8um x 100mm x 2.1mm) linked by 2cm of peak tubing to a Waters Symmetry C18 column (2.7um, 10cm x 2.1mm).

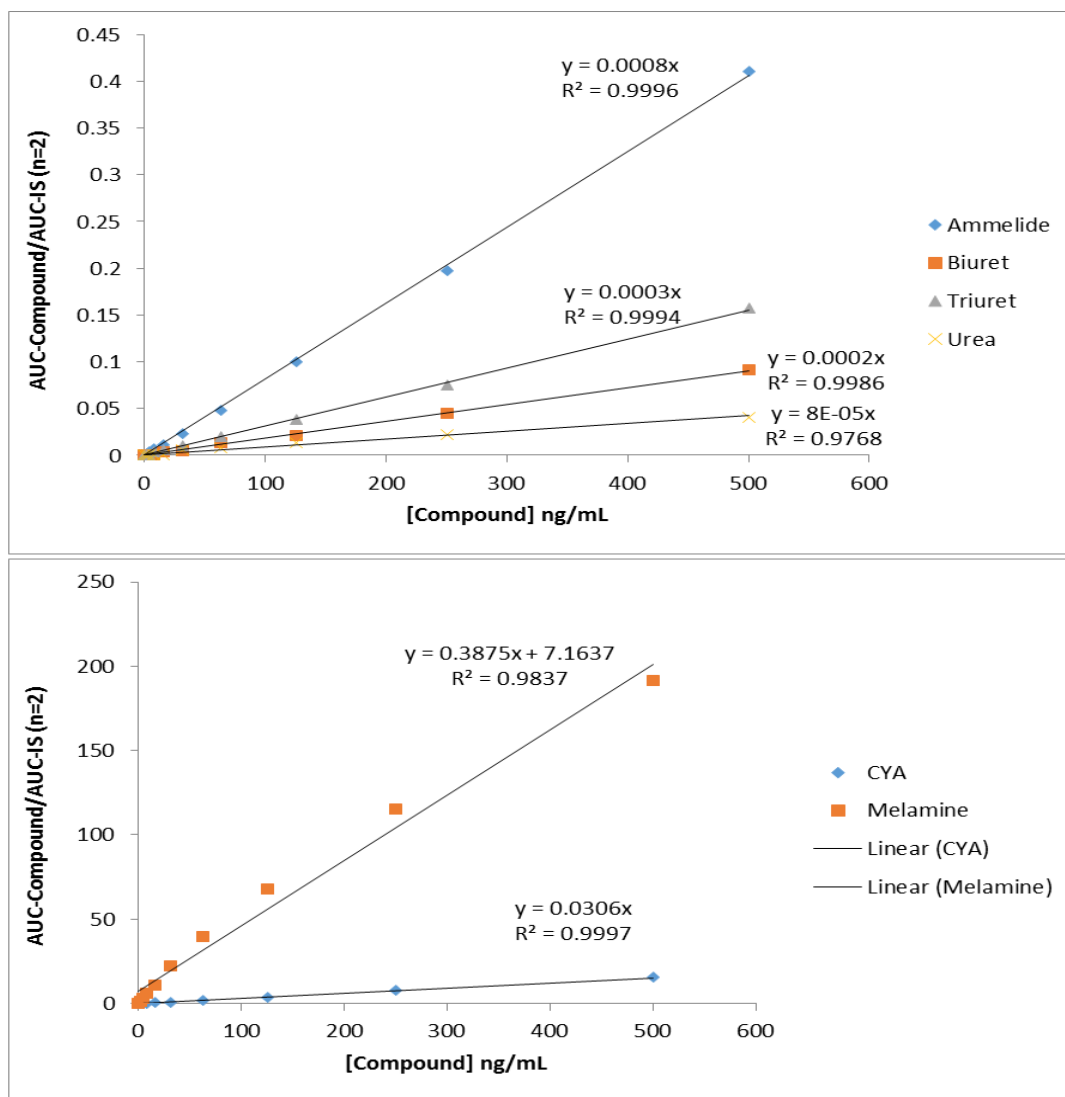


Figure 6.10 Standard Curves for Dual Column Setup
(Standards were made by serial dilution for 6 compounds. A linear response was observed for the all standards)

Solvent was delivered at 0.4mL/min across the gradient. Solvent A: 0.1% formic acid in water; Solvent B: 0.1% FA in acetonitrile. Initial conditions were 0%B followed by a 1.5min hold at 0%B, 0.5min ramp to 98%B, hold for 1.25min at 98%B, 0.5min ramp to 0%B, and hold at 0%B for 1.5min. Total run time 5.25min. The column was not heated (room temperature ~21 °C) and the samples cooled to 20 °C in the autosampler.

Due to the lack of signal for lower concentrations of biuret and urea, the lower limit of quantitation (LLOQ) will be quite high (likely >50ng/mL). Signal for all compounds were observed (Figure 6.11). Two compounds, triuret and biuret, had the same retention time (Figure 6.11). However, their masses were sufficiently different that no signal overlap would occur.

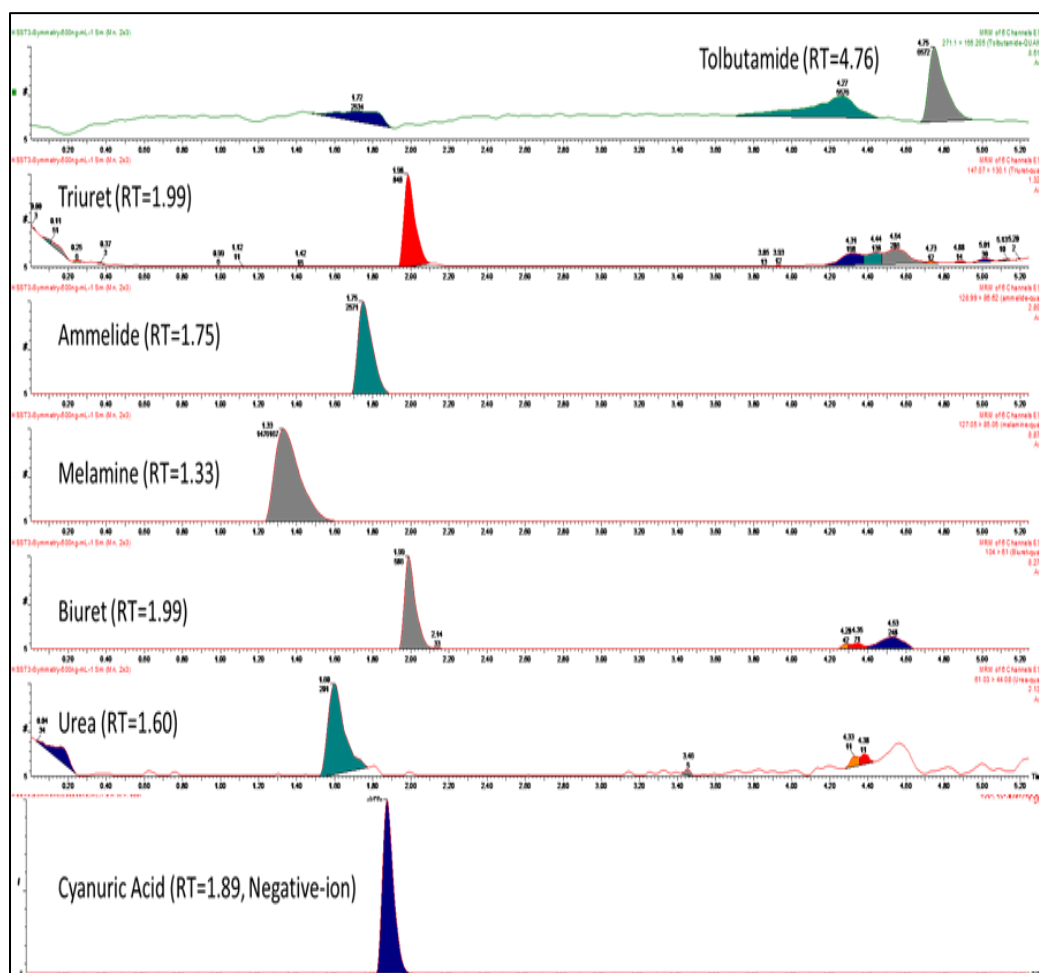


Figure 6.11 Compound Separation and Retention for Dual Column (Samples (10uL injection) were separated using a dual column set-up comprising Waters HSS-T3 column (1.8um x 100mm x 2.1mm) linked by 2cm of peak tubing to a Waters Symmetry C18 column (2.7um, 10cm x 2.1mm))

Sample analysis: The two-column set up was not reliable for sample analysis. During one of the runs, the system leaked after injection #6 and ended up not having any data. In another test, the system over-pressured and did not have standard curve data to calculate ng/mL amounts in the sample.

6.6.3. HILIC Column. HILIC column was tested with all 7 standards. The samples were suspended at 2mg/mL in 0.1% NaOH and diluted 1:500 for analyses. One mg/mL stocks of each compound were freshly prepared as follows: ammeline, 1mg/mL in DMSO; cyanuric acid, 1mg/mL in DMSO; biuret, 1mg/mL in water; urea 1mg/mL in water; triuret, 1mg/mL in DMSO; and melamine 1mg/mL in water; and ammeline, 1mg/mL in 0.1% NaOH.

Standards were made by serial dilution as follows: all 7 compounds were mixed at 1ug/mL final concentration in 90% acetonitrile, 0.1% formic acid. That standard was then mixed 1:5 with 90/0.1 solvent. All compounds, except urea ($R^2=0.88$), showed a linear response ($R^2>0.99$) (Figure 6.12).

The instrument was operated in positive-ion and negative-ion modes. One transition was used for each compound (Table 6.1). Most compounds were measurable in positive-ion mode, except for cyanuric acid. Urea yielded very poor response for MS/MS MRM transition. Urea was subsequently acquired in SIR mode (selected ion recording), no collision energy applied, intact molecule examined.

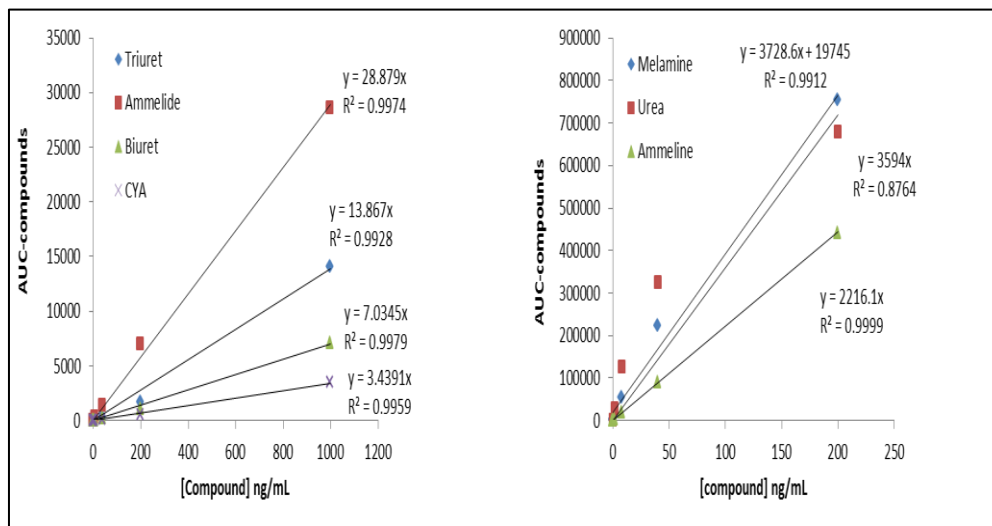


Figure 6.12 Standard Curves for HILIC Column
(All compounds, except urea ($R^2=0.88$), showed a linear response ($R^2>0.99$))

Table 6.1 LC-MRM Transition

| Compound | Precursor | Fragment | Ionization mode |
|---------------|-----------|----------|-----------------|
| Ammelide | 128.99 | 86.62 | + |
| Biuret | 104 | 61 | + |
| Cyanuric acid | 128 | 42 | - |
| Melamine | 127.05 | 85.05 | + |
| Triuret | 147.07 | 130.1 | + |
| Urea (SIR*) | 61.03 | 61.03 | + |
| Ammeline | 128.0 | 86.0 | + |

Cross-talk phenomenon: Each standard preparation was injected separately without mixing. Results indicated that urea was very abundant in the melamine standard; the ammelide standard contained a significant amount of ammeline; biuret contained

significant amount of triuret (Figure 6.13). Since CYA was acquired in negative-ion mode, there was no cross-talk with the others.

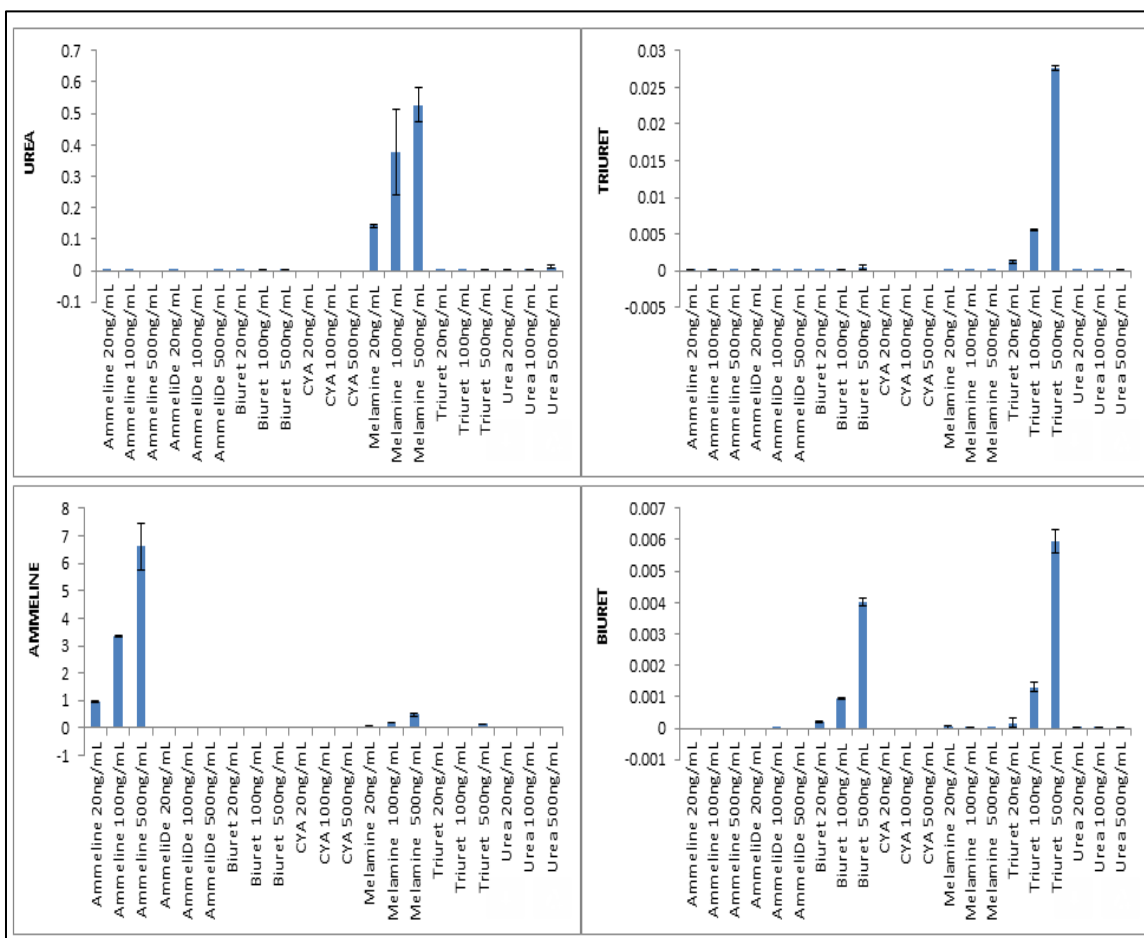


Figure 6.13 Cross-Talk Phenomenon in HILIC Column
(Urea was abundant in melamine standard; ammelide standard contained ammeline;
biuret contained triuret)

The analytical method developed by Yassin et al. [69] had used ammonium formate in the aqueous mobile phase which resulted in co-elution of melamine and ammeline. This was fixed by removing ammonium formate and including 0.1% formic acid. This was also observed by Eakle et.al [67].

In our analysis, ammonium acetate was replaced with 0.1% formic acid to prevent the cross-talk phenomenon.

Final Method Used for Chemical Quantitation: Materials: Urea(>99.9% assay) was purchased from Fisher Scientific, triuret(>95%) was purchased from Enamine LLC (Cincinnati, OH), ammeline (>98.0% assay) was purchased from Tokyo Chemical Industry Co. Ltd. (Portland, OR), biuret(>98%), ammeline(100%), CYA(>98%), and the SeQuant ZIC-HILIC column (3.5 μ m, 100Å, 50mm x 2.1 mm) were purchased from Sigma-Aldrich(St.Louis,MO) .

Compounds were quantified using the methods outlined in Eakle et .al [63] with the following modifications: samples were resuspended at 1mg/mL in 0.5 % (v/v) NaOH in water. Samples were then diluted 1:10 and 1:1000 in solvent (50% acetonitrile, 0.1% formic acid) and then 10 μ L injected onto the SeQuant ZIC-HILIC column. Data were acquired in positive and negative-ion modes (separate acquisitions, as outlined in Table X) using an Acquity UPLC (Waters Corp, Milford, MA) and a Xevo TQ-S QQQ mass spectrometer (Waters Corp.). Area under curve (AUC) data were generated using Target Lynx software (Waters Corp) and compounds quantified using a mixed standard curve of 7 compounds. Due to the lack of retention of urea on the 50mm HILIC column, a dual column set-up was used for all subsequent analyses as follows: a Waters Acquity UPLC BEH C18 VanGuard pre-column (1.7 μ m, 2.1mm x 5mm) was attached to a Waters Symmetry C18 column (2.7 μ m, 10cm x 2.1mm) and then linked to the front of the HILIC column with peek tubing (3cm x 1.6mm o.d. x 0.127mm i.d.). A 15min gradient was used to elute the compounds: initial conditions were 87%B (A: 0.1% formic acid in water, B: 99.9% acetonitrile, 0.1% formic acid), followed by 5min of isocratic flow (at 87%B),

gradient to 40%B over 4min, hold at 40%B for 3min, then ramp back to (1 min) and hold at (3 min) initial conditions.

Data were acquired in positive and negative-ion modes using an Acquity UPLC (Waters Corp, Milford, MA) and a Xevo TQ-S QQQ mass spectrometer (Waters Corp.). Area under curve (AUC) data were generated using Target Lynx software (Waters Corp) and compounds quantified using a mixed standard curve of 7 compounds.

6.7. AMMONIUM CARBAMATE CHARACTERIZATION

A separate test was conducted at Faurecia Clean Mobility's R&D center to study the conversion of urea to ammonium carbamate. The products from different test conditions were sent to Missouri S&T to detect the presence of ammonium carbamate(Figure 6.14).

Samples: 4 bottles of specimens were collected:

- a. Reactor-1: DEF leftover from conversion test(R1)
- b. Reservoir -1: Ammonia Carbamate from 150°C and 180°C hot plate. System was closely sealed(S1)
- c. Reservoir-2: Ammonia Carbamate from 150°C and 180°C hot plate. System had open hole on reservoir(S2)
- d. Reservoir-3: Ammonia Carbamate from 300°C hot plate. System had open hole and then closed sealed(S3)

TGA and Gas Chromatography-Mass Spectroscopy (GC-MS) was used to detect the presence of ammonium carbamate in the sample.



Figure 6.14 Ammonium Carbamate Test Samples
 (R1:DEF leftover from conversion test; S1: Ammonia Carbamate-closely sealed between 150-180°C; S2: Ammonia Carbamate-open hole on reservoir between 150-180°C; S3: Ammonia Carbamate from 300°C hot plate)

6.7.1. Thermogravimetric Analysis Samples (S1, S2 and S3) were stable in closed containers but decomposed rapidly when exposed to air even at room temperatures. TGA analysis was conducted on all 3 samples along with pure ammonium carbamate. Sample S1, S2, S3 had very similar composition and decomposed at less than 100°C. According to Gary Fulks et al. [70], ammonium carbamate had a single step decomposition process (Figure 6.15). Samples S1, S2 and S3 had single step decomposition similar to ammonium carbamate.

Sample R1 curve was similar to the TGA of DEF. The sample decomposed above 300°C.

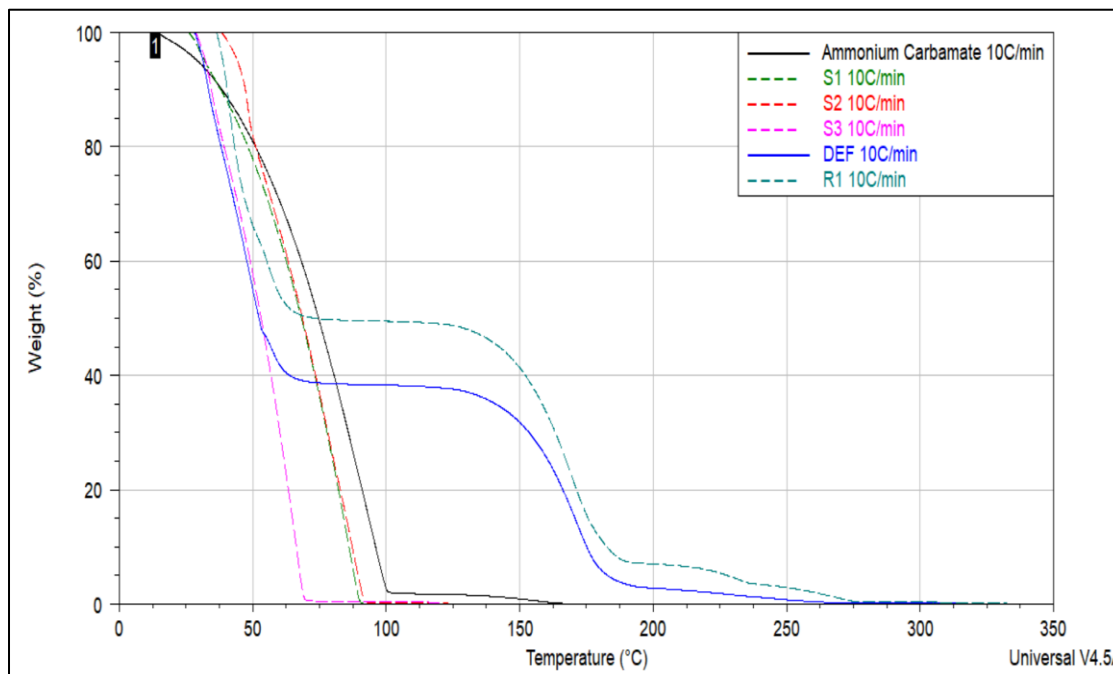


Figure 6.15 TGA Curves of Ammonium Carbamate Samples
(Samples S1, S2 and S3 had single step decomposition similar to ammonium carbamate)

6.7.2. Gas Chromatography-Mass Spectroscopy (GC-MS) GC-MS was

used to detect the presence of ammonium carbamate. The derivatized extracts were analyzed for non-targeted metabolic profiling using an Agilent 6890 GC coupled to a 5973N MSD mass spectrometer with a scan range from m/z 50 to 650 (Agilent Technologies, Inc). 1 μ l of sample was injected into the GC column with a split ratio of 1:15. Separation was achieved with a temperature program of 80 $^{\circ}$ C for 2 min, then ramped at 5 $^{\circ}$ C /min to 315 $^{\circ}$ C and held at 315 $^{\circ}$ C for 12 min on 60m DB-5MS column (J&W Scientific, 0.25 mm ID, 0.25 μ m film thickness) and a constant flow of 1.0 ml/min of helium gas. A standard alkane mix was used for GCMS quality control and retention index calculations. The water blank showed clearly a peak at retention time of 5.6 min. This peak appeared in all the samples as well as in the standard (Figure 6.16)

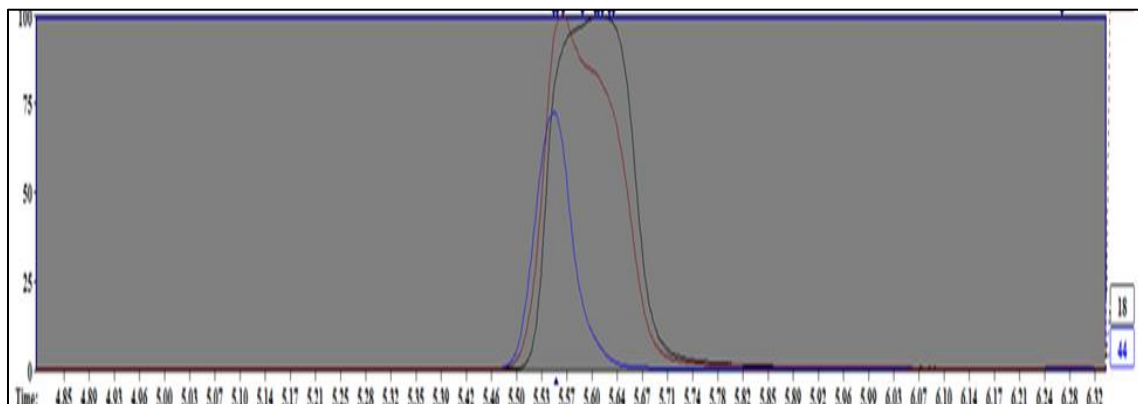


Figure 6.16 Peak Retention Time

(The derivatized extracts were analyzed for non-targeted metabolic profiling using an Agilent 6890 GC coupled to a 5973N MSD mass spectrometer with a scan range from m/z 50 to 650)

Ammonium carbamate is a salt of carbamic acid. Generally, fragmentation pattern of ions is detected in GC-MS. Both the sample had the same spectrum with 84% match to carbamic acid (NH_2COO^-) (Figure 6.17). Samples had higher 18 m/z peak that corresponded to NH_4^+ (Figure 6.18).

| | |
|-------------|------------------------------|
| 5.5484 - 72 | >Carbon dioxide |
| 5.5484 - 72 | >Carbon dioxide |
| 5.5535 - 23 | >Carbamic acid, monoammonium |
| 5.5535 | >Water |
| 5.6073 | >Water |
| 5.6115 | >Water |
| 5.6115 | >Water |
| 5.6173 | >Water |
| 5.6173 | >Water |
| 5.6274 - 8 | >Methyl Alcohol |
| 5.6330 | >Ammonia |

| | |
|------------------|------------------|
| Component: | Match: |
| Width = >36 | Weighted = 84 |
| Purity = 75% | Reverse = 84 |
| Model = 16 m/z | Corrections: n/a |

Figure 6.17 Predicted Retention Time
(Spectrum had 84% match to carbamic acid)

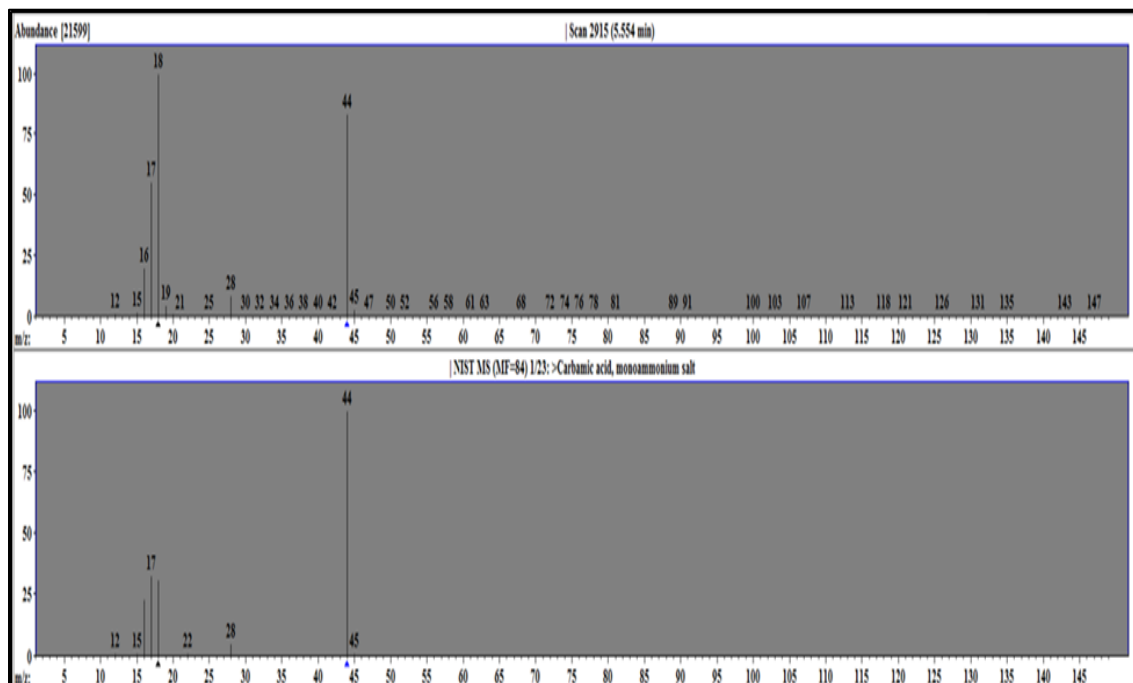


Figure 6.18 GC-MS Peaks
(Samples with 18 m/z peak and 44 m/z corresponded to carbamic acid)

The library entry for carbamate looks just as an overlap of a water peak and a carbon dioxide peak. The standard was not showing any appreciable peak for m/z 44. So, either the samples are extremely concentrated or there is a presence of dissolved carbon dioxide. The ratio of m/z 17 to m/z 18 is increased for the samples, but that could be from the presence of ammonia. We also tried running the standard dissolved in methanol, but still didn't get much of a presence of m/z 44. It basically looked like a methanol blank. Thus, it seemed that the results are ambiguous.

6.8. INFERENCE

The challenge with deposit characterization was due to the presence of complex mixtures. Different analytical methods were applied to evaluate the chemical composition

of deposit samples. TGA analysis qualitatively differentiated between the deposits formed at different exhaust conditions by comparing it with the standard curves. ESI-MS method was used to detect the relative abundance of compounds in the samples. Most of the compounds were detected in positive-ion mode except CYA. Liquid chromatography was used to separate the mixture where different columns were tested for compound retention and separation. HILIC had better retention and separation compared to amide and C-18 columns. MS/MS was used to perform quantitation, a technique that had high specificity. Ammonium carbamate was characterized using the GC-MS and the TGA. The fragmentation pattern of carbamate and ammonium ions were detected using the GC-MS.

7. CONCLUSION

Urea decomposition and deposit study was investigated through numerous experiments. The data from TGA showed the range of temperatures at which urea and its derivative compounds decomposed. DEF solution was heated in an open system and pressurized system. In an open system, most of the water evaporated before urea decomposition initiated. At higher pressures, due to the presence of water at wider temperature range, urea underwent hydrolysis and the deposit residual weight decreased.

Single-droplet experiment study further supported that deposit forming mechanisms were surface based. Within a liquid film, increase in heating rates and temperatures, accelerated deposit initiation.

Finally, deposit test was conducted on a truck with the complete after-treatment layout. Deposit initiating local surface temperatures were identified independent of operating parameters-exhaust flow rate, exhaust gas temperature. Critical injection rate for different gas temperatures were identified and the effect of gas flow rate on deposit generation was studied in the same test. LC-MRM with a HILIC column was used to accurately quantify the compounds in deposit mixture.

To design a better mixer, the first risk was the droplet impingement on the wall. From previously published literature, it was understood that droplets larger than 50 μ m do not have enough residence time for complete evaporation. To prevent the surface impingement, droplet size had to be reduced. The second risk was the wall wetting and the film formation. This can be minimized and prevented by having high heat transfer at the droplet impingement location. The third risk was the deposit generating from liquid film.

From the experiments, there was enough evidence to conclude that deposit would generate when a liquid film was present. The experiments indicated that deposit growth rate can be reduced with lower heat transfer. Finally, if the generated deposits plug the exhaust system, the only solution was to decompose it above $\sim 500^{\circ}\text{C}$.

8. FUTURE WORK

Future work should focus on testing more points to study the effect of gas flow rate in the wall film regime and to deconvolute the effect of gas velocity and flowrate. Repeating the deposit initiation temperature test with different plate thickness would deconvolute the effect of temperature and the plate thermal energy on deposit initiation. To build a more accurate regression model, the gas can be passed through the non-impingement side of the plate so that the local impingement DEF flow rate and global flow rate are the same. To predict the deposits at the end of test cycle, studying the effect of temperature on critical injection flow rate with respect to deposit growth rate is important.

In the pressurized system test, the reaction mechanism needs to be characterized by simultaneously measuring liquid and gaseous composition at different time intervals. Measuring isocyanic acid, ammonia, carbon-dioxide and water vapor in the gas phase and measuring carbamate/carbonate ions, urea in liquid phase could be one of the approaches.

Studying the droplet size, surface roughness, surface tension and urea concentration on a single droplet aqueous urea solution would provide us better understanding of different factors interacting in the spray-wall interaction model. This can guide new ideas like applying surface coating or modifying the urea solution or improving the nozzle design.

Characterization and Analytical Chemistry- Identifying the oligomer structure present in the deposit. Insoluble from the deposit samples must be separated and by applying either X-Ray Diffraction (XRD) or Maldi-ToF (Time of Flight) might help us identify the oligomer structure.

REFERENCES

- [1] T. Holmstrom and L. Wallin, "Investigation of urea deposit formation in vehicles with Selective Catalytic Reduction System," 2014.
- [2] M. Nahavandi, "Selective Catalytic Reduction (SCR) of NO by Ammonia Over V2O5/TiO2 Catalyst in a Catalytic Filter Medium And Honeycomb Reactor: A Kinetic Modeling Study," *Brazilian Journal of Chemical Engineering*, 2015.
- [3] H. J. Seong, "Selective Catalytic Reduction (SCR) of NO by NH3 in a Fixed-bed Reactor," 2009.
- [4] B. J. Cooper, A. McDonald, A. Walker and J. Matthey, "The Development and On-Road Performance AND Durability of the Four-Way Emission Control SCRT System," in *9th Diesel Engine Emissions reduction Conference(DEER)*, Newport, 2003.
- [5] Z. Qi, S. Li and X. Guo, "Development, Application and Direction of Development of Urea-SCR," *International Journal of Multimedia and Ubiquitous Engineering*, 2016.
- [6] W. A. Majewski, "Selective Catalytic Reduction," 2005. [Online]. Available: https://www.dieselnet.com/tech/cat_scr.php.
- [7] A. Jain, B. Jyotirmoy , K. Patchappalam and S. Gedela, "A Study on the Factors Affecting the Formation of Urea Crystals and Its Mitigation for SCR After-Treatment Systems," *SAE International*, 2017.
- [8] S. Toma, "Your Guide to AdBlue - What Is It, Who Needs It, and How to Refill It," 22 Feb 2016. [Online]. Available: <https://www.autoevolution.com/news/your-guide-to-adblue-what-is-it-who-needs-it-and-how-to-refill-it-104882.html#>.
- [9] A. Johansson, U. Wallin, M. Karlsson, A. Isaksson and P. Bush, "Investigation on Uniformity Indices Used for Diesel Exhaust Aftertreatment Systems," no. 2008-01-0613, 2008.
- [10] C. Bai and A. D. Gosman, "Development of Methodology for Spray Impingement Simulation," *SAE Technical Paper Series*, 1995.
- [11] H. Smith, M. Zochbauer and T. Lauer, "Advanced Spray Impingement Modelling for an Improved Prediction Accuracy of the Ammonia Homogenisation in SCR Systems," *SAE International*, 2015.

- [12] L. Möltner, A. Giovannini and S. Verena , "Analysis of Heat and Mass Transfer on Free Moving Urea/Water-Droplets in SCR-Systems by Numerical Methods," *INTERNATIONAL JOURNAL OF MECHANICS*, 2016.
- [13] S. Grout, J. Blaisot, K. Pajot and G. Osbat, "Experiemental Investigation on the Injection of an Urea-Water Solution in Hot Air Stream for SCR Applications," *Fuel*, 2012.
- [14] M. Koebel and E. O. Strutz, "Thermal and Hydrolytic Decomposition of Urea for Automotive Selective Catalytic Reduction Systems: Thermochemical and Practical Aspects," *Industrial and Engineering Chemistry Research*, 2003.
- [15] G. Chaussonnet, "Modeling of Liquid Film and Break Up Phenomena in Large-Eddy Simulations of Aeroengines Fueled by Airblast Atomizer," *HAL*, 2014.
- [16] F. Birkhold, U. Meingast, P. Wassermann and O. Deutschmann, "Analysis of the Injection of Urea-Water-Solution for Automotive SCR DENOX-Systems:Modeling of Two-Phase Flow and Spray/Wall Interaction," *SAE Technical Paper Series*, 2006.
- [17] G. Zheng, "CFD Modeling of Urea Spray and Deposits for SCR Systems," *SAE International*, 2016.
- [18] A. Munnannur, M. Chiruta and G. Liu, "Thermal and Fluid Dynamic Considerations in Aftertreatment System Design for SCR Solid Deposit Mitigation," *SAE International*, 2012.
- [19] W. Brack, B. Heine, F. Birkhold, M. Kruse and O. Deutschmann, "Formation of Urea-Based Deposits in an Exhaust System: Numerical Predictions and Experimental Observations on a Hot Gas Test Bench," *Emiss.Control Sci.Technol*, 2016.
- [20] H. L. Fang and H. F. DaCosta, "Urea Thermolysis and NO_x reduction with and without SCR Catalyst," *Applied Catalysis*, vol. 46, pp. 17-34, 2003.
- [21] P. M. Schaber, J. Colson, S. Higgins, D. Thielen, B. Anspach and J. Brauer, "Thermal Decomposition(Pyrolysis) of Urea in an Open Reaction Vessel," *Thermochimica Acta*, vol. 424, pp. 131-142, 2004.
- [22] A. Lundstrom, B. Andersson and L. Olsson, "Urea Thermolysis Studied Under Flow Reactor Conditions using DSC and FT-IR," *Chemical Engineering Journal*, vol. 150, pp. 544-550, 2009.
- [23] M. Eichelbaum, R. Farrauto and M. Castaldi, "The Impact of Urea on the Performance of Metal Exchanged Zeolites for the Selective Catalytic Reduction of NO_x Part 1. Pyrolysis and Hydrolysis of Urea over Zeolite Catalysts," *Applied Catalysis B:Environmental*, pp. 90-97, 2010.

- [24] J. Liu, T. Zhang, Z. Wang, G. Dawson and W. Chen, "Simple Pyrolysis of Urea into Graphitic Carbon Nitride with Recyclable Adsorption and Photocatalytic Activity," *Journal of Materials Chemistry*, vol. 21, pp. 14398-14401, 2011.
- [25] A. M. Bernhard, I. Czekaj, M. Elsener, A. Wokaun and O. Krocher, "Evaporation of Urea at Atmospheric Pressure," *The Journal of Physical Chemistry*, vol. 115, pp. 2581-2589, 2011.
- [26] S. Sebelius, T. T. Le, L. J. Pattersson and H. Lind, "Identification of Urea Decomposition From An SCR Perspective: A Combination of Experimental Work and Molecular Modeling," *Chemical Engineering Journal*, vol. 231, pp. 220-226, 2013.
- [27] W. Brack, B. Heine, F. Birkhold, M. Kruse, G. Schoch, S. Tischer and O. Deutschmann, "Kinetic Modeling of Urea Decomposition Based on Systematic Thermogravimetric Analysis and Its Most Important By-Products," *Chemical Engineering Science*, vol. 106, pp. 1-8, 2014.
- [28] W. Brack, B. Heine, F. Birkhold, M. Kruse and O. Duetschmann, "Formation of Urea-Based Deposits in an Exhaust System: Numerical Predictions and Experimental Observations on a Hot Gas Test Bench," *Emission Control Science and Technology*, vol. 2, pp. 115-123, 2016.
- [29] S. Tisher, M. Bornhorst, J. Amsler, G. Schoch and O. Deutschmann, "Thermodynamics and Reaction Mechanism of Urea Decomposition," *Physical Chemistry Chemical Physics*, vol. 21, pp. 16785-16797, 2019.
- [30] R. Hartley, C. Henry and S. Eakle, "Deposit Reduction in SCR Aftertreatment Systems by Addition of Ti-Based Coordination Complex to UWS," *SAE International*, no. 2019-01-0313, 2019.
- [31] H. Zhang, Y. Xi, C. Su and Z. Liu, "Lab Study of Urea Deposit Formation and Chemical Transformation Process of Diesel After Treatment System," *SAE Technical Paper*, 2017.
- [32] H. Smith, T. Lauer and M. Mayer, "Optical and Numerical Investigations on the Mechanisms of Deposit Formation in SCR Systems," *SAE International*, no. 2014-01-1563, 2014.
- [33] Manufacturers of Emission Controls Association, "Technology Feasability for Model Year 2024 Heavy-Duty Diesel Vehicles in Meeting Lower NO_x Standards," Arlington, VA, 2019.

- [34] C. Sharp, C. C. Webb, S. Yoon, M. Carter and C. Henry, "Achieving Ultra Low NOX Emissions Levels with a 2017 Heavy Duty on Highway TC Diesel Engine-Comparison of Advanced Technology Approaches," *SAE International*, no. 2017-01-0956, 2017.
- [35] R. Sala, P. Bielaczyc and M. Brzezanski, "Concept of Vaporized Urea Dosing in Selective Catalytic Reduction," *Catalysts*, no. 307, 2017.
- [36] P. Pierz and L. D. Tikk, "Superheated Urea Injection for Aftertreatment Applications". United States Patent US 20070119153A1, 31 May 2007.
- [37] P. Larsson, W. Lennard, O. Andersson and P. Tunestal, "A Droplet Size Investigation and Comparison Using a Novel Biomimetic Flash -Boiling Injector for Adblue Injections," *SAE International*, no. 2016-01-2211, 2016.
- [38] N. V. Vuuren and J. Qin, "High Speed Video Measurements with Water of a Planar Laser Illuminated Heated Tip Urea Injector Spray," *SAE International*, no. 2013-01-1073, 2013.
- [39] G. Brizi and L. Postrioti, "Experimental Analysis of SCR Spray Evolution and Sizing in High-Temperature and Flash Boiling Conditions," *SAE International Journal of Fuels and Lubricants*, no. 04-12-02-0006, 2019.
- [40] N. Rapoport, "Phase Shift, Stimuli-Responsive Perfluorocarbon Nanoparticles for Drug Delivery to Cancer," *Wiley Interdisciplinary Reviews.Nanomedicine Nanobiotechnology*, pp. 492-510, 2012.
- [41] H. B. Cooper and H. W. Spencer, "Methods for the Production of Ammonia from Urea and/or Biuret, and uses for Nox and/or Particulate Matter Removal". United States Patent 6077491, 20 June 2000.
- [42] D. L. Wojichowski, "Methods of Converting Urea to Ammonia for SCR , SNCR and Flue Gas Conditioning". United States Patent 20030211024A1, 13 November 2003.
- [43] D. G. Jones, "Method for Converting Urea to Ammonia". United States Patent 5827490, 27 October 1998.
- [44] J. Shorter, "The Conversion of Ammonium Cyanate into Urea-a Saga in Reaction Mechanisms," *Chemical Society Reviews*, no. 1, 1978.
- [45] A. G. Dana, G. E. Shter and G. S. Grader, "Thermal Analysis of Aquous Urea Ammonium Nitrate Alternative Fuel," *Royal Society of Chemistry*, no. 4, pp. 34836-34848, 2014.

- [46] M. C. Stumpe and H. Grubmuller, "Aqueous Urea Solutions: Structure, Energetics and Urea Aggregation," *The Journal of Physical Chemistry B*, no. 111, pp. 6220-6228, 2007.
- [47] Y. A. Cengel, *Heat Transfer: a practical approach*, New york: McGraw-Hill, 2002.
- [48] A. Wiranata, I. Pranoto, W. H. Mitrakusuma, D. and S. Kamal, "Experimental study on the effect of surface temperature and weber number to spreading ratio of multiple droplets on a horizontal surface," in *AIP Conference Proceedings*, 2016.
- [49] J. D. Bernardin and I. Mudawar, "The Leidenfrost Point: Experimental Study and Assessment of Existing Models," *Journal of Heat Transfer*, vol. 121, pp. 894-903, 1999.
- [50] C. Kruse, T. Anderson, C. Wilson, C. Zuhlke, D. Alexander, G. Gogos and S. Ndao, "Extraordinary Shifts of the Leidenfrost Temperature from Multiscale Micro/Nanostructured Surfaces," *Langmuir*, p. 9798–9806, 2013.
- [51] M. Bornhorst and O. Deutschmann, "Single Droplet Impingement of Urea Water Solution on a Heated Substrate," *International Journal of Heat and Fluid Flow*, vol. 69, pp. 55-61, 2018.
- [52] G. Wasow and E. O. Strultz, "Method for minimizing the diameter of a urea solution and use of a surfactant in urea solution". United States Patent US 9,050,560 B2, 9 June 2015.
- [53] S. Sebelius, "Additive to Urea Solutions". Euopean Patent Specification Patent EP2488283B1, 01 January 2010.
- [54] V. O. Strots, S. Santhanam, B. J. Adelman, G. A. Griffin and E. M. Derybowski, "Deposit Formation in Urea-SCR Sytems," *SAE International Journal of Fuels and Lubricants*, 2009.
- [55] A. Roppertz, S. Fuger and S. Kureti, "Investigation of Urea-SCR at Low Temperature," *Topics in Catalysis*, vol. 60, pp. 199-203, 2017.
- [56] S. Prabhu, N. Nayak, N. Kapilan and V. Hindasageri, "An experimental and numerical study on effects of exhaust gas temperature and flow rate on deposit formation in Urea-Selective Catalytic Reduction(SCR) system of modern automobiles," *Applied Thermal Engineering*, vol. 111, pp. 1211-1231, 2017.
- [57] A. Spiteri and P. D. Eggenschwiler, "Experimental Fluid Dynamic Investigation of Urea-Water Sprays for Diesel Selective Catalytic Reduction-DeNO_x Application," *Industrial and Engineering Chemistry Research*, vol. 53, pp. 3047-3055, 2014.

- [58] P. Gaynor, B. Reid, G. Hargrave, T. Lockyer and J. Wilson, "An Experimental Investigation into DEF Dosing Strategies for Heavy Duty Vehicle Applications," *SAE International*, no. 2015-01-1028, 2015.
- [59] D. Kuhnke, "Spray / Wall-interaction Modelling by Dimensionless Data Analysis," PhD Thesis Universitat Darmstadt, 2004.
- [60] M. Bornhorst, S. Langheck, H. Weickenmeier, C. Dem, R. Suntz and O. Deutschmann, "Characterization of Deposits from Urea Water Solution Injected Into a Hot Gas Test Rig," *Chemical Engineering Journal*, vol. 377, 2019.
- [61] S. Eakle, S. Kroll, A. Yau, J. Gomez and C. Henry, "Investigation of Urea Derived Deposits Composition in SCR Systems and Their Potential Effect on Overall PM Emissions," *SAE International*, 2016.
- [62] A. Munnannur, M. Chiruta and G. Liu, "Thermal and Fluid Dynamic Considerations in Aftertreatment System Design for SCR Solid Deposit Mitigation," *SAE International*, no. 2012-01-1287, 2012.
- [63] G. Zheng, A. Fila, A. Kotrba and R. Floyd, "Investigation of Urea Deposits in Urea SCR Systems for Medium and Heavy Duty Trucks," *SAE International*, no. 2010-01-1941, 2010.
- [64] K. W. Ku and J. G. Hong, "Thermo Fluid Effect of the Urea Thermal Decomposition in a Lab-Scaled Reactor," *Chemical Engineering Journal*, vol. 264, pp. 625-632, 2015.
- [65] S. Eakle, S. Kroll and C. Henry, "Investigation of Urea Derived Deposits Composition in SCR Systems," *SAE International*, 2016.
- [66] C. L. Weeks, D. R. Ibeling, S. Han and L. Ludwig, "Analytical Investigation of Urea Deposits in SCR System," *SAE International*, no. 2015-01-1037, 2015.
- [67] M. Yassine, "Development of a Hydrophilic Interaction Liquid Chromatography-Mass Spectrometry Method for Detection and Quantification of Urea Thermal Decomposition By-Products in Emission from Diesel Engine Employing SCR Technology," *Journal of Chromatography*, vol. 1229, pp. 208-215, 2012.
- [68] G. Fulks, G. B. Fisher, K. Rahmoeller, M. Cheng, E. Herde and J. Tan, "A Review of Solid Materials as Alternative Ammonia Sources for Lean NO_x Reduction with SCR," *SAE International*, no. 2009-01-0907, 2009.
- [69] M. Kapoor, "Review of Diesel Emissions Conference India," in *platinummetalreview.com*, Delhi, 2012.

- [70] M. Eichelbaum, R. J. Farrauto and M. J. Castaldi, "The impact of urea on the performance of metal exchanged zeolites for the selective catalytic reduction of NO_x," *Applied Catalysis B:Environmental*, vol. 97, pp. 90-97, 2010.
- [71] H. Dong, S. Shuai and J. Wang, "Effect of Urea Thermal Decomposition on Diesel NO_x-SCR Aftertreatment Systems," *SAE International*, no. 2008-01-1544, 2008.
- [72] F. Rodriguez and F. Posada, "Future Heavy-Duty Emission Standards," The International Council on Clean Transportation, 2019.
- [73] H. Smith and K. Gabel, "Evaluation and Prediction of Deposit Severity in SCR Systems," *SAE International*, no. 2016-01-0970, 2016.
- [74] G. Chaussonnet, "Modeling of Liquid Film and Breakup Phenomena in Large-Eddy Simulations of Aeroengines Fueled by AirBlast Atomizer," HAL, 2014.
- [75] H. Lan, J. L. Wegener, B. F. Armaly and J. A. Drallmeier, "Developing Laminar Gravity-Driven Thin Liquid Film Flow Down an Inclined Plane," *Journals of Fluids Engineering*, vol. 132, 2010.

VITA

Anand earned his bachelor's degree in Chemical Engineering from Amrita Vishwa Vidyapeetham, Ettimadai. He completed his B. Tech degree in October of 2013.

Anand joined the graduate school Missouri University of Science and Technology in January of 2014 for a master's degree. There, he was given an opportunity to work as a graduate research assistant under Dr. Joseph Smith. He was also a graduate teaching assistant and course instructor during his time as a graduate student in the Chemical and Biochemical Engineering Department. Anand Alembath graduated with his M.S. in Chemical Engineering in May of 2016.

Anand worked as a CFD engineer in Elevated Analytics for a brief period before enrolling in the doctoral program at Missouri S&T under Dr. Joseph Smith in Spring 2017. Anand was offered for his doctoral dissertation, a project on investigating urea deposits in diesel exhaust after-treatment system. The research was in collaboration with Faurecia Clean Mobility, Columbus, IN. As a part of his research, Anand pursued an internship as SCR product specialist at Faurecia's R&D Centre in summer 2017. Anand obtained his PhD in Chemical Engineering from Missouri University of Science and Technology in December 2020.